

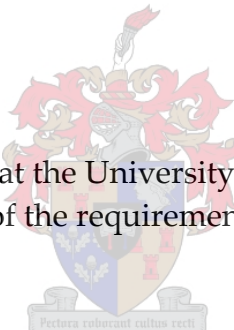


UNIVERSITEIT•STELLENBOSCH•UNIVERSITY
jou kennisvennoot • your knowledge partner

APPLICATION OF TURBOCHARGERS IN SPARK IGNITION PASSENGER VEHICLES

By

Wallace William Bester



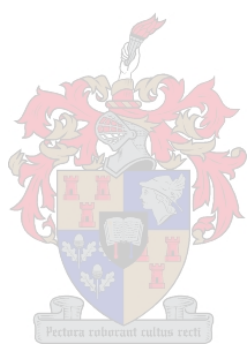
Thesis presented at the University of Stellenbosch in
partial fulfilment of the requirements for the degree of

Master of Science in Mechanical Engineering

Department of Mechanical Engineering
Stellenbosch University
Private Bag X1, 7602 Matieland
South Africa

Supervisor: Dr A. B. Taylor
Co-supervisor: Dr C. Scheffer

April 2006

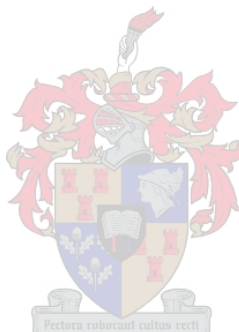


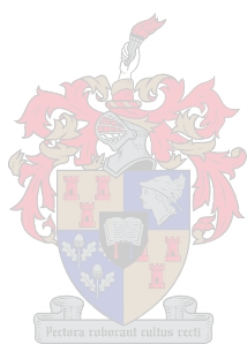
DECLARATION

I, the undersigned, hereby declare that the work contained in this thesis is my own work and that I have not previously in its entirety or in part submitted it at any university for a degree.

Signature:.....

Date:.....





ABSTRACT

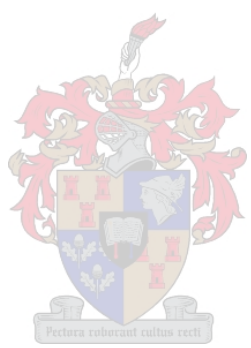
The quest for higher efficiency of the internal combustion engine will always be pursued. Increasingly stringent emission regulations are forcing manufacturers to downsize on engine displacement and increase specific power. By adding a turbocharger, the airflow through the engine and hence the specific power can be increased.

The advantages of a small turbocharged engine over a naturally aspirated (NA) engine of similar power is that it is lighter, having better part load efficiency when operating at the same load, while producing less emissions. Component sharing, increased production volume and lower development costs are further possible advantages that turbocharging could hold for the manufacturer.

The objective in this study was to determine the accuracy with which a one-dimensional flow simulation package can predict the performance of a NA and turbocharged engine. The implications of adding a turbocharger to a NA engine were also investigated.

Different exhaust manifold concepts were evaluated for the turbocharged engine. A NA engine was turbocharged and its performance was compared to the simulated results. Simulation predicted the actual NA engine performance to within 6% and the actual turbocharged engine performance to within 9% when developing the same boost pressure. Turbocharging increased the maximum power by 37% and the torque by 48%. 82% of the maximum torque was available from 2000 rev/min up to 5500 rev/min. The turbocharged engine could match the fuel efficiency of the NA engine both at full load and part load. Thus it is justified that a turbocharger can be used to increase the specific power while still maintaining part load efficiency. However turbocharging does increase the mechanical loads on the engine components, the extent of which was quantified.

It was found that one-dimensional analysis is a valuable tool for the use in the application of turbochargers on SI engines.



OPSOMMING

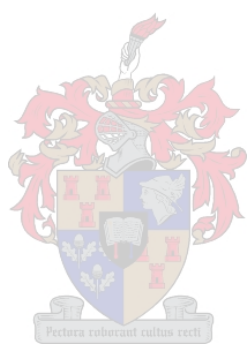
Daar sal altyd gestreef word om die effektiwiteit van binnebrandenjins te verhoog. Die toenemende streng uitlaatgas regulasies verplig vervaardigers om enjins se verplasing te verminder, maar terselfdertyd die spesifieke kraguitset te verhoog. Die toevoeging van 'n turbo-aanjaer kan die lugvloei deur die enjin vermeerder en dienooreenkomsdig ook die krag uitset.

Die voordele van 'n klein turbo-aangejaagde (TA) enjin teenoor 'n onaangejaagde (OA) enjin met gelyke werkverrigting is dat die TA enjin lichter is, beter deellas effektiwiteit het wanneer beide by dieselfde las toestand opereer terwyl dit minder emissies vrystel. Onderdeel deling, verhoogde produksie volume en laer ontwikkelingskoste is moontlike voordele wat turbo-aanjaging vir die vervaardigers kan inhoud.

Die doelwit was om die akkuraatheid te bepaal waarmee 'n 1-dimensionele vloeianalise pakket die werkverrigting van 'n OA en TA enjin voorspel kan word. Die implikasies van die toevoeging van 'n turbo-aanjaer op 'n OA enjin is ook ondersoek.

Verskillende uitlaat spruitstuk konsepte is geëvalueer vir die TA enjin met behulp van die 1-dimensionele simulasie pakket. 'n OA enjin is omgebou na 'n TA enjin en die gemete werkverrigting is vergelyk met die voorspelde resultate. Die simulasie het die werkverrigting van die OA enjin met 'n akkuraatheid van 6% voorspel. Die werkverrigting van die TA enjin is met 'n akkuraatheid van 9% voorspel wanneer dieselfde aanjagings druk ontwikkel is. Turbo-aanjaging het die maksimum drywing verhoog met 37% en die wringkrag met 48%. 82% van die maksimum wringkrag is beskikbaar vanaf 2000 opm. tot by 5500 opm. Die TA enjin het die brandstof verbruik van die OA enjin ge-ewenaar beide by deel las sowel as vollas. Die turbo-aanjaer verhoog egter die meganiese belasting op die komponente en hierdie toename is gekwantifiseer.

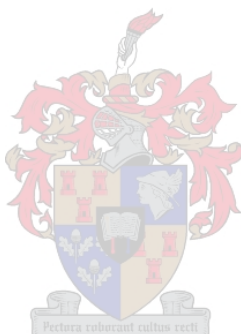
Dit is bevind dat 1-dimensionele simulasie 'n nuttige hulpmiddel is in die implementering van turbo-aanjaers op vonkontstekings enjins.



ACKNOWLEDGEMENTS

I would like to thank the following people for their involvement in the completion of this project:

- Dr Andrew Taylor, my supervisor, for his guidance and motivation throughout my studies;
- All CAE personnel for their help and contributions, and especially Gerhard Lourens for his assistance in the laboratory;
- Anton van den Berg at SMD for his patience and accuracy in manufacturing components needed for this project.



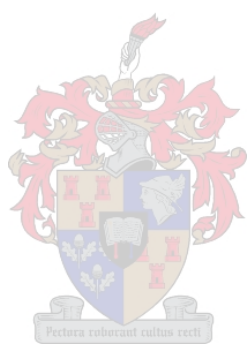


TABLE OF CONTENTS

DECLARATION	i
ABSTRACT	ii
OPSOMMING.....	iii
ACKNOWLEDGEMENTS.....	iv
TABLE OF CONTENTS	v
LIST OF FIGURES.....	vii
LIST OF TABLES	xi
LIST OF SYMBOLS AND ABBREVIATIONS	xii
1. INTRODUCTION.....	1
2. PROJECT OBJECTIVES AND OVERVIEW	3
3. LITERATURE REVIEW	7
3.1. Supercharging.....	7
3.2. Turbocharging	8
3.2.1. Turbocharger Theory	10
3.2.2. Turbocharging CI or SI engines	16
3.2.3. Energy Available in the Exhaust Gas.....	18
3.2.4. Constant Pressure Turbocharging.....	20
3.2.5. Pulse Turbocharging	22
3.2.6. Pulse Converters in Turbocharger Applications.....	26
3.3. Engine Management Systems.....	28
3.3.1. Electronic Throttle Control	29
3.3.2. Torque-Based Engine Management	29
3.3.3. Boost Control	31
3.4. Engine Performance Simulation	33
3.4.1. Flow Modelling	34
3.4.2. Combustion Modelling	35
3.4.3. Modelling of Compressors and Turbines.....	37
4. ENGINE SIMULATION.....	40
4.1. Engine Simulation Model – 1.6 litre Ford Rocam.....	40
4.2. Engine Optimisation	41
4.2.1. Modelling Strategy for Wastegate Control	43
4.2.2. Exhaust Manifold Simulation.....	45
4.2.3. Valve Timing Optimisation	46
4.3. Exhaust Manifold Concept Evaluation.....	53

5. EXPERIMENTAL APPARATUS.....	58
5.1. Exhaust Manifold Design.....	58
5.1.1. Pulse interference.....	60
5.1.2. Exhaust Manifold: Concept 1	61
5.1.3. Exhaust Manifold: Concept 2	64
5.2. Intake Piping Design	64
5.2.1. Pre-Compressor Pipe.....	65
5.2.2. Post-Compressor Pipe	66
5.3. Variable Wastegate Actuator Design	67
5.4. Oil Feed and Return lines	70
5.5. Fuel System Upgrade	72
5.6. Exhaust System Upgrade	73
5.7. Experimental Set-up	73
5.7.1. Combustion Analysis	74
5.7.2. Power Correction	77
5.7.3. Exhaust Gas Measurement	78
5.7.4. Engine Calibration	81
6. RESEARCH RESULTS.....	82
6.1. NA Results: Simulation versus Experiments	82
6.2. Turbocharged Results: Simulation versus Experiments	90
6.3. Comparison of the NA and Turbocharged Results.....	101
6.3.1. Comparison of Turbocharged Boost Settings	101
6.3.2. Force Analysis	105
6.3.3. Energy Balance	111
6.3.4. Performance Comparison	116
6.3.5. Part-load Comparison	129
7. CONCLUSION	137
8. RECOMMENDATIONS	140
9. REFERENCES	142
APPENDIX A OPTIMISATION ALGORITHMS	145
A.1. Nelder-Mead Algorithm	145
A.2. Initial Value Scaling for Optimisation.....	146
APPENDIX B TURBOCHARGER OIL FLOW	147
APPENDIX C POWER CORRECTION FACTORS.....	148
APPENDIX D FORCE ANALYSIS	149

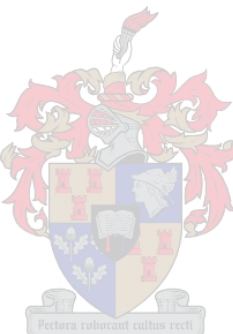
LIST OF FIGURES

Figure 2-1 Engine Output Target.....	4
Figure 3-1 Automotive Turbocharger (Venter, 1999)	8
Figure 3-2 Components of a Radial Compressor (Sayers, 1990)	11
Figure 3-3 h-s Diagram for a Radial Compressor (Watson & Janota, 1984)	13
Figure 3-4 Components of a Radial Turbine (Watson & Janota, 1984)	15
Figure 3-5 h-s diagram for a radial turbine (Watson & Janota, 1984).....	15
Figure 3-6 Naturally Aspirated Ideal Limited Pressure Cycle (Watson & Janota, 1984)	18
Figure 3-7 Turbocharged Ideal Pressure Limited Cycle (Watson & Janota, 1984)	19
Figure 3-8 Schematic of Birmann pulse converter (Watson & Janota, 1984)....	26
Figure 3-9 Exhaust manifold with pulse converter (Watson & Janota, 1984) ..	28
Figure 3-10 Components of ME7 (Gerhardt <i>et al.</i> , 1998).....	30
Figure 3-11 Conventional Boost Control Layout (Audi AG, 1998).....	32
Figure 3-12 Typical Electronic Boost Control Layout (Audi AG, 1998).....	32
Figure 3-13 3-way Solenoid Valve (Normally open)	33
Figure 3-14 Wiebe Combustion Curve Shape.....	36
Figure 3-15 Wiebe Cumulative Combustion Curve Shape.....	37
Figure 4-1 Simulation model: Ford RSI Turbo.....	41
Figure 4-2 Measured Rack Travel and Calculated Wastegate Area versus Boost Pressure	43
Figure 4-3 Wastegate Area Calculation	44
Figure 4-4 Simulation Model of Exhaust Manifold: Concept 1.....	45
Figure 4-5 Simulation Model of Exhaust Manifold: Concept 2.....	46
Figure 4-6 Effect of Optimised Valve and Wastegate Settings on Torque.....	52
Figure 4-7 Exhaust Concept Evaluation: Wastegate Area	54
Figure 4-8 Exhaust Concept Evaluation: Torque.....	54
Figure 4-9 Exhaust Concept Evaluation: Volumetric Efficiency	55
Figure 4-10 Exhaust Concept Evaluation: Airflow.....	55
Figure 4-11 Exhaust Concept Evaluation: Average Residual Mass.....	56
Figure 5-1 Positioning Rig	59
Figure 5-2 Four-cylinder engine's valve timing (firing order 1-3-4-2)	60
Figure 5-3 Exhaust manifold: Concept 1, CAD model	61
Figure 5-4 Exhaust Manifold Force Diagram.....	63
Figure 5-5 Exhaust Manifold: Concept 2, CAD model.....	64
Figure 5-6 Pre-Compressor Pipe	65
Figure 5-7 Guide Vanes in a Sharp Bend	66
Figure 5-8 Post-Compressor Pipe	67

Figure 5-9 Variable Wastegate Actuator.....	68
Figure 5-10 VWA Diaphragm Test.....	69
Figure 5-11 Oil Return Schematic	71
Figure 5-12 LogP-LogV of motored test	75
Figure 5-13 Normalised Cumulative Heat Release (NA engine, WOT at 4000 rev/min)	77
Figure 5-14 Thermocouple Set-up (Ricardo, 2002)	78
Figure 5-15 Exhaust Port versus Downstream Temperatures.....	80
Figure 6-1 NA Simulation vs Experiment: Torque	83
Figure 6-2 NA Simulation vs Experiment: Volumetric Efficiency	84
Figure 6-3 NA Simulation vs Experiment: Airflow	84
Figure 6-4 NA Simulation vs Experiment: Maximum Combustion Pressure..	85
Figure 6-5 NA Simulation vs Experiment: Motored in-cylinder Pressure (1500 rev/min)	86
Figure 6-6 NA Simulation vs Experiment: Exhaust Backpressure	87
Figure 6-7 NA Simulation vs Experiment: Specific Fuel Consumption.....	88
Figure 6-8 NA Simulation vs Experiment: Manifold Absolute Pressure.....	88
Figure 6-9 NA Simulation vs Experiment: Intake Manifold Air Temperature	89
Figure 6-10 Turbocharged Simulation versus Experiment: Torque	91
Figure 6-11 Turbocharged Simulation versus Experiment: Absolute Boost Pressure	91
Figure 6-12 Turbocharged Simulation vs Experiment: Volumetric Efficiency	92
Figure 6-13 Turbocharged Simulation versus Experiment: Airflow	93
Figure 6-14 Turbocharged Simulation versus Experiment: Max. Combustion Pressure	94
Figure 6-15 Turbocharged Simulation versus Experiment: SFC.....	95
Figure 6-16 Turbocharged Simulation versus Experiment: MAP	95
Figure 6-17 Turbocharged Simulation versus Experiment: Intake Manifold Air Temperature	96
Figure 6-18 Turbocharged Simulation versus Experiment: Compressor Outlet Temperature	97
Figure 6-19 Turbocharged Simulation versus Experiment: Wastegate Area ...	98
Figure 6-20 Turbocharged Simulation versus Experiment: Wastegate Area as function of mass flow	99
Figure 6-21 Turbocharged Simulation versus Experiment: Turbine Pressure Ratio	99
Figure 6-22 Turbocharged Simulation versus Experiment: Turbine Inlet Temperature	100
Figure 6-23 Turbocharged Boost Settings: Boost Pressure.....	102
Figure 6-24 Turbocharged Boost Settings: Lambda	103
Figure 6-25 Turbocharged Boost Settings: Ignition Timing.....	103

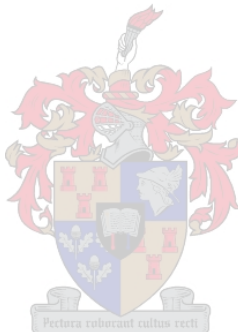
Figure 6-26 Turbocharged Boost Settings: Compressor Operating Points	104
Figure 6-27 Turbocharged Boost Settings: Torque	105
Figure 6-28 Piston Velocity and Acceleration Correlation.....	106
Figure 6-29 Small-End Bearing Force Comparison: Analytical versus Simulation	107
Figure 6-30 Big-End Bearing Force Comparison: Analytical versus Simulation	107
Figure 6-31 Analytically Determined Bearing Forces.....	108
Figure 6-32 NA versus Turbocharged Results: Gas Force on Piston.....	109
Figure 6-33 NA versus Turbocharged Results: Small-end Bearing Forces....	110
Figure 6-34 NA versus Turbocharged Results: Big-end Bearing Forces.....	110
Figure 6-35 Extrapolation of Specific Heat.....	112
Figure 6-36 NA versus Turbocharged Results: Heat Rejection.....	113
Figure 6-37 NA versus Turbocharged Results: Oil Temperature	114
Figure 6-38 NA engine: Energy Balance at WOT	115
Figure 6-39 Turbocharged Engine: Energy Balance at WOT	115
Figure 6-40 NA Engine Torque	116
Figure 6-41 NA versus Turbocharged Results: Torque and Power.....	117
Figure 6-42 NA versus Turbocharged Results: Ignition Timing.....	118
Figure 6-43 NA versus Turbocharged Results: Lambda	118
Figure 6-44 NA versus Turbocharged Results: SFC.....	119
Figure 6-45 NA versus Turbocharged Results: MAP and TMAP	120
Figure 6-46 NA versus Turbocharged Results: Wastegate Area.....	120
Figure 6-47 NA versus Turbocharged Results: Intake Manifold Air Density	121
Figure 6-48 NA versus Turbocharged Results: Ambient and Intake Manifold Air Temperature.....	122
Figure 6-49 NA versus Turbocharged Results: Airflow	122
Figure 6-50 NA versus Turbocharged Results: Volumetric Efficiency	123
Figure 6-51 NA versus Turbocharged Results: Exhaust Manifold Pressure..	123
Figure 6-52 NA versus Turbocharged Results: Pressure Difference (Intake Manifold - Exhaust Manifold).....	124
Figure 6-53 NA versus Turbocharged Results: Exhaust Backpressure.....	125
Figure 6-54 NA versus Turbocharged Results: Exhaust Manifold Temperature	126
Figure 6-55 NA versus Turbocharged Results: Fuel consumption vs Power Output.....	127
Figure 6-56 NA versus Turbocharged Results: Spark Advance and Lambda	127
Figure 6-57 NA versus Turbocharged Results: Burn Duration.....	128
Figure 6-58 NA versus Turbocharged Results: 50% Burn Point	128
Figure 6-59 NA versus Turbocharged Results: Maximum Combustion Pressure	129

Figure 6-60 NA versus Turbocharged Results: Part load SFC	130
Figure 6-61 NA versus Turbocharged Results: Part load Spark Advance	131
Figure 6-62 NA versus Turbocharged Results: Part load Lambda	131
Figure 6-63 NA versus Turbocharged Results: Part load Energy Balance at 2500 rev/min	133
Figure 6-64 NA versus Turbocharged Results: Part load Fuel Flow	133
Figure 6-65 Required Engine Power	134
Figure 6-66 2.0L NA versus Turbocharged SFC at 4000 rev/min.....	135
Figure 6-67 2.0L NA versus Turbocharged SFC at 2500 rev/min.....	136
Figure B-1 K03 Oil Flow Specification (Kühnle, Kopp, Kausch, 1994).....	147
Figure D-1 Piston-Crank: Free Body Diagram.....	149



LIST OF TABLES

Table 2-1 Test Engine Specifications	3
Table 4-1 Initial Values for Full Factorial Valve Optimisation.....	49
Table 4-2 Full Factorial Results	49
Table 4-3 Simplex Optimisation Results (30 iterations).....	52
Table 5-1 Material Properties of Mild Steel at High Temperatures (British Iron and Steel Research Association Metallurgy, 1953).....	62
Table 6-1 Estimated Fuel Saving.....	136
Table C-1 ECE-Standard Reference Conditions	148



LIST OF SYMBOLS AND ABBREVIATIONS

AFR	Air Fuel Ratio
ATDC	After Top Dead Centre
BDC	Bottom Dead Centre
BMEP	Brake Mean Effective Pressure
CA	Crank Angle
CAD	Computer-aided Design
CFD	Computational Fluid Dynamics
CI	Compression Ignition
CR	Compression Ratio
ECU	Electronic Control Unit
EGR	Exhaust Gas Recirculation
EMS	Engine Management System
ETA	Engine Test Automation
ETC	Electronic Throttle Control
EVC	Exhaust Valve Closure
EVO	Exhaust Valve Opening
ID	Inside Diameter
IVC	Intake Valve Closure
IVO	Intake Valve Opening
KLSA	Knock Limited Spark Advance
MAP	Manifold Absolute Pressure
MBT	Most Beneficial Timing
NA	Naturally Aspirated
OD	Outside Diameter
OEM	Original Equipment Manufacturer
PLC	Programmable Logic Controller
SFC	Specific Fuel Consumption
SI	Spark Ignition
TDC	Top Dead Centre
VWA	Variable Wastegate Actuator
WOT	Wide-Open Throttle

1. INTRODUCTION

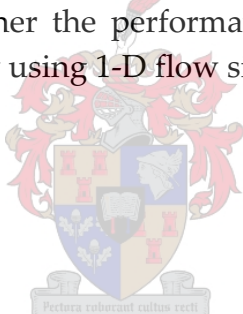
Turbocharged spark ignition (SI) engines have been around since the 1970s, but their popularity outside the motorsport sector has been small until the recent advances in engine control. The lack of popularity could partly be due to the drivability issues associated with early turbocharged engines. The engine's response to a sudden increase in driver's demand was delayed due to turbocharger lag. The lag was then usually followed by a rapid increase of power which resulted in loss of traction and possible loss of control over the car. The advances and developments made in the electronic control and management of internal combustion engines made it possible to overcome most of these drivability limitations. Passenger vehicles with turbocharged SI engines are now becoming more common. Audi, Volvo and VW all offer different passenger vehicle models with turbocharged SI engines. In the performance sector Mitsubishi, Porsche, and Subaru offer turbocharged engines whereas Mercedes offers supercharged and turbocharged engines. In the quest for more efficient engines, turbocharged engines will most probably increase in popularity.

The operating principle of a turbocharger is to use energy recovered from the exhaust gases to force more air into the combustion chamber. This increases the amount of oxygen in the combustion chamber and hence more fuel can be burned. If more fuel can be burned, more power can be produced. Therefore a turbocharged engine can produce more power than a similar-size NA engine. It is claimed that the displacement of a turbocharged engine can be reduced by up to 40% relative to a NA engine, without compromising power output. Thus the turbocharged engine could be smaller, lighter and more fuel-efficient as well as produce less emissions. Therefore this is an attractive option for manufacturers who need to lower their fleet average fuel consumption, but also for those who must meet emission standards without compromising performance.

Engine simulation and performance prediction are playing an increasingly important role in engine development. With engine simulation and performance prediction much iteration in the development phase can now be done in simulation, which not only costs less than actual testing but also leads to faster development times. There are a number of engine simulation packages available on the market today ranging from packages to simulate combustion, engine and driveline dynamics, control systems, cooling system and the valve train, to packages which combine some or all the above into one.

If a one-dimensional (1-D) flow simulation could be used to replicate and predict the complicated three-dimensional (3-D) flow found in reality, it would significantly reduce the computation time. The simpler a simulation package, the faster it would yield results. Shortening simulation time would enable more iteration in a specific time frame, enabling a higher level of optimisation and in the end, a better product. Simplifying the simulation, certain assumptions must be made, causing inaccuracies. Certain processes in the internal combustion engine such as flow through a compressor or turbine are difficult to predict with 1-D simulation only. Thus complex 3-D computational fluid dynamics (CFD) may be necessary to accurately simulate the reality. By using 3-D CFD only for certain complex processes rather than for the whole engine model, it would be possible to retain a high degree of accuracy while not compromising excessively on computation time.

The research questions that are addressed in this project are firstly to ascertain what the implications would be of adding a turbocharger to a NA engine and, secondly, to determine whether the performance of a turbocharged engine can be predicted accurately by using 1-D flow simulation.



2. PROJECT OBJECTIVES AND OVERVIEW

The objective of the project is to address the following two research questions:

- What is the implication of adding a turbocharger to a NA engine;
- Can 1-D simulation predict the performance of a turbocharged engine accurately?

In order to address the above questions, a standard NA engine was converted to a turbocharged engine and a simulation model of each engine was used for comparative purposes. A 1.6 litre Ford Rocam engine was chosen for the project. The maximum power output target was set as 100 kW and a torque curve as flat as possible for a wide as possible engine speed range. The target speed range was set as 2000 rev/min up to 5000 rev/min. The engine specifications and output targets are represented in Table 2-1 and Figure 2-1.

Table 2-1 Test Engine Specifications

Specification:	Standard	Target
Engine Size [cc]	1594	
No. of Cylinders	4	
Valves Per Cylinder	2	
Compression Ratio	9.48	
Bore x Stroke [mm]	82 x 75.48	
Max Power [kW]		100
Engine Speed @ Max Power [rev/min]	5500	
Max. Torque [N·m]	137	174
Engine Speed @ Max Torque [rev/min]	2500	2000-5000
Fuel Injection		Yes
Fuel Injectors	BOSCH 110 g/min	BOSCH 160 g/min
Fuel Pressure Regulator	BOSCH 2.7 bar	BOSCH 3.0 bar
Turbocharger	No	Yes
Intercooler		No
Fuel Octane	95	102.6
Exhaust Manifold	STD Cast iron	Custom
Exhaust System	STD (35 mm ID)	Custom (51 mm ID)

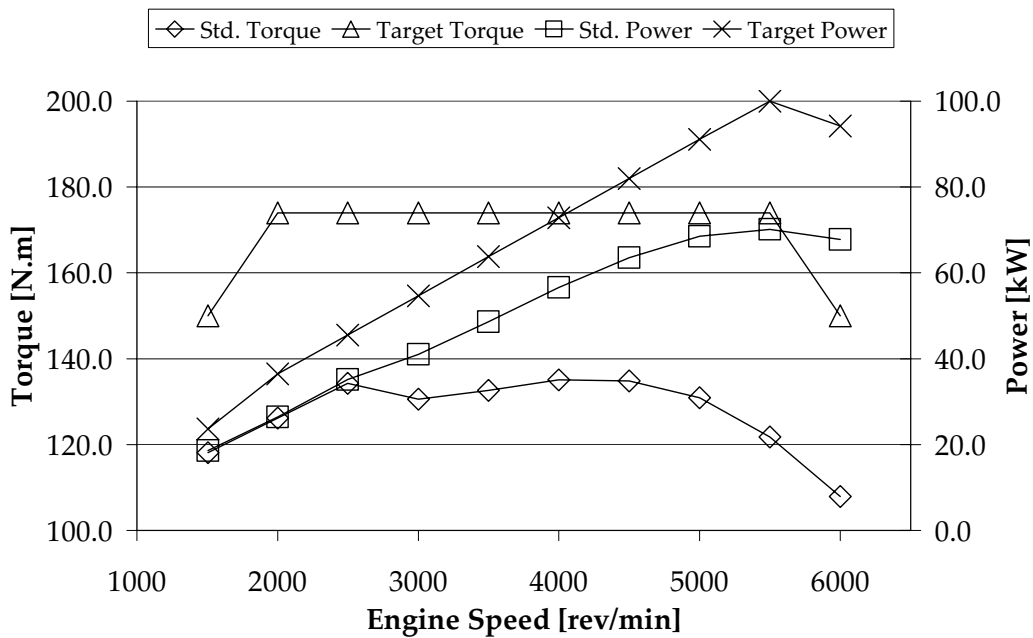


Figure 2-1 Engine Output Target

In order to minimise cost and time, the modifications to the engine were limited. The complete package was also required to fit in the original car's engine bay without any modifications to it. This posed a very challenging packaging exercise since the transversely mounted engine is of the cross flow type with the exhaust-side of the engine close to the firewall.

The modifications included the design and manufacture of an exhaust manifold to accommodate the turbocharger. Oil and water were supplied to the turbocharger and pipes were made to connect the air filter to the compressor and the compressor to the intake manifold. Due to the increased airflow, the exhaust had to be replaced by a larger diameter free-flow exhaust to keep the exhaust backpressure within reasonable limits. The standard fuel injectors were replaced with injectors that would be capable to supply the increased amount of fuel. The fuel pressure regulator was also changed since the higher flow injectors required a higher fuel pressure.

The intake manifold pressure sensor had to be replaced with a sensor that would be able to measure pressures above atmospheric pressure. A knock sensor was added to the engine control unit (ECU) to enable it to retard the ignition timing in the event of knock. High octane fuel would be used during testing to reduce the likelihood that knock would occur. The time frame and budget of the project did not allow for engine failure, thus the use of high octane fuel was a precautionary measure and not a technical requirement. The fuelling and timing maps of the ECU were adjusted for maximum performance at full load. At part load the air fuel ratio was kept the same for both engines as far as possible (limited by exhaust port temperature), but the ignition timing was optimised for maximum power output.

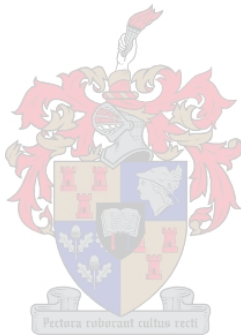
The first limitation on engine change was that the compression ratio (CR) of the engine would not be reduced. It was not envisaged that high boost pressures would be needed to develop the target output, thus reducing the CR was not a requirement. Knock would have been a limitation, but by using the high octane fuel this should be overcome. Reducing CR severely impairs the efficiency of the engine. Since the aim is to improve engine efficiency, reducing the CR would contradict the initial intention.

The second limitation was that the valve timing would not be altered. The result would be non-optimal valve timing for the turbocharged engine. The valve timing is a critical part of the gas exchange mechanism and directly influences the breathing characteristics of an engine. Optimising the valve timing could benefit low-end torque or high-end power, or a compromise between these two extremes. Developing camshafts and cam profiles is a science outside the scope of this project. Valve timing optimisation was done with the simulation in order to demonstrate its advantage.

Thirdly an intercooler would not be used. An intercooler would have a two-fold benefit. It would reduce the intake charge temperature, reducing the chances of knock and by lowering the temperature it would effectively increase the density of the air, while using the same boost pressure. Since high boost pressure would not be required, an intercooler would add unnecessary cost and complexity to the system. Due to the space limitations on passenger vehicles, packaging of the intercooler would also pose a very challenging exercise.

The fourth limitation was that only mechanical boost control would be utilised. This is a major simplification since the mechanical wastegate responds directly to the boost pressure. Using electronic boost control would further aid the ability to develop a flat torque curve but the complexity and time needed to implement such a system would be beyond the scope of this project. However a mechanical wastegate actuator was developed which would facilitate independent adjustment of the spring stiffness and the preset compression of the spring.

This concludes the objectives and overview and defines the framework in which this project was executed.



3. LITERATURE REVIEW

This project was concerned with the turbocharging of a four-stroke petrol engine. Turbocharged four-stroke diesel engines will also be discussed briefly and differences will be highlighted. The discussion, however, omits two-stroke engines due to their different gas exchange processes.

3.1. Supercharging

Supercharging can be defined as the introduction of air (or air/fuel mixture) into an engine cylinder at a density greater than ambient density. This allows a proportional increase in the fuel that can be burned and hence raises the potential power output. The principal objective of supercharging is to increase power output, not to improve efficiency, although efficiency may benefit.

Various methods of supercharging are available. These methods can be classified into two categories. The first category uses a compressor driven by the engine output shaft to compress the air to a density greater than ambient density. The compressor can be any positive displacement pump such as a Roots-type blower, a centrifugal compressor or a vane-type blower. The speed of the supercharger is proportional to the engine speed, thus at low engine speeds the centrifugal compressor might be ineffective because the output pressure varies approximately as the square of the impeller speed.

The second category, known as turbocharging, uses the energy available in the exhaust gas to compress the charged air (or air/fuel mixture). The energy is recovered by expanding the high-pressure exhaust gas in a turbine. This energy is then used to drive the compressor. In big diesel engines axial turbines and compressors may be used, while radial compressors and turbines are more common in medium-size and small engines. Turbocharging will be discussed in more detail in the next section.

The main advantage of turbocharging as opposed to supercharging is that turbocharging uses the energy in the hot exhaust gas that would have been lost. Supercharging uses power from the engine's crankshaft and thus less power is available for propulsion.

3.2. Turbocharging

The author acknowledges that the basis of the theory represented in this section was extracted from Watson and Janota (1984) and Sayers (1990).

The exhaust-driven turbocharger was invented by a Swiss engineer named Buchi, who fitted his creation to a diesel engine back in 1909. However, he only achieved success many years later (around 1925). It took a long time for turbochargers to become established, but it is now recognised that their characteristics are particularly suited to the diesel engine, the reason being that only air is compressed, and no throttling is used. As a result, turbocharged diesel engines are becoming recognised as suitable, even desirable, for private cars as well as for commercial vehicles.

A typical turbocharger consists of a radial turbine, which recovers the energy from the hot exhaust gases. The turbine is coupled to a radial compressor, which increases the pressure in the intake manifold. Between the two is a wide supporting bearing, usually in the form of a free-floating journal bearing, because an ordinary roller bearing would not survive the high rotational speed (up to 250 000 rev/min) of which a small turbine is capable. Figure 3-1 shows a typical turbocharger used in automotive applications.

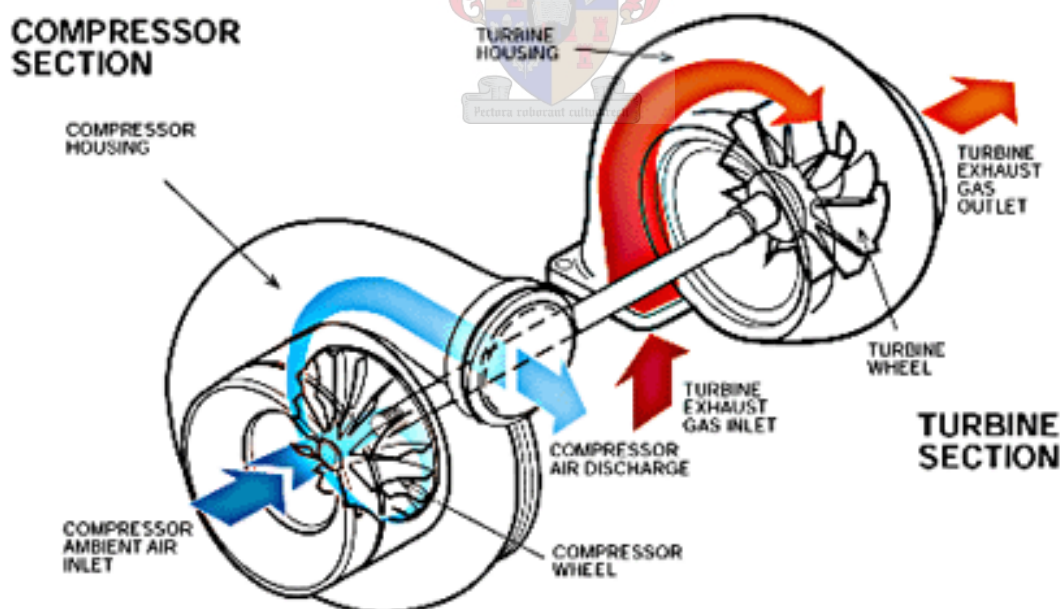


Figure 3-1 Automotive Turbocharger (Venter, 1999)

There have been concerns that the increased exhaust backpressure caused by the turbine is a disadvantage, but analysis refutes this statement. When the exhaust valve first opens, the pressure inside the cylinder is very much higher than the pressure in the exhaust manifold. As the cylinder pressure drops, a stage is reached where the ascending piston has to drive out the gases, because the pressure in the exhaust system is higher due to the turbine. This higher backpressure could also increase the amount of residual exhaust gas inside the combustion chamber.

This represents a loss of energy. However, when the inlet valve opens, the extra pressure created by the compressor supplies extra energy to force the piston down on the intake stroke, which represents a net gain in energy. During the period of valve overlap, the extra pressure in the intake manifold may even help scavenge the residual exhaust gases out of the clearance volume, representing a further gain in energy. All this presupposes a well-designed system, with the turbocharger being efficient enough to raise the boost pressure above the exhaust pressure of the engine. Actual temperature measurements at full power have shown a significant drop in exhaust gas temperature across the turbine, which is a measure of the energy removed. This energy would have gone to waste if the turbocharger were not there. There are currently two ways of utilising the high pressure of the gas inside the combustion chamber at the moment of valve opening, namely: constant pressure turbocharging and pulse turbocharging, each of which has its own merits and will be discussed in later sections (3.2.4 and 3.2.5).

Maximum allowable boost on Compression Ignition (CI) engines depends only on the mechanical strength of the engine, because they have no knock limitations. On SI engines the boost pressure is limited by knock (self-ignition of the end-gas under high temperature and pressure). Thus, if the boost pressure is high on SI engines, the CR must be sufficiently low, high-octane fuel must be used or the ignition timing must be retarded. The difference between CI and SI combustion are discussed in more detail in section 3.2.2.

3.2.1. Turbocharger Theory

The operating characteristics of turbomachines such as compressors and turbines are completely different from those of the reciprocating internal combustion engine. Thus matching these two completely different machines to operate together is an optimisation problem with many parameters. The basic theory of turbomachines will be briefly reviewed to highlight certain key aspects that must be borne in mind when combining turbomachines with reciprocating internal combustion engines.

The most common turbocharger assembly used in the automotive industry consists of a radial compressor coupled to a radial turbine. The bearings are generally of the plain journal bearing type; however, for racing applications ceramic ball bearings are being used more frequently. On big engines such as those used for rail and marine applications, where the operating range is very narrow and operation is mostly steady state, an axial turbine coupled to a radial compressor is the most common configuration. Axial turbines are preferred for their superior efficiency to those of a radial turbine, but a radial turbine's operating range is much wider. This makes radial turbines more suitable for automotive applications, where the operating range is very wide. Radial compressors also have a much wider operating range and are thus more widely used than axial compressors in turbocharger applications. Radial compressors are limited to a pressure ratio of about 3.5, because higher pressure ratios will cause supersonic flow and cause shockwaves to form at the compressor inlet. This will cause a rapid deterioration in the compressor efficiency.

Before discussing the working and characteristics of turbomachines, pressure and temperature measurements will be revisited and their significance discussed.

3.2.1.1. Total and Static Pressure and Temperature

The static pressure (P_1) of a fluid flowing in a duct is that measured at the surface of the wall. The total or stagnation pressure (P_{01}) is the pressure that will be measured in the stream if the fluid were brought to rest isentropically. Thus P_{01} can be related to P_1 as in Eq 3-1.

$$P_{01} = P_1 \left(\frac{T_{01}}{T_1} \right)^{\gamma/(\gamma-1)} \quad \text{Eq 3-1}$$

Where gamma (γ) represents the polytropic coefficient (ratio of specific heats). Similarly the static temperature (T_1) is the free stream temperature and the total (or stagnation) temperature (T_{01}) is the temperature that will be measured if the gas were brought to rest. For a perfect gas it can be shown that Eq 3-2 holds.

$$T_{01} = T_1 + \frac{1}{2} \frac{C_1^2}{c_p} \quad \text{Eq 3-2}$$

Where C_1 is the velocity of the gas and c_p the specific heat at constant pressure.

3.2.1.2. The Radial Compressor

Figure 3-2 shows the three important parts of a radial compressor: impeller, diffuser ring and volute casing. In some applications there might be a diffuser ring included. The diffuser ring is optional and may or may not be present depending on size, use and cost of the compressor.

The impeller is a solid rotating disc with curved blades standing out axially from the face of the disc. In most turbocharger applications the blade tips are left open and the casing of the compressor itself forms the solid outer wall of the blade passages. In some cases the blade tips may be covered with another flat disc to give shrouded blades. The advantage of the shrouded blade is that no leakage can take place from one passage to the next. The disadvantage of having shrouded blades is extra weight and a more complicated manufacturing process. In turbocharger applications where very high rotational speeds are required, the disadvantage of leakage is more than offset by the reduced weight of the impeller.

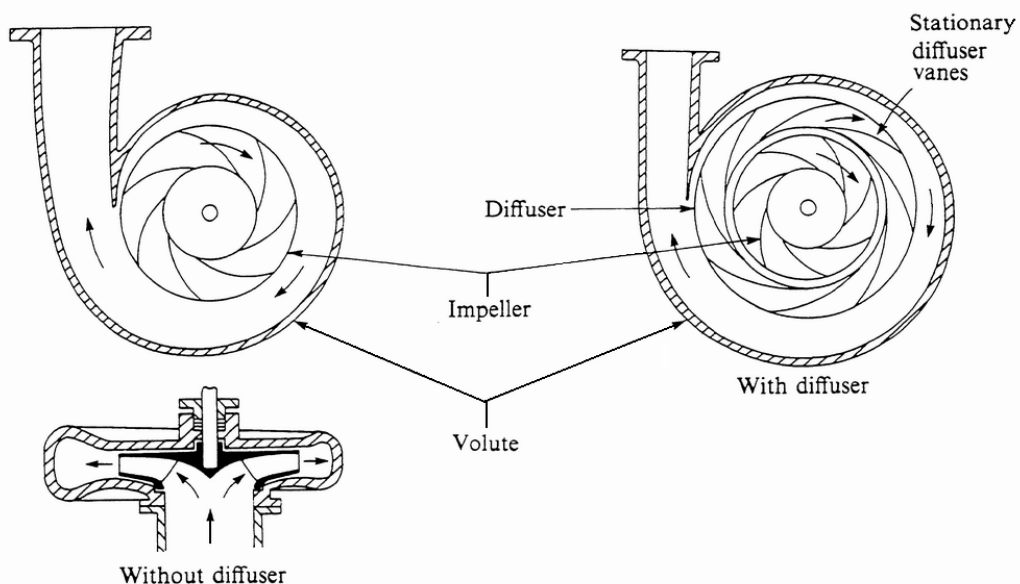


Figure 3-2 Components of a Radial Compressor (Sayers, 1990)

As the impeller rotates, the fluid (air) that is drawn into the blade passages at the impeller inlet is accelerated as it is forced radially outwards. In this way, the static pressure at the outlet radius is much higher than at the inlet radius. The fluid has a very high velocity at the outer radius of the impeller and, to recover this kinetic energy by changing it to pressure energy, diffuser blades mounted on the diffuser ring may be used. The stationary blade passages so formed have an increasing cross-sectional area as the fluid moves through them, the kinetic energy of the fluid being reduced, while the pressure energy is further increased. Vaneless diffuser passages may also be utilised.

Finally, the fluid moves from the diffuser blades into the volute casing, which collects it and conveys it to the compressor outlet. As the fluid moves along the volute casing, further pressure recovery occurs. Sometimes only the volute casing exists without the diffuser.

This process can be plotted on an enthalpy versus entropy diagram as shown in Figure 3-3, so that any departures from isentropic compression can be shown. Station 01 represents ambient pressure of the air. Acceleration of the fluid in the inlet causes a pressure drop from P_{01} to P_1 (or P_{00} to P_1 when considering losses in the inlet), the change in enthalpy being equivalent to the increase in kinetic energy ($C_1^2/2$). Isentropic compression to the delivery stagnation pressure P_{05s} is shown by the vertical line 01-05s. Energy transfer to the fluid takes place in the impeller and the line 1-2 indicates this process. The corresponding isentropic process is shown by 1-2_s. If the total kinetic energy of the fluid leaving the impeller ($C_2^2/2$) were converted to pressure, isentropically, the delivery pressure would be P_{02} (point 02). Since the diffusion process is not accomplished isentropically (2-5), and some kinetic energy remains at the diffuser exit (velocity C_5), the static delivery pressure at point 5 is P_5 .

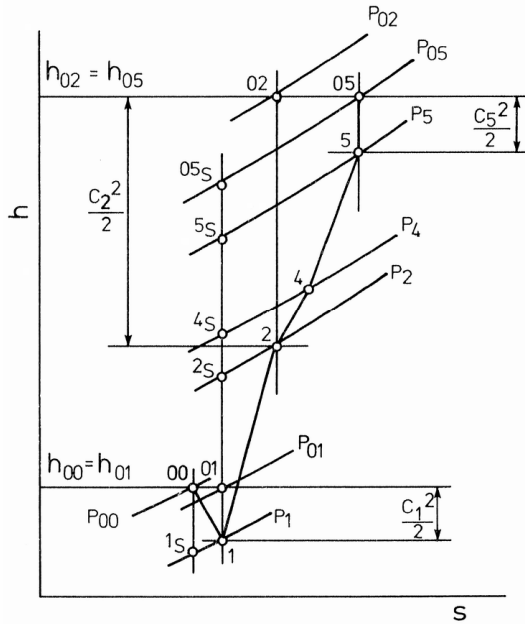


Figure 3-3 h-s Diagram for a Radial Compressor (Watson & Janota, 1984)

This describes the basic working of a radial compressor. For more detailed analyses and literature on compressor design the reader is referred to Sayers (1990) or Watson and Janota (1984).

3.2.1.3. Compressor Efficiency

The efficiency of the radial compressor can be defined as the work required for ideal adiabatic compression divided by the actual work required to achieve the same pressure ratio. From the second law of thermodynamics it is clear that this definition is equivalent to Eq 3-3.

$$\eta_c = \frac{\text{isentropic work}}{\text{actual work}} \quad \text{Eq 3-3}$$

From the first law of thermodynamics, assuming that the heat transfer rate to and from the compressor can be neglected as well as the change in potential energy, Eq 3-3 can be rewritten in the following form:

$$\eta_{cTT} = \frac{h_{02s} - h_{01}}{h_{02} - h_{01}} \quad \text{Eq 3-4}$$

Assuming that air is a perfect gas, thus c_p is constant.

$$\eta_{cTT} = \frac{T_{02s} - T_{01}}{T_{02} - T_{01}} \quad \text{Eq 3-5}$$

The expressions are for total-to-total isentropic efficiency.

An evaluation based on Eq 3-5 assumes that all the kinetic energy at the compressor outlet can be used. This is true in the case of a gas turbine, since the velocity at the compressor delivery is maintained at the combustion chamber. However, the compressor of a turbocharger must supply air via a relatively large inlet manifold to the cylinders. Hence the engine will only ‘feel’ the static pressure at the compressor delivery and is unlikely to benefit from the kinetic energy at the compressor outlet. Thus a turbocharger compressor should be designed for high kinetic to potential energy conversion before the outlet duct.

Since the engine benefits little from the kinetic energy of the air leaving the compressor, a more realistic definition of the compressor efficiency is based on static delivery temperature as in Eq 3-6, where TS denotes total-to-static.

$$\eta_{cTS} = \frac{T_{2s} - T_{01}}{T_{02} - T_{01}} \quad \text{Eq 3-6}$$

It is common practice for manufacturers to quote total-to-total efficiencies for turbocharger compressors, and quite often those are quoted without declaring the basis on which the efficiency values are calculated.

3.2.1.4. The Radial Turbine

The radial flow turbine consists of a scroll or inlet casing, a set of inlet nozzles (sometimes omitted) followed by a short vaneless gap and the turbine wheel itself (Figure 3-4). Most small turbochargers’ turbines use a vaneless casing; the nozzle is then in the form of a slot running all the way between the scroll and turbine wheel. A vaneless casing can be used to improve flow range at some penalty in peak performance, while also reducing cost. However, considering the more conventional type with nozzles, the function of the inlet casing is purely to deliver a uniform flow of inlet gas to the nozzle entries. The nozzles accelerate the flow, reducing pressure and increasing the kinetic energy. A short vaneless space prevents the rotor and nozzle blades from touching and allows wakes coming off the trailing edge of the nozzle blades to mix out. Energy transfer occurs solely in the impeller, which should be designed for minimum kinetic energy at the exit.

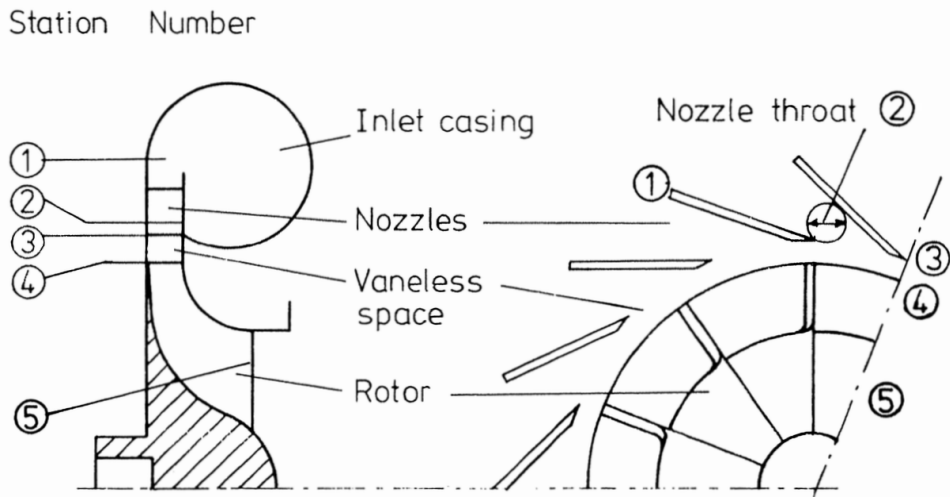


Figure 3-4 Components of a Radial Turbine (Watson & Janota, 1984)

The flow process through the turbine may be plotted on an enthalpy versus entropy diagram as shown in Figure 3-5. Station 01 refers to stagnation conditions at the entry to the casing. The gas will already have a significant velocity (C_1), hence the stagnation pressure is P_{01} . The inlet nozzles accelerate the flow from station 1 to 2. If this process were isentropic, the end point would be 2_s. Energy transfer occurs in the rotor, between station 4 and 5 (4 and 5_s if isentropic) down to the exit pressure P_5 . The stagnation P_{05} will be higher than P_5 since the exit velocity will remain significant. Station 3 is the nozzle exit or the nozzle throat, denoted as station 2.

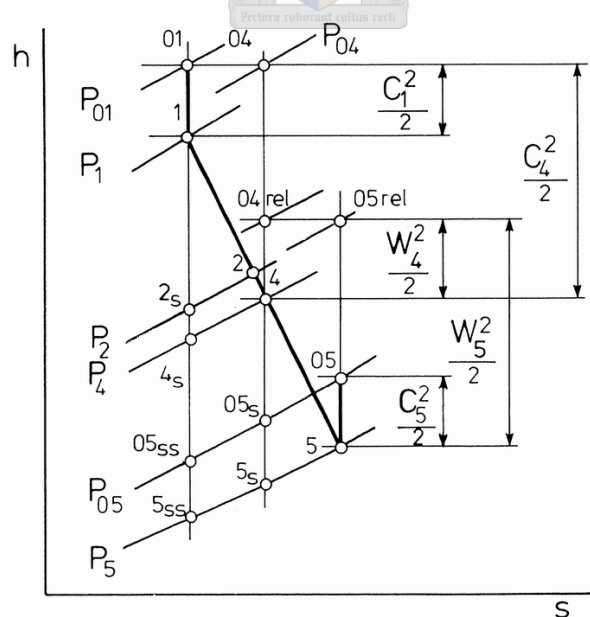


Figure 3-5 h-s diagram for a radial turbine (Watson & Janota, 1984)

3.2.1.5. *Turbine Efficiency*

The isentropic efficiency of a turbine may be defined as the actual work output divided by that obtained from reversible adiabatic (isentropic) expansion between the same two pressures.

$$\eta_t = \frac{\text{actual work}}{\text{isentropic work}} \quad \text{Eq 3-7}$$

Assuming a perfect gas ($cp = \text{constant}$) and following the same reasoning as with compressors, it can be shown that Eq 3-7 can be expressed in terms of temperatures as in Eq 3-8.

$$\eta_{tTT} = \frac{T_{03} - T_{04}}{T_{03} - T_{04s}} \quad \text{Eq 3-8}$$

The total-to-total efficiency given in Eq 3-8 assumes that the kinetic energy leaving the turbine exit can be harnessed. In most applications this is not possible. The energy leaving the turbine exit goes to waste through the exhaust pipe. Thus a more relevant isentropic efficiency could be based on the static exit temperature. The total-to-static isentropic efficiency would be defined as the actual work output divided by isentropic expansion between the stagnation inlet and static outlet pressures.

$$\eta_{tTS} = \frac{T_{03} - T_{04}}{T_{03} - T_{4s}} \quad \text{Eq 3-9}$$

3.2.2. *Turbocharging CI or SI engines*

Today, turbocharged CI engines are more common than turbocharged SI engines. There are sound reasons for this, both economic and technical. The principal reasons stem from the difference between the combustion and control systems of SI and CI engines. The SI engine uses a carburettor or fuel injection system to mix air and fuel in the inlet manifold so that a homogeneous mixture is compressed in the cylinder. A spark is used to control the initiation of combustion, which then spreads throughout the mixture. It follows that the mixture temperature during compression must be kept below the self-ignition temperature of the fuel.

Once combustion has started, it takes time for the flame front to move across the combustion chamber burning the fuel. During this time, the un-burnt end-gas (furthest from the sparkplug) is heated by further compression and radiation from the flame front. If it reaches the self-ignition temperature before the flame front arrives, a large quantity of mixture may burn very rapidly, producing severe pressure waves in the combustion chamber. This situation is commonly referred to as knock and may result in severe cylinder head and piston damage. Lowering the CR, using fuel with a higher octane number or retarding the ignition timing are ways to prevent the occurrence of knock.

In the CI engine cylinder, air alone is compressed. Fuel is injected directly into the combustion chamber from an injector, only when combustion is required. This fuel vaporises and mixes with the air, it self-ignites and, in contrast to SI combustion, it follows that in a CI engine the CR must be high enough for the air temperature during compression to exceed the self-ignition temperature of the fuel. Because injection takes time, only some of the fuel is in the combustion chamber when ignition starts. Since much of the fuel has not fully vaporised and mixed with the air, the initial rate of combustion is not sufficient to initiate destructive pressure waves as in the case of knocking in a SI engine, and thus does not lead to engine damage.

The maximum CR of the SI engine, but not the CI engine, is therefore limited by the ignition properties of the fuel. The minimum CR is limited by the resulting low overall engine efficiency. Turbocharging results in not only a higher compression pressure, but also a higher temperature.

Unless the CR of a SI engine is reduced the temperature at the end of compression stroke may be too high and the engine may knock. The engine may remain knock free under mild boost – but only because there is a sufficiently safe knock-free margin. Thus the potential power output of a turbocharged SI engine is limited. The CI engine has no such limit and can therefore use a much higher boost pressure.

SI engines cost substantially less to produce than CI engines of equivalent power output, primarily as a result of higher operating speeds and cheaper fuel injection system. The cost of the turbocharger on a CI engine is more than offset by the reduced engine size required for a specific power output (with the exception of very small engines). This situation will rarely occur in the case of a SI engine.

3.2.3. Energy Available in the Exhaust Gas

Figure 3-6 shows the ideal limited pressure engine cycle in terms of a pressure/volume diagram for a naturally aspirated engine. Superimposed is a line representing isentropic expansion from point 5, at which the exhaust valve opens, down to the ambient pressure (P_a), which could be obtained by further expansion if the piston were allowed to move to point 6. The shaded area 1-5-6 represents the maximum theoretical energy that could be extracted from the exhaust system; this is called the blow-down energy.

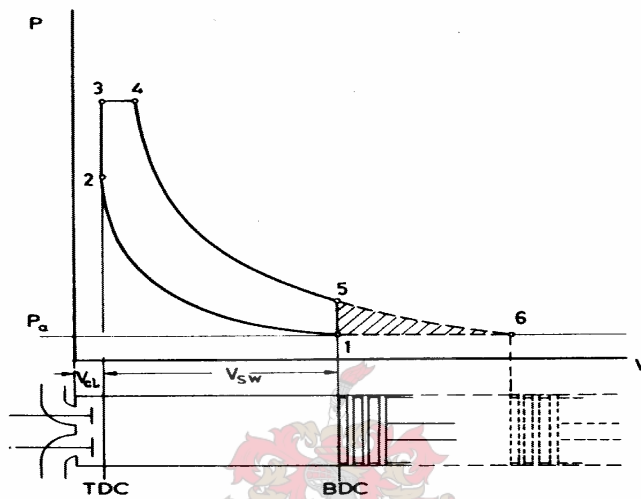


Figure 3-6 Naturally Aspirated Ideal Limited Pressure Cycle (Watson & Janota, 1984)

Consider now the turbocharged engine; the ideal four-stroke pressure/volume diagram would appear as shown in Figure 3-7, where P_1 is the turbocharging or boost pressure and P_7 is the exhaust manifold pressure. Process 12-1 is the induction stroke, during which fresh air at the compressor delivery pressure enters the cylinder. Process 5-1-13-11 represents the exhaust process. When the exhaust valve first opens (point 5) some of the gas in the cylinder escapes to the exhaust manifold expanding along 5-7, if the expansion is isentropic. Thus the remaining gas in the cylinder is at P_7 , when the piston moves toward top dead centre (TDC), displacing the cylinder contents through the exhaust valve against the backpressure P_7 . At the end of the exhaust stroke the cylinder retains a volume (V_{cl} , clearance volume) of residual combustion products, which for simplicity can be assumed to remain there. The area 7-8-10-11 will represent the maximum possible energy that could be extracted during the expulsion stroke, where 7-8 represents isentropic expansion down to the ambient pressure.

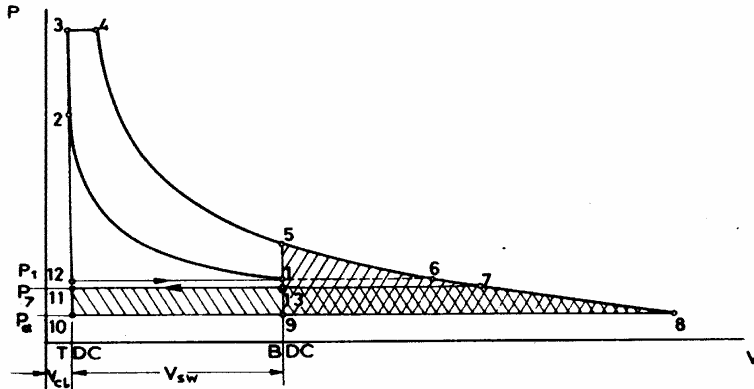


Figure 3-7 Turbocharged Ideal Pressure Limited Cycle (Watson & Janota, 1984)

There are two distinct areas in Figure 3-7 representing energy available from the exhaust gas, the blow-down energy (area 5-8-9) and the work done by the piston (area 13-9-10-11). The maximum possible energy available to drive the turbocharger turbine will clearly be the sum of these two areas. Although the energy associated with one area is easier to harness than the other, it is difficult to devise a system that will harness all the energy. To harness all the energy; the turbine inlet pressure must rise instantaneously to P_5 when the exhaust valve opens, followed by isentropic expansion of the exhaust gas through P_7 to the ambient pressure ($P_8=P_a$). During the displacement part of the exhaust process (expulsion stroke) the turbine inlet pressure must be held at P_7 . Such a series of processes is impractical.

Consider the simpler process in which a large chamber is fitted between the engine and the turbine inlet, in order to damp out the pulsating exhaust gas flow. By forming a restriction to flow, the turbine may maintain its inlet pressure at P_7 for the whole cycle. The available work at the turbine will then be given by area 7-8-10-11. This is the ideal constant pressure turbocharging system. Next consider an alternative system, in which a turbine wheel is placed directly downstream of the engine close to the exhaust valve. If there were no losses in the port, the gas would expand directly out through the turbine alone line 5-6-7-8, assuming isentropic expansion. If the turbine area were sufficiently large, both cylinder and turbine inlet pressures would drop to P_9 before the piston has moved significantly up the bore. Hence the available energy at the turbine would be given by area 5-8-9. This can be considered the ideal pulse turbocharging system. The systems commonly referred to as 'constant pressure turbocharging' and 'pulse turbocharging' are based on the above principles, but in practice they differ from the ideal theoretical cycles.

3.2.4. Constant Pressure Turbocharging

With constant pressure turbocharging, the exhaust ports from all cylinders will be connected to a single exhaust manifold, whose volume will be sufficiently large to damp down the unsteady flow, caused by the blow-down and expulsion, from each cylinder in turn. Only one turbocharger need be used, with a single entry. When the exhaust valve of a cylinder opens, the gas expands down to the (constant) pressure in the exhaust manifold without doing any useful work. However, not all of the blow-down energy is lost. From the law of conservation of energy, the only energy actually lost between cylinder and turbine will be due to heat transfer. With a well-insulated manifold, this loss will be very small and can be neglected.

Consider what happens to the exhaust gas leaving the cylinder, expanding down into the exhaust manifold and then flowing through the turbine. At the moment of exhaust valve opening, the cylinder pressure will be much higher than the exhaust manifold pressure. During early stages of valve opening (when the throat area of the valve is very small) the pressure ratio across the valve or port will be above the choked value. Hence the gas flow will accelerate to sonic velocity in the throat followed by a shock wave at the valve throat and sudden expansion to the exhaust manifold pressure. Due to turbulent mixing and throttling, no pressure recovery occurs. The stagnation enthalpy remains unchanged and hence the flow from valve to turbine is accompanied by an increase in entropy.

As the valve continues to open, the cylinder pressure will fall and flow through the valve becomes subsonic. The flow will continue to accelerate through the valve throat and expand to the pressure in the exhaust manifold. The energy available to do useful work in the turbine is given by the isentropic enthalpy change across the turbine, whereas the actual energy recovered is given by the enthalpy change across the turbine. Clearly it is the lack of recovery of the kinetic energy leaving the valve throat and the throttling losses that lead to poor exhaust gas energy utilisation with the constant pressure system.

The volume of the exhaust manifold should be sufficient to damp pressure pulsations down to a low level. Thus the volume required will depend on the cylinder release pressure and frequency of the exhaust gas pulsations coming from each cylinder in turn. Pulse amplitude will be a function of engine load, the timing at which the exhaust valve opens, turbine area and exhaust manifold volume. Frequency will be dependent on the number of cylinders and engine speed. The effect of engine speed will be less significant, since the duration of the exhaust process from each cylinder will be relatively constant in terms of crank angle, rather than time, and a suitable turbine area will be chosen at the operating speed and load.

If the exhaust manifold is not sufficiently large, the blow-down or first part of the exhaust pulse from the cylinder will raise the general pressure in the manifold. If the engine has more than three cylinders, it is inevitable that at the moment when the blow-down pulse from one cylinder arrives in the manifold, another cylinder is nearing the end of its exhaust process. The pressure in the latter cylinder will be low, hence any increase in exhaust manifold pressure will impede or even reverse its exhaust processes. This will be particularly important where the cylinder has both intake and exhaust valves partially open (valve overlap) and is relying on a through-flow of air for scavenging of the burnt combustion products.

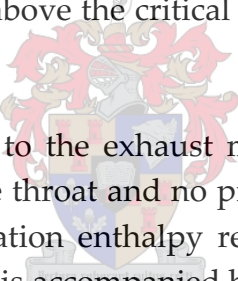
The constant pressure system has some advantages and disadvantages:

- Conditions at turbine entry are steady, thus losses in the turbine that result from unsteady flow are absent;
- A single-entry turbine may be used, eliminating 'end-of-sector' losses (losses associated with flow from one turbine nozzle to another);
- Use of a single turbocharger implies a larger turbocharger and larger machines have higher efficiencies than smaller ones;
- A turbine designed for constant pressure operation may have high degree of reaction, coupled with an exhaust diffuser, bringing additional gains in efficiency;
- From a practical point of view, the exhaust manifold is simple to construct, but is rather bulky, particularly relative to small engines with few cylinders;
- Transient response of a constant pressure system is poor. Due to the large volume of gas in the exhaust manifold, the pressure is slow to rise, resulting in poor engine response and making it unsuitable for applications with frequent load or speed changes.

3.2.5. Pulse Turbocharging

In the practical pulse system an attempt is made to utilise the energy represented by both the pulse and constant pressure areas of Figure 3-7. The objective is to make the maximum use of the high pressure and temperature that exist in the cylinder at the moment of exhaust valve opening, even at the expense of creating highly unsteady flow through the turbine. In most cases the benefit from increasing the available energy will more than offset the loss in turbine efficiency due to unsteady flow.

The constant pressure system was discussed in detail in the previous section. Now consider a much smaller exhaust manifold. Due to the small volume of the exhaust manifold, a pressure build-up will occur during the exhaust blow-down period. This results from a flow rate of gases entering the manifold through the exhaust valves exceeding that of gas escaping through the turbine. At the moment the exhaust valve starts to open, the pressure in the cylinder will be 6 to 10 times atmospheric pressure, whereas the pressure in the exhaust manifold will be close to atmospheric. Thus the initial pressure drop across the valve will be above the critical value at which choking occurs and the flow will be sonic.



Further expansion of the gas to the exhaust manifold pressure occurs by a sudden expansion at the valve throat and no pressure recovery occurs due to turbulent mixing. The stagnation enthalpy remains constant, consequently the flow from the valve throat is accompanied by an entropy increase. Finally the gas expands through the turbine to atmospheric pressure, doing useful work. The out-flowing gas from the cylinder loses a very large part of its available energy in throttling and turbulence after passing the minimum section of the exhaust valve throat. The throttling losses are very high if the ratio of valve throat area to manifold cross-section area is very small and the pressure drop across the valve is large, as during the initial stages of exhaust valve opening.

Following further opening of the exhaust valve, the cylinder pressure falls, but the pressure in the exhaust manifold increases, reducing the throttling losses across the valve. The pressure drop across the turbine is now much larger, transferring the available energy to the turbine, which represents a much larger proportion of the available energy in the cylinder. During the last portion of valve opening the flow is sub-sonic and the throttling loss is reduced and is equivalent to the kinetic energy at entry to the exhaust manifold. During the exhaust stroke, the flow process follows approximately the constant pressure pattern as described in the previous section. At the exhaust valve, the pressure in the exhaust manifold approaches atmospheric value.

With pulse operation, a much larger portion of the exhaust energy can be made available to the turbine by considerably reducing throttling losses across the exhaust valve. The speed at which the exhaust valve opens to its full area and the size of the exhaust manifold become important factors as far as energy utilisation is concerned. If the exhaust valve can be made to open faster, the throttling losses become smaller during the initial exhaust period. Furthermore, the smaller the exhaust manifold, the faster the rise in manifold pressure becomes, contributing to a further reduction in throttling losses in the early stages of the blow-down period. A small exhaust manifold also causes a much more rapid fall of the manifold pressure towards the end of the exhaust process improving scavenging and reducing pumping work. This discussion has thus far focussed on a single-cylinder engine connected to a small exhaust manifold.

The problem becomes more complicated when considering a multi-cylinder engine. Since the turbocharger may be located at one end of the engine, narrow pipes are used to connect the cylinders to the turbine to keep the size of the manifold as small as possible. By using narrow pipes the area increase following the valve throat is greatly reduced, keeping throttling losses to a minimum. But by using narrow pipes the flow resistance and losses due to friction become important factors.

Consider again a single-cylinder engine, connected to a turbine by a long narrow pipe. Since a large quantity of the exhaust energy becomes available in the form of pressure waves, which travel along the pipe to the turbine at sonic velocity, the conditions at the exhaust valve and turbine are not the same at a given time instant. For simplicity, pressure wave reflections in the pipe will be ignored. During the first part of the exhaust process, in the choked region of flow through the valve, the gas is accelerated to sonic velocity at the throat. Since the contents of the pipe are initially at rest at atmospheric pressure, sudden expansion takes place across the valve throat. However, some of the kinetic energy is retained, depending on the ratio of valve throat area to pipe cross-section area.

As the valve opens further the pressure at the exhaust pipe entry rises rapidly. This is, firstly, because a certain time is required for the acceleration of the outgoing gases, and secondly, because the gases enter the exhaust pipe from the cylinder at a higher rate than they are leaving the exhaust pipe at the turbine end. The rapid pressure rise at the pipe entry is transmitted along the pipe in the form of a pressure wave, travelling at sonic velocity, and will arrive at the turbine displaced in time. This phase shift is a function of pipe length and gas properties (composition, temperature and pressure).

The pressure drop across the valve is noticeably reduced due to the rapid drop in cylinder pressure and the rise in pipe pressure, and also because the ratio of valve throat area to pipe area has increased. Both effects considerably reduce throttling losses. The velocity at the turbine end of the pipe is greater than the velocity after the valve, due to the arrival of the high-pressure wave at the turbine end. In the sub-critical flow region of the blow-down period, the pressure in the exhaust falls at the same time as that in the cylinder. The velocity at the valve throat is equal to the velocity in the pipe, assuming the valve throat area is equivalent to the area of the pipe when the valve is fully open. At the turbine the exhaust gas expands to atmospheric pressure, doing useful work in the turbine.

It has been established that the pulse turbocharging system results in greater energy availability at the turbine. As the pressure wave travels through the pipe, it carries a large portion of pressure energy and a small portion of kinetic energy, which is affected by friction. The gain obtained by using a narrow exhaust pipe is achieved partly by reducing the throttling losses at the early stages of the blow-down period and partly by preserving kinetic energy. Thus the small-diameter exhaust pipes are essential and, up to a point, the smaller the better, since this will preserve high gas velocity from the valve to turbine. However, if the pipes are made too narrow the viscous friction at the pipe wall will become excessive. The optimum exhaust manifold pipe diameter will be a compromise, but the cross-sectional area should not be significantly greater than the geometric valve area at full lift.

The actual flow through a pulse exhaust system is highly unsteady and is affected by pulse reflections from the turbine and closed exhaust valves. It will be evident that as engine speed changes, the effective time of arrival of a reflected pulse, in crank-angle terms, will vary. Hence the exhaust pipe length is critical and must be optimised to suit the speed range of the engine. The interference of reflected pressure waves with the scavenging process is the most critical aspect of a pulse turbocharging system, particularly on engines with a very long valve overlap. Due to this phenomenon it is impossible to connect an engine with more than 3 cylinders to the same turbine without using a twin-entry turbine or introducing losses on the intake or exhaust processes.

The ideal pulse turbocharging system must have the following two characteristics. Firstly, the peak of blow-down pulse must occur just before the bottom dead centre (BDC) of that cylinder, followed by a rapid pressure drop to below boost pressure. The boost pressure must be above exhaust manifold pressure to aid the scavenging process during valve overlap. Secondly, the effectiveness of pulse system is governed by the gas exchange process and overall efficiency of the turbocharger under unsteady flow conditions. The principal advantage of the pulse system over the constant pressure system is that the energy available for conversion to useful work in the turbine is greater. However, this benefit is reduced or eliminated if the energy conversion process is inefficient (Watson & Janota, 1984).

3.2.6. Pulse Converters in Turbocharger Applications

The pulse turbocharging system has been found to be superior to the constant pressure system on the majority of today's diesel engines. Generally, it is used on all but highly rated engines designed for constant speed and load or marine applications. In the previous section it was made clear that the pulse turbocharging system is usually most effective when groups of three cylinders are connected to a single turbine or a single-entry turbine. When one or two cylinders are connected to a turbine entry, the average turbine efficiency and expansion ratio tends to fall due to the wide spacing of exhaust pulses. The 'pulse converter' has been developed to overcome some of these disadvantages on certain engines as a compromise between the pulse and constant pressure turbocharging system.

Birmann first used the term 'pulse converter' (Birmann, 1946). His objective was to design a device that preserved the unsteady flow of gases from the cylinder during the exhaust and valve overlap periods, yet maintained steady flow at the turbine. In this way he hoped to achieve good scavenging and high turbine efficiency. Figure 3-8 shows one of the devices proposed. All the cylinders are connected to a single-entry turbine, resulting in a continuous, almost steady flow and high turbine efficiency. To achieve good scavenging, Birmann proposed a 'jet-pump' system, using high velocity jets of gas issuing from a central nozzle to reduce the pressure in short pipes at the exhaust valves. This high jet should create a suction effect in the surrounding area, due to the conservation of momentum. The by-pass tube was used to provide the jet for the first cylinder and to maintain an almost constant pressure at the jet nozzles.

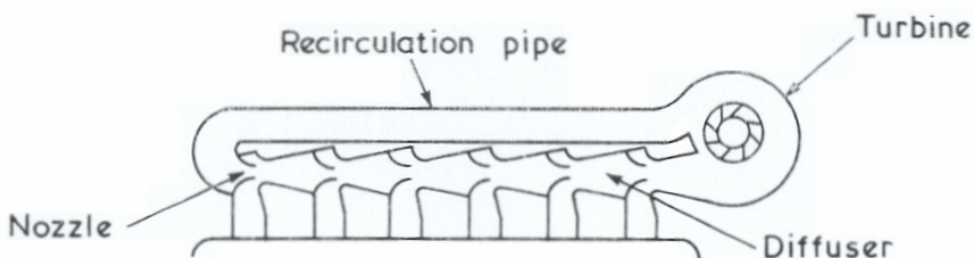


Figure 3-8 Schematic of Birmann pulse converter (Watson & Janota, 1984)

The system proposed in Figure 3-8 has several disadvantages:

- There is insufficient length between exhaust ports to permit efficient recovery in diffusers;
- Each nozzle must be larger than the last, resulting in high manufacturing cost;
- Frictional and diffusion losses will be high, since much of the exhaust gas will pass through several ejectors and diffusers;
- The whole installation is bulky and complex;
- The large total volume of the installation can result in poor performance when starting and accelerating, as in the constant pressure turbocharging system.

Birmann gradually developed refinements, but the converter never achieved wide acceptance, possibly due to the problem of trying to optimise the size of the ejector nozzles and amount of recirculation. Furthermore, the extremely turbulent nature of the gas flow entering the diffusers must have resulted in poor diffusion which, when combined with high jet velocities, would imply high losses. Consequently the energy available during expansion through the turbine is reduced, although the steady flow conditions would aid efficient conversion of the energy into useful work.

The majority of pulse converters in use today are based on the concept of minimum energy loss, even if this means not only a loss of all suction effect, but also some pressure wave interference during scavenging. To avoid high mixing losses at the junction, the area reduction in the inlet nozzles is usually small (junction area $> 50\%$ of pipe area), while the mixing length and plenum and often even the diffuser are omitted completely, as suggested by Petak (as cited in Watson & Janota, 1984). These simple pulse converters have the added advantage of adding little over-all length to the exhaust system. A typical example from a four-stroke engine is shown in Figure 3-9.

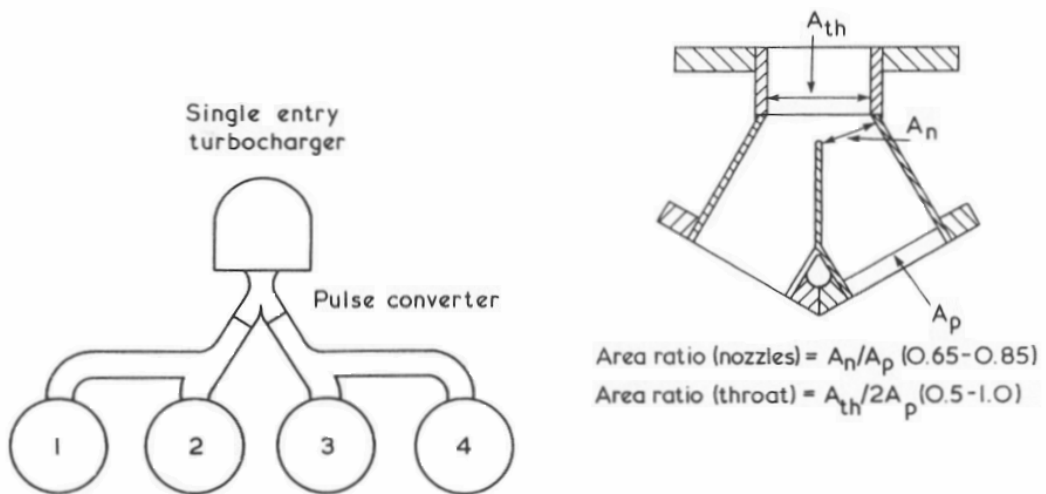


Figure 3-9 Exhaust manifold with pulse converter (Watson & Janota, 1984)

The pulse converter is specified by the nozzle and throat area ratios. Clearly such a pulse converter will generate no suction, but the flow losses through it will be very much less than in more complex designs. Tests on a model pulse converter by Watson & Janota (1971) have shown that the area reduction at the nozzles has to be severe to reduce pulse propagation substantially. The penalty accompanying large area reductions in the inlet nozzles is higher internal losses and hence reduces the amount of energy available for useful expansion through the turbine. In practice this means that the minimum possible area reduction is used, consistent with reasonable scavenging. It follows that the design of the pulse converter is a compromise between minimum losses and reduction of pulse interaction between the inlet branches. The compromise adopted may vary from one engine design to another, depending on the amount of pulse interference, etc.

3.3. Engine Management Systems

The functional structure of the SI engine management systems has evolved over several years. Starting with carburetors and mechanically controlled ignition timing evolving to a simple injection system with a separate ignition unit in the early 1970s. Injection and ignition were integrated into one single electronic control unit during the 1980s. A modern engine management system (EMS) is comprised of a large number of subsystems, and not only controls basic EMS functions such as injection duration and timing, ignition timing, emission control such as closed loop lambda control and catalyst heating, but also manages additional functions such as continuous camshaft control, resonance flap actuation or the engine fan. A modern EMS must also be equipped with a full onboard diagnostic and monitoring system.

3.3.1. Electronic Throttle Control

Electronic throttle control (ETC) systems have been in production since 1986. These were add-on devices to conventional engine management systems, including fuel injection and ignition control. Such an add-on system as proposed by Streib and Bischof (1978), consists of an accelerator pedal sensor, a separate electronic control unit, and a throttle valve with integrated electric drive and position sensors. ETC replaces the mechanical link between accelerator pedal and throttle valve and also eliminates the idle speed actuator, because ETC controls the idle speed via the main throttle valve. The major reasons for introducing ETC at that time were traction control, programmable engine response characteristics, cruise control and emission improvements.

Costs of these add-on systems were relatively high due to the separate ECU and an actuator design which was not optimised for mass production. Therefore application was limited to high-performance vehicles with traction control. In January 1995 Bosch started the production of a new ETC generation. This generation is the first ETC system which has the electronics of ETC and of the conventional engine control functions integrated into the same ECU with one microcontroller. The integrated electronics and a new actuator design were suited for high-volume production and resulted in a sharp decline of system costs.

Within the last few years additional requirements for engine and power train control functions have evolved in order to improve emissions, fuel economy and driveability. These new requirements, combined with the reduction of system costs have expedited the introduction of ETC in a large and steadily growing number of cars.

3.3.2. Torque-Based Engine Management

The introduction of ETC as a drive-by-wire system, with its adjustable relationship between the pedal position and throttle position, enables the EMS to now control all torque-influencing outputs over the entire operating range of the engine. With stand-alone ETC systems, mutual functional impacts have to be considered, such as idle-speed control, which must be divided into the two subsystems (Azzoni *et al.*, 1998). The fully integrated system with control of injection, ignition and cylinder charge can eliminate this drawback, but then a complete redesign of the entire system is required. The BOSCH ME7 is a model-based EMS and the basic components are shown in Figure 3-10.

This discussion is included because the use of the BOSCH ME7 was investigated, but the calibration and application of such a system requires two years and was thus beyond the scope of this project to change the ECU.

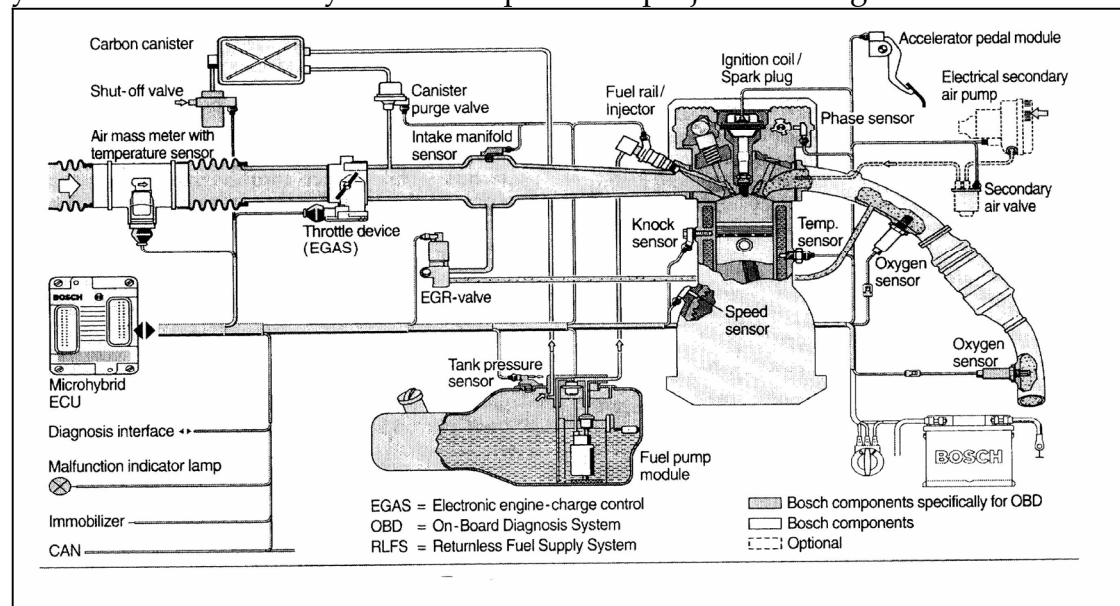


Figure 3-10 Components of ME7 (Gerhardt et al., 1998)

The functional architecture of the BOSCH ME7 system is characterised by the following main features: (Gerhardt et al., 1998):

- Centrally coordinated torque management:
The engine torque represents the central system variable. Thus engine control parameters are adjusted to meet the torque requirements as calculated by the EMS;
- Centrally coordinated AFR management:
Similarly, all mixture demands are coordinated in one central manager. Based on the operating conditions, a set of basic functions control A/F ratio within the physical limits defined by the flammability of the mixture;
- Subsystems based on physical models with physically defined interfaces:
The use of physically based functions improves the transparency of the system's architecture. Computed values can be directly compared with physically measurable values.

Using physically based functions in combination with centrally coordinated torque and AFR management allows for an improved handling of function variants. Due to their relationship to the physical structure, single functions as well as functionally linked groups of functions, subsystems could easily be compared with customer's requests using physically measured values. Therefore a set of basic platform functions was realised and applied over the entire EMS family (Gerhardt *et al.*, 1998).

3.3.3. Boost Control

In a spark ignition engine the primary parameter controlling power output is the amount of air induced into the engine per cycle. By definition conventional spark ignition engines operate at a stoichiometric or near-stoichiometric air-fuel ratio. Thus the amount of fuel injected is directly proportional to the amount of air induced. The amount of air induced is dependent on the density of air in the intake manifold. At wide-open throttle (WOT) for a turbocharged engine the density of air in the intake manifold is proportional to the boost pressure. Thus to control the power output of the engine, the boost pressure must be controlled.

The boost pressure developed by the compressor is proportional to the amount of energy extracted by the turbine from the exhaust gas. By using a by-pass valve to route some of the exhaust gas directly to the exhaust system and not through the turbine, it is possible to control the boost pressure. The traditional way of controlling the by-pass valve (or wastegate) is by actuating it with a pneumatic piston. The piston is spring loaded, with a predetermined preload. The preload on the spring determines the opening boost pressure and the spring stiffness determines the relationship between wastegate opening area and boost pressure. A typical layout is shown below in Figure 3-11.

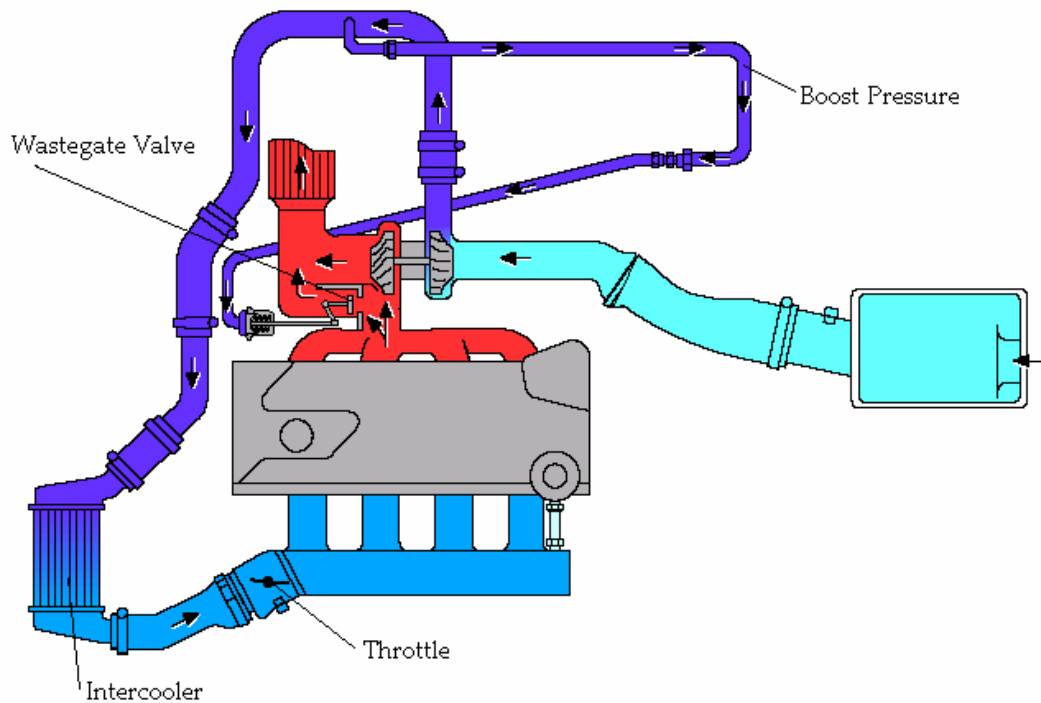


Figure 3-11 Conventional Boost Control Layout (Audi AG, 1998)

With the increased power and capability of the modern ECU, electronic boost control is becoming more common. This can be implemented by manipulating the pressure that acts on the diaphragm of the wastegate actuator. Manipulation of the pressure can be realised with the use of a 3-way solenoid valve. A typical layout can be seen in Figure 3-12 and connections within the valve can be seen in Figure 3-13.

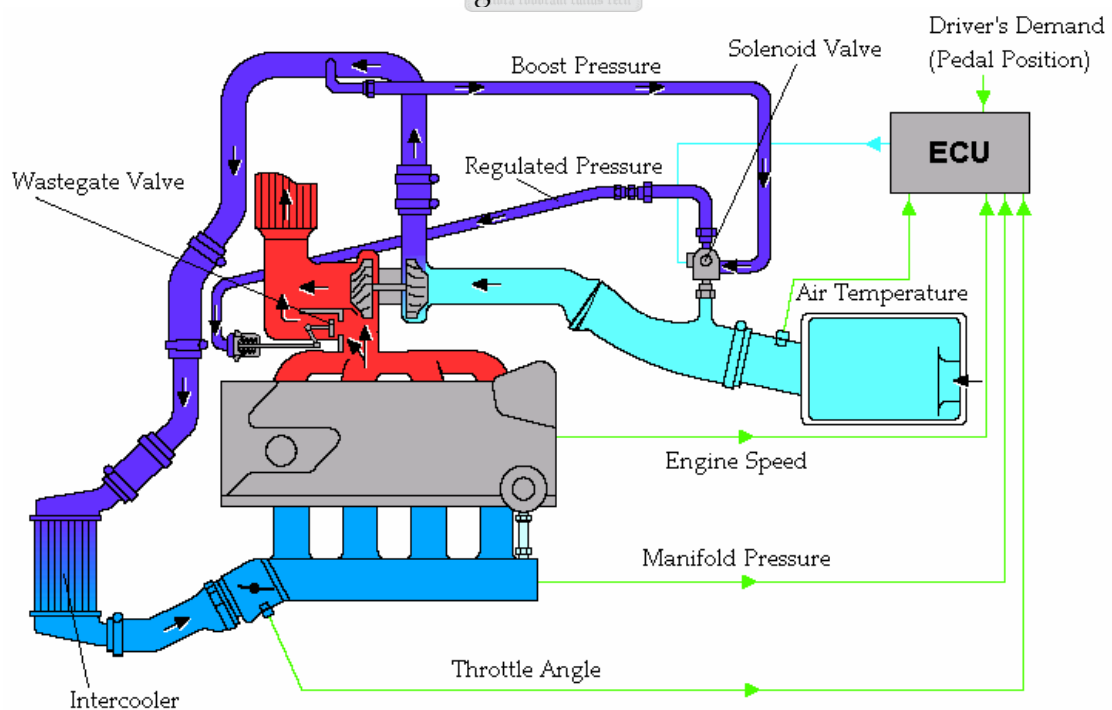


Figure 3-12 Typical Electronic Boost Control Layout (Audi AG, 1998)

In the valve's normal (de-energised or OFF) position the wastegate (2) is connected directly to the boost pressure (3). If the valve is energised (switched ON) the wastegate (2) is connected to atmosphere (1) and the wastegate will not open, thus maximum boost will be developed. Switching the solenoid valve on and off repeatedly, the pressure on the actuator piston can be varied between atmospheric pressure and the boost pressure. The actual pressure generated at (2) will depend on the switching duty cycle.

The result is that the higher the switching duty cycle, the lower the pressure on the actuator piston. This will result in a smaller opening of the wastegate and thus a higher boost pressure could be developed. The advantage of using the valve in its normal open position is that, should the electronics fail, the wastegate will open as in the conventional case, producing a lower boost pressure than with electronic control.

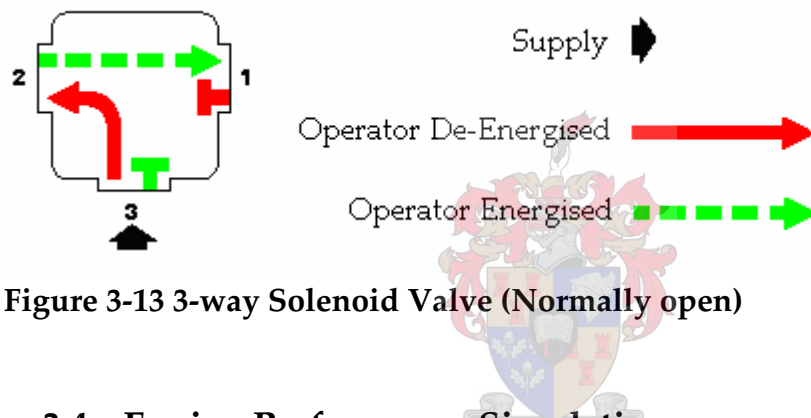


Figure 3-13 3-way Solenoid Valve (Normally open)

3.4. Engine Performance Simulation

WAVE is a computer-aided engineering code developed by Ricardo to analyse the dynamics of pressure waves, mass flows and energy losses in ducts, plenums and the intake and exhaust manifolds of various systems and machines. WAVE provides a fully integrated treatment of time-dependent fluid dynamics and thermodynamics by means of a one-dimensional finite-difference formulation incorporating a general thermodynamic treatment of working fluids including air, air-hydrocarbon mixtures, products of combustion, freons and liquid fuels. In addition, WAVE provides a completely coupled interface to Ricardo's CFD code, VECTIS, which allows various system components to be simulated as a full three-dimensional model. Finally, WAVE provides a completely coupled interface to external models which are user-defined to specifically describe the physics in a system component.

WAVE can model general networks of pipes, volumes and junctions in terms of a set of building blocks, which include:

- Constant area or conical pipes or ducts;
- Passages with abrupt changes of area;
- Junctions of multiple ducts;
- Elbows, orifices and plenums;
- Terminators such as infinite plenums (ambients) and anechoic boundaries.

WAVE also includes a library of machinery components such as engine cylinders, piston compressors, turbocharger compressors and turbines, and pumps. These components can be attached to the pipe networks to serve as the sources or absorbers of pulsating flows.

The basic methodology incorporated in WAVE has been extensively tested against a set of reference test cases (Ricardo, 2002). These included: shock-wave propagation in a duct, pressure-wave reflection from closed and open ends of a duct, steady-state flow through a duct with an abrupt change of cross-sectional area, flow through an orifice, pipe flow with friction, pipe flow with heat transfer and flow through junctions of three ducts.

3.4.1. Flow Modelling

The details of the flow in ducting systems are obtained as a solution of quasi-one-dimensional compressible flow equations governing the conservation of mass, momentum and energy. The duct system is discretized into a series of small volumes and the governing equations are then written in a finite difference form for each of these elementary volumes. A staggered mesh system is used, with equations of mass and energy solved for each volume and the momentum equation solved for each boundary between volumes. The equations are written in an explicitly conservative form as:

$$mass = \frac{dm}{dt} = \sum \dot{m} \quad \text{Eq 3-10}$$

$$energy = \frac{dme}{dt} = \sum \dot{mh} + sources \quad \text{Eq 3-11}$$

$$momentum = \frac{dmu}{dt} = -A \frac{dp}{dx} dx + \sum \dot{mu} - losses \quad \text{Eq 3-12}$$

The thermodynamic properties of the fluids are based on the appropriate governing relations, such as perfect gas equations for the thermo-chemistry of hydrocarbon/air mixtures for general C/H/O/N type fuels, or real gas equations for fluids such as freons or oils.

The solution of the governing equations is obtained by the application of a finite difference technique utilizing the finite-volume approach to the discretization of the partial differential equations. The time-differencing is based on the explicit technique, with the time-step governed by the Courant condition.

This approach is superior to the method of characteristics, because it does not require the inaccurate and cumbersome ad hoc treatment of many of the terms of the governing equations and of the geometry. These ad hoc treatments, which are inherent in the method of characteristics, introduce inaccuracies specifically in the areas of source terms such as heat transfer, friction, and distributed losses, boundary conditions at locations of abrupt area change, junctions of multiple ducts, and bends. WAVE, on the other hand, because of its basic formulation and solution technique, is able to handle these effects accurately and with no special difficulty.

3.4.2. Combustion Modelling

WAVE contains a number of relatively simple but fully integrated combustion models such as:

- Standard diesel combustion;
- SI combustion model (Wiebe-based);
- Stratified charge combustion model.

Since this thesis is focused on SI engines, only the SI combustion model will be discussed in more detail.

The correlative combustion model for premixed charge spark-ignited engines is based on a Wiebe function relationship widely used to describe the rate of mass burned in thermodynamic calculations. This relationship allows the independent input of function shape parameters and of burn duration. It is known to represent quite well the experimentally observed trends of combustion heat release. When using the Wiebe correlation, the cumulative mass fraction burned as a function of crank angle is given by the following:

$$W = 1 - EXP \left(- AWI \left(\frac{\Delta\theta}{BDUR} \right)^{(WEXP + 1)} \right) \quad \text{Eq 3-13}$$

where: W = cumulative mass fraction burned

$\Delta\theta$ = crank degrees past start of combustion

$BDUR$ = user-entered 10 % – 90 % burn duration in crank degrees

$WEXP$ = user-entered Wiebe exponent

AWI = internally calculated parameter to allow $BDUR$ to cover the range of 10 % - 90 %.

When using the Wiebe model, the combustion rate is controlled by three user-defined parameters. These are the location, in degrees, of the 50 % burned point of the total heat release; the burn duration, in degrees, from 10 % to 90 % mass burned; and the Wiebe function exponent. The main effect of the Wiebe exponent is the shift of the 10 % and 90 % points with respect to the 50 % point. This is illustrated in Figure 3-14 and Figure 3-15. In both figures the 50 % burn point and combustion duration were held constant at 10 °CA and 25 °CA respectively. It can be seen that a $WEXP = 2$ shift the 50 % burn point earlier in respect to the burn duration than would a higher value for $WEXP$.

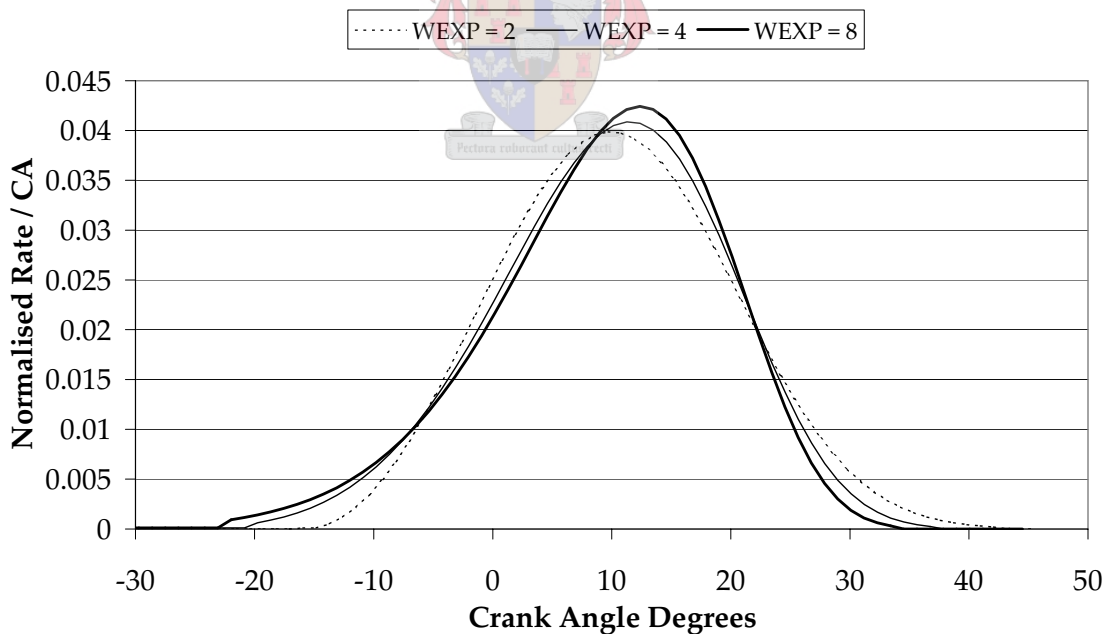


Figure 3-14 Wiebe Combustion Curve Shape

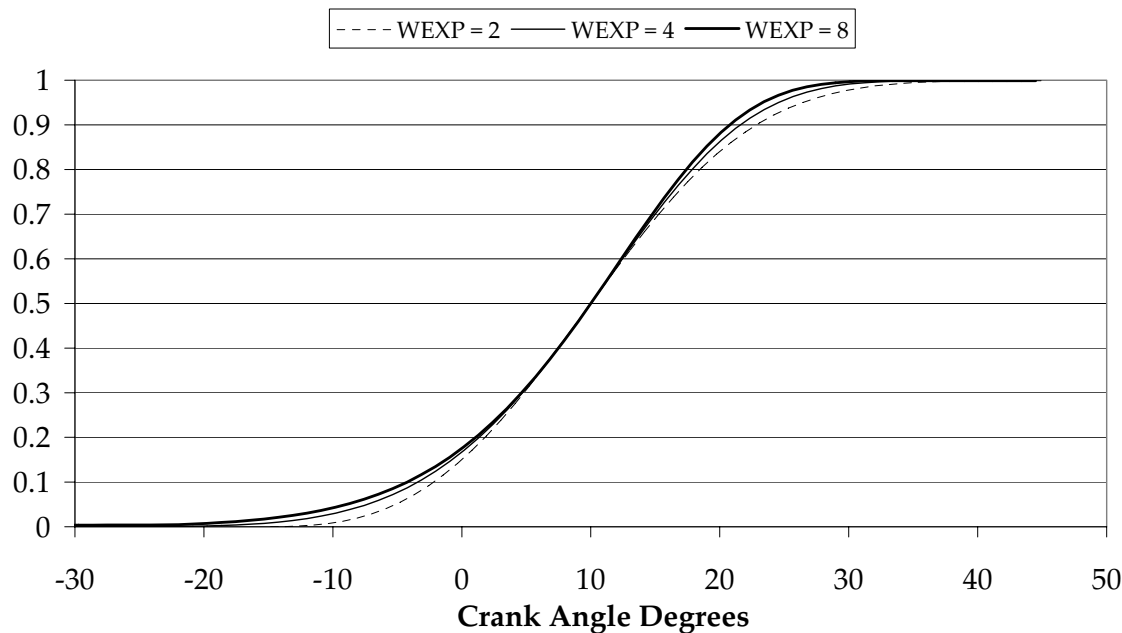


Figure 3-15 Wiebe Cumulative Combustion Curve Shape

3.4.3. Modelling of Compressors and Turbines

In WAVE a turbocharger is modelled as two separate components, a compressor and a turbine. There may be more than one of each in a given simulation. A compressor may be driven by an associated turbine or may be gear-driven by the engine. Similarly, a turbine may be driven at a fixed speed for simulation of turbocompounded components. A compressor's boost pressure or speed can be controlled by actuating a wastegate or variable geometry nozzle of its associated turbine. A turbine may be of fixed or variable geometry with an optional wastegate. Each component is represented by a map that relates mass flow, pressure ratio, rotational speed and efficiency. Standard dimensional maps are pre-processed for use in WAVE by the TCMAP pre-processor, which smoothes and extends the maps and produces an input file for WAVE. This is done to allow optional user-prescribed scaling of the turbocharger to match it to an engine.

The compressor and turbine are each modelled as type 1 junctions, which are plane boundaries between adjacent duct sub-volumes. The compressor junction requires two ducts, one inlet and one or more outlets. Both the fixed and the variable geometry turbine junctions allow multiple inlet ducts and one output duct.

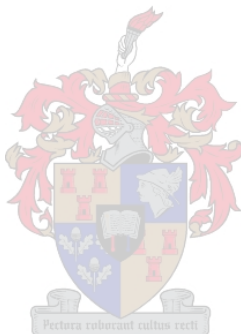
A variable geometry turbine is defined in WAVE by supplying a series of turbine performance maps, each at a different nozzle angle (rack position). The code determines the actual turbine characteristics by interpolating between the supplied maps to any rack position. An integral wastegate may be defined for any turbine in the system. WAVE simulates the wastegate opening as an additional flow path from the entrance duct to the exit duct of the turbine. A fixed-opening integral wastegate can be defined for each turbine in the system. To model an external wastegate, one which does not lead directly from the turbine inlet duct to the turbine outlet duct, a separate flow path around the turbine may be constructed, using an orifice junction or dashpot-driven check-valve junction to represent the wastegate itself.

The calculation of flow through a compressor or a turbine is carried out in WAVE in the following manner. At each time-step of the simulation of a compressor/turbine, the code accesses the appropriate steady-state map in a quasi-steady manner. The inputs used to read the maps are the instantaneous values of inlet pressure and temperature and outlet pressure (values are total or static as appropriate), and the compressor/turbine speed. The outputs obtained from the maps are the instantaneous mass flow and adiabatic efficiency. From these values the simulation computes the resulting instantaneous mass and enthalpy fluxes out of the compressor or turbine. Also, the instantaneous work done or extracted by a compressor/turbine is calculated. The works of the compressor and turbine are integrated in time to calculate the change of speed of the turbocharger.

For multiple-entry turbines, WAVE makes a default assumption that all of the entries are identical. If a multiple-entry turbine is not symmetrical, the user can override this assumption by assigning individual flow capacities to each turbine entry. The total mass flow through the turbine is then the sum of the mass flows calculated separately for each entry. Any leakage between the multiple entries of the turbine must be accounted for by the user by constructing a leakage orifice between the entries. For compressors with multiple exits, the assumption is made that all of the exits are identical. The above procedures represent a simplified treatment of two unsteady features:

- The gas pressure and temperature entering a turbine can be substantially non-uniform in time, while the turbine maps were acquired under steady-state conditions. This introduces an error of unknown magnitude into the simulation;
- Under the conditions of partial admission (twin-entry turbines), the instantaneous mass flow through each entry of the turbine may not be equal to one half of the full map value as assumed above.

Under steady-state conditions, the above procedure perfectly reproduces the steady-state map data. The situation under unsteady conditions is less clear. Comparisons of simulation results to available turbocharged engine data made by Ricardo suggest that, despite the simplified treatment, the agreement with data is quite good, at least within the typical inaccuracies due to measurements of gas temperature and, to a lesser degree, pressures and speed. (Ricardo, 2002)



4. ENGINE SIMULATION

The process of engine design and development can be time consuming and laborious. If a numerical model can be used to predict engine performance and calculate mechanical and thermal stresses, the results may be used for optimisation of the engine. This optimisation may include, but is not limited to, swept volume, CR, valve timing, turbocharger matching, and inlet and exhaust manifold geometry. This optimisation may be done with the required power output and/or reliability as the objective. With the use of numerical models, the engineer will be able to develop a prototype engine that is much more refined and closer to the optimum match than would be possible in the same time without such a tool. Development time, and hence cost is reduced, resulting in a better end product.

4.1. Engine Simulation Model – 1.6 litre Ford Rocam

Development and modelling of the test engine had previously been done with WAVE; thus a model representing this engine existed, thus it was not necessary to build a completely new model. The existing model was updated to reflect the design changes made to the engine. Changes were made to the exhaust manifold to accommodate the turbine, the exhaust system was altered to represent the geometry of the system as used in actual engine testing and the intake piping was adapted to accommodate the compressor. Figure 4-1 shows the graphical representation of the simulation model.

The values needed for combustion simulation were the Wiebe exponent, burn duration and 50% burn point. These values were carried over from the previous model, since no combustion data were initially available to update these values. Therefore the simulated combustion and actual combustion might differ.

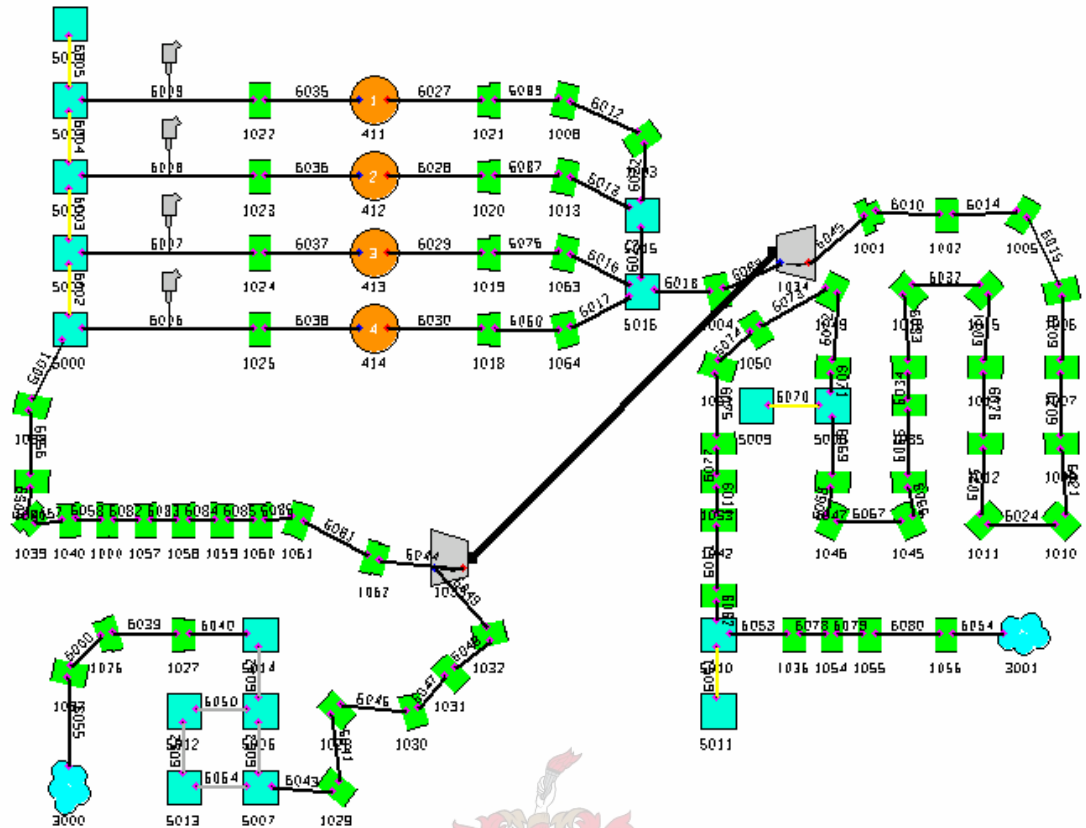


Figure 4-1 Simulation model: Ford RSI Turbo

The design and simulation of the exhaust manifold were done using the old combustion data from the NA model. Since the comparison between the exhaust manifold concepts was done with the focus on engine breathing, the influence of the combustion data was deemed not to be an important factor. It was only after everything was built and the engine was set up and running that combustion data were measured and used for final correlation between the actual test data and simulations.

4.2. Engine Optimisation

When developing an up-rated engine or doing a turbocharged conversion on a NA engine, a target output must be set and decisions must be made on which engine parameters may be changed in order to achieve the desired output. As mentioned earlier, there are numerous parameters that can be changed or optimised. All possible changes can be classified as primary and secondary changes.

Engine design, performance simulation and optimisation are iterative procedures; thus it is very difficult to separate the discussions of engine simulation and optimisation from that of the next section, namely design and modification. Primary and secondary changes will be indicated in this section, but the influence of and the decisions taken regarding them will be discussed in the next section.

In this project, where a turbocharger conversion is done on a NA engine, the primary changes would be all changes that are necessary to fit the turbocharger to the engine and make the basic configuration work. These primary changes would typically include:

- Redesigned exhaust manifold to accommodate the turbocharger;
- Connecting the turbine outlet to the exhaust pipe;
- Rerouting the clean air piping to include compressor before the intake manifold;
- Supplying oil to the turbocharger bearings and returning it to the sump;
- Supplying water for the cooling of the turbocharger bearings;
- Upgrading the fuel injectors and fuel pressure regulator to supply the extra fuel needed;
- Changing the manifold absolute pressure (MAP) sensor to enable boost pressure measurement by the ECU;
- Adjusting fuelling and timing maps on the ECU.

Secondary changes can be defined as those changes that are not essentially necessary, but would be beneficial to make. These changes could entail the following:

- Charge air cooling;
- Valve timing optimisation;
- Lowering of CR;
- Electronic boost control;
- Electronic throttle control.

Simulations at an early stage indicated that the objectives could be met with only the primary changes. Therefore none of the secondary changes was made, but when the simulation model has been correlated to the actual engine, they could be used to illustrate the advantage that each secondary change could have.

4.2.1. Modelling Strategy for Wastegate Control

The simulation package used has the capability to control the wastegate opening area to a set target or limit on Brake Mean Effective Pressure (BMEP), boost pressure or compressor speed. In reality, if a pneumatic actuator is used, the boost pressure developed is proportional to the stiffness of the spring and the opening pressure is proportional to the preset compression of the spring. This relationship can be seen in Figure 4-2. The data were obtained by doing a simple test with the actual wastegate actuator fitted to the turbocharger used.

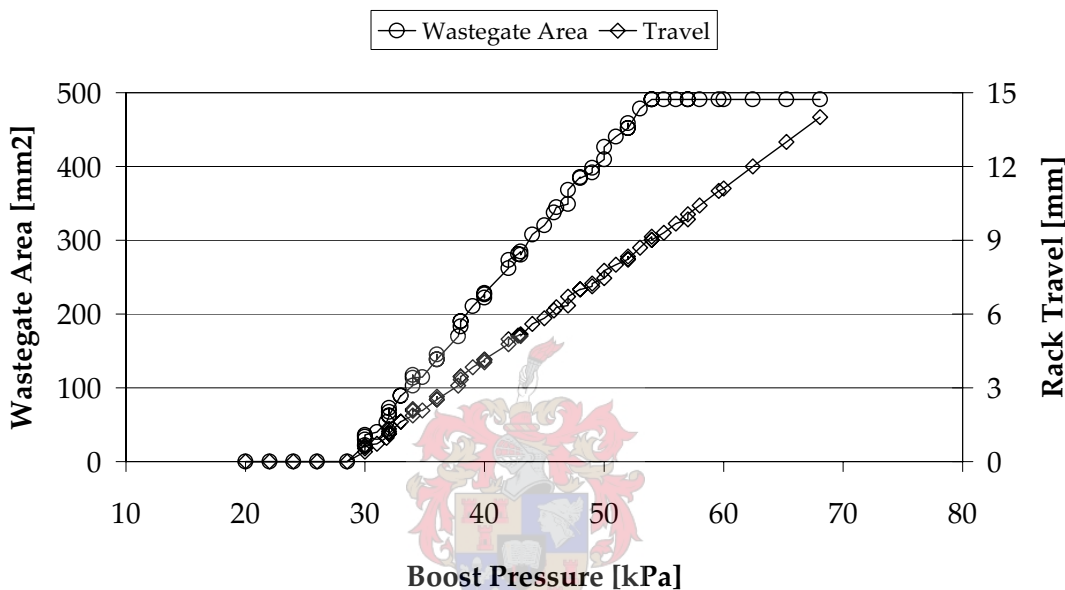


Figure 4-2 Measured Rack Travel and Calculated Wastegate Area versus Boost Pressure

Pressure was applied with a hand pump and then the rack travel was measured. Because the area cannot be measured directly, it has to be calculated. With reference to Figure 4-3, the physical opening area can be calculated by assuming that the flow area is the surface area of a cylinder that is cut by a plane that is at an angle to the centreline of the cylinder. The flow height BB', height of the centreline of the cut cylinder, is equal to the travel height AA' multiplied by the ratio OB:OA. Thus the area can be calculated by Eq 4-1.

$$Area = 2 \cdot \pi \cdot R \cdot AA' \cdot \frac{OB}{OA} \quad \text{Eq 4-1}$$

If the flow area calculated with Eq 4-1 is bigger than the area of the hole in the casing of the turbine, the area of the hole is used. This explains why the wastegate area in Figure 4-2 remains constant for boost pressures exceeding 55 kPa. Thus the maximum wastegate area is equal to the area of the hole in the turbine casing, which is equal to 490 mm^2 for the turbocharger being used.

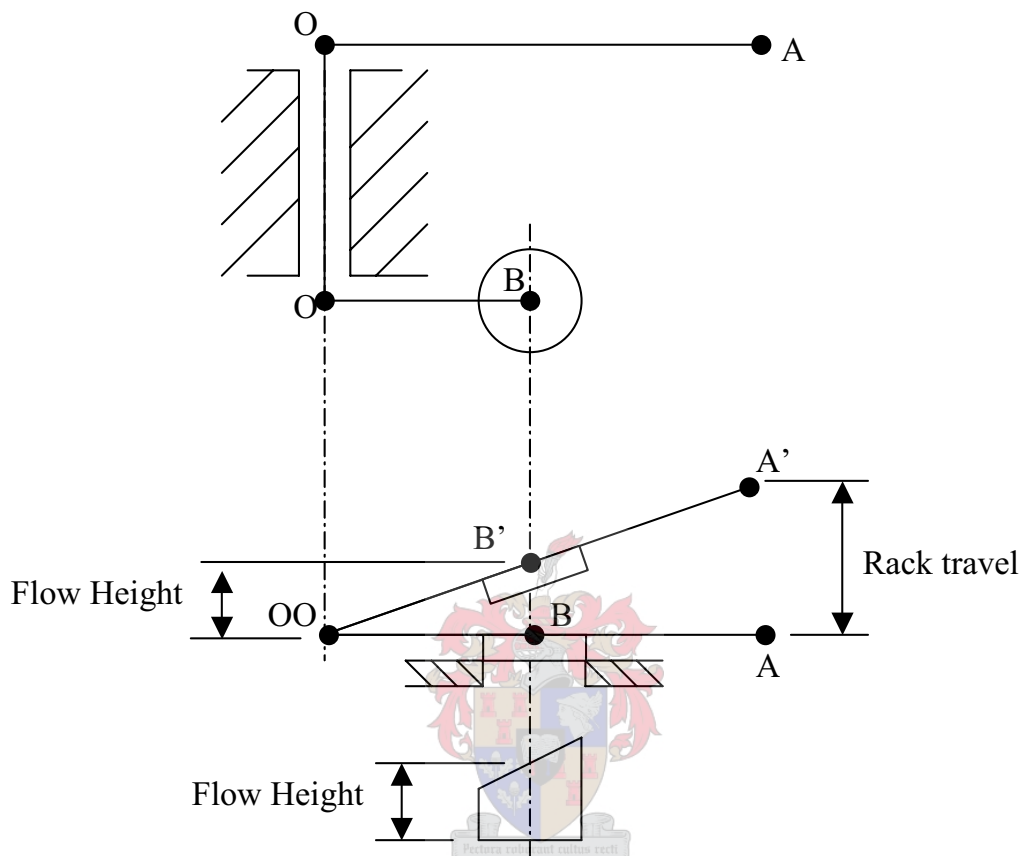


Figure 4-3 Wastegate Area Calculation

A Visual Basic program (WG_control) was written to control the wastegate area in an iterative manner until the area versus boost pressure corresponds to the spring stiffness and preset compression. A simplified algorithm for WG_control is outlined below:

- Execute WAVE simulation with user specified starting value for wastegate area;
- Read results from output file after simulation finished;
- Determine shortest distance between operating point and wastegate characteristic line;
- Adjust wastegate area in input file and execute WAVE simulation;
- Repeat process until operating point lies within the specified tolerance from wastegate characteristic line.

This code was written as a subroutine that it could easily be incorporated into another program to fulfil this function.

4.2.2. Exhaust Manifold Simulation

The exhaust manifold had to be redesigned in order to accommodate the turbocharger's turbine. Two concepts for the exhaust manifold were evaluated with the aid of simulations. The objective was to compare the amount of internal exhaust gas recirculation (EGR) and exhaust manifold pressure of the two concepts.

The detailed concepts are discussed in section 5, but the modelling of the concepts in WAVE will be discussed here. Figure 5-3 and Figure 5-5 show the computer-aided design (CAD) models of the two concepts.

The two concepts are built up of ducts, orifices and complex junctions in WAVE. The representation is shown in Figure 4-4 and Figure 4-5 respectively. Concept 1 consists of 2 complex junctions, 12 ducts and 6 orifices. Orifices are used to connect two ducts together. If the ducts are of the same diameter, the orifice plays no role other than connecting two ducts, but if the diameters differ, it acts as an abrupt change in area. Complex junctions were used to model the junctions between the different cylinders in order to model the flow and duct orientation correctly. Complex junctions take into account the duct orientation and represent the volume where two or more ducts join together.

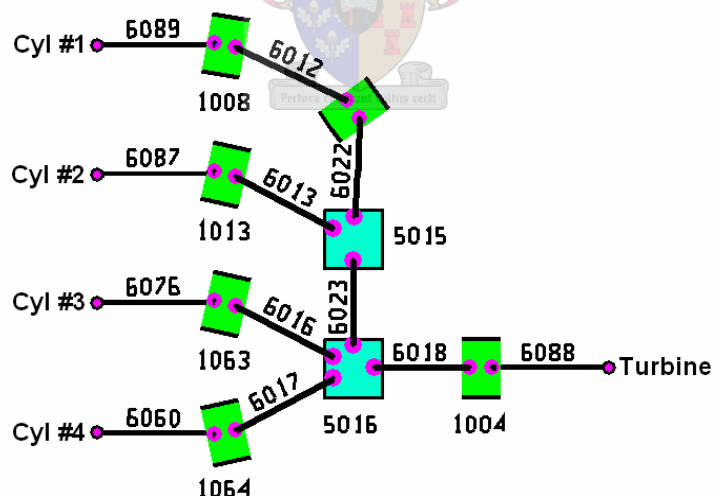


Figure 4-4 Simulation Model of Exhaust Manifold: Concept 1

Concept 2 consists of 15 ducts, 8 orifices and 3 complex junctions. Concept 2 has more components to account for the simple pulse converters used. Ducts 6013, 6016, 6018, 6022, 6023 and 6091 cross-sectional area decreases in the flow direction to simulate nozzles. The complex junctions are used to simulate the collector between two nozzles and connection to the next duct.

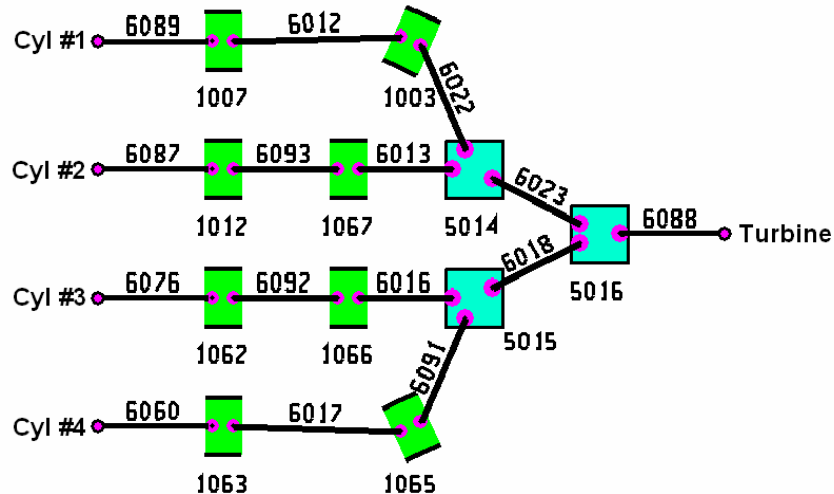


Figure 4-5 Simulation Model of Exhaust Manifold: Concept 2

Simulations were done with all inputs identical but with the two different exhaust manifold concepts. During the simulations the focus was shifted to the turbocharger's performance and the engine's breathing characteristics. The approach taken was to run engine simulations in such a way as to emulate the methodology that would have been used in an engine prototype development process. Thus the wastegate was opened according to a spring stiffness that was pre-defined. Since the actual turbocharger used for this project came with a wastegate actuator, its standard opening characteristics were used in the simulation. This test was done at different engine speeds in order to investigate each concept's performance across the engine's entire operating speed range.

4.2.3. Valve Timing Optimisation

The valve timing plays an important role on the breathing of an engine. The requirements for a turbocharged engine differ from that of a naturally aspirated engine. In general the valve timing of a naturally aspirated engine can be optimised for either higher torque at low engine speeds, compromising power at high engine speeds or vice versa.

In general for NA engines the exhaust valve closure (EVC) and intake valve opening (IVO) are the important parameters, whereas on turbocharged engines the exhaust valve opening (EVO) and intake valve closure (IVC) are more important (Watson & Janota, 1984). Furthermore, the amount of valve overlap plays a significant role. Valve overlap is defined as the crank angle during which both exhaust and intake valves of the same cylinder are open.

Another factor that plays a significant role is the amount of exhaust valve overlap. This can be defined as the crank angle that the exhaust valves of two cylinders, which fire in succession and are on the same exhaust manifold, are open simultaneously.

As mentioned earlier, valve timing optimisation falls under the secondary engine changes. This optimisation was done only using simulations and is used to illustrate its advantages.

4.2.3.1. Optimisation Strategy

Optimising the valve timing and lift is a trade off between higher torque at low engine speeds and power at high engine speeds. The initial aim of this project was to achieve a torque curve, as flat as possible, over a wide engine operating speed range at 150 N·m and to produce 100 kW at 6366 rev/min. This odd engine speed was due to the fact that the gearbox that this engine is mostly used with, was rated at 150 N·m maximum; therefore to achieve 100 kW at this torque the engine speed must be 6366 rev/min.

Thus optimising the valve timing for low engine speeds would result in very little boost being required to achieve the target of 150 N·m, but with high boost being required at high engine speeds. Due to the fact that the compression process in the compressor is not isentropic and the higher the boost pressure, the higher the compressed air temperature, the initial charge temperature would be higher, which would make the engine even more susceptible to knock because initial charge temperature and pressure would be higher than normal.

If the valve timing was optimised for a specific engine speed, the same airflow could be achieved with lower boost pressure than when the valve timing was not optimised, but with higher boost. Therefore when considering the above, it was decided to optimise the valve timing for high engine speeds in order to decrease the boost pressure necessary to achieve the 100 kW target, while higher boost pressure would be used at low engine speeds to achieve the 150 N·m target.

However, the higher boost pressure at low engine speeds could result in a situation where the boost pressure is high enough and the airflow is low enough to cause the compressor to surge. Thus care must be taken to ensure that the compressor operates with an adequate safety margin from the surge-line on the compressor map.

Knock at low engine speeds are generally more severe and damaging than at high engine speeds. The boost pressure and charge air temperature would be higher than optimal at low engine speeds, but would still be lower than at high engine speeds, even if the valve timing is optimised for high engine speeds. Therefore it was not expected that knock would occur at low engine speeds. Since knock was not simulated and the optimised valve timing would not be implemented, it was assumed that knock would not occur for the purpose of this investigation.

4.2.3.2. Full Factorial Simulation

The optimisation of valve timing and lift is basically the optimisation of a function which is not explicitly known and which has six variables (EVO, EVC, IVO, IVC, exhaust valve lift, intake valve lift). There exist numerous optimisation algorithms each applicable to certain kinds of problems (Press *et al.*, 2001). Most optimisation algorithms require quite a number of iterations before arriving at a solution. Therefore it was decided that, as a starting point, a full factorial optimisation would be done.

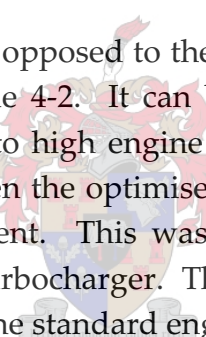
Valve lift is limited by the maximum acceleration the valve train can withstand. The acceleration is inversely proportional to the time the valve is open and proportional to the valve lift. The result would be that the longer a valve is open, the more lift is possible and vice versa for a given maximum acceleration. Thus to keep the maximum acceleration the same, the amount of lift must be adjusted according to the valve open time. In the full factorial search the simplification was made that the lift for both the valves remains constant. With this decision the variables were reduced to four.

Assigning four values to each variable it resulted in four to the power of four simulations, which is equal to 256. Table 4-1 lists the initial values used for each variable. This would give a relatively coarse search, but refinement can be done in an iterative way. The simulations only require computer time and not actual testing and set-up time, thus it was cost effective to perform such a full factorial search. The search was done at an engine speed of 6366 rev/min and 2000 rev/min. 256 simulations at a single engine speed took about five days to complete on a personal computer with an AMD 1.2 GHz Duron processor and with 128 MB of memory.

Table 4-1 Initial Values for Full Factorial Valve Optimisation

IVO	IVC	EVO	EVC
270	540	90	360
300	570	130	390
330	600	150	420
360	630	180	450

After the simulations were completed, the results were sorted in order of descending engine torque and increasing boost pressure. Thus the top results were the highest torque with the lowest boost pressure. The top 20 results showed that the best IVC was as late as possible. Thus IVC was held constant during further refinement. A second optimisation process was undertaken with only 3 variables and 5 values for each. After the refined optimisation was completed, the results were again sorted as described above. The search was iterated until each of the remaining 3 variables' values was within 1 degree of each other.



The end results for each speed opposed to the standard engine's valve timing can be summarised as in Table 4-2. It can be seen that the required valve timing differs a lot from low to high engine speeds. The standard engine's intake valve timing fits between the optimised results, but that found for the exhaust valve is totally different. This was due to the different breathing characteristics caused by the turbocharger. The valve overlap at 6366 rev/min of 63°CA was close to that on the standard engine of 70°CA.

Table 4-2 Full Factorial Results

Engine Speed [rev/min]	IVO [°CA ATDC]	IVC [°CA ATDC]	EVO [°CA ATDC]	EVC [°CA ATDC]
2000	301	580	172	421
6366	342	630	125	405
STD Engine	328	614	112	398

4.2.3.3. Optimisation Using a Search Algorithm

In the previous section valve optimisation was done at two engine speeds. Thus a solution for both the high and low engine speeds was obtained. This would not necessarily result in a flat torque curve. The ability to optimise the wastegate actuator together with the valve timing to obtain the desired torque curve could not be done using the full factorial method. Since the target was a nearly flat torque curve over a wide as possible engine speed range, an optimisation problem was setup to optimise for the whole engine speed range. The target torque curve can be specified and the optimisation algorithm will optimise the valve timing and wastegate actuators characteristics to obtain the desired torque curve while using minimal boost pressure.

Increasing the number of variables increases the complexity of the optimisation process considerably. In order to make a decision on which optimising algorithm must be used, some of the characteristics of the function that must be optimised must be known. The function in this specific case had multiple variables, was not explicitly known and thus it was impossible to calculate the function's gradient (derivative) directly. The method of finite differences could have been used to determine the function's gradient but this would have resulted in more function evaluations (simulations), which is time consuming. The fact that the output torque doesn't vary much with small variations in valve timing (0.25 degrees) further complicates the determination of the function's gradient.

It was decided to use a direct search method, such as the Simplex method. There are various variations of the Simplex method available. The Nelder-Mead Simplex algorithm was the choice from Press W H, *et al.*(2001). The program example was easily rewritten in Visual Basic and was combined with the wastegate control program mentioned earlier enabling optimisation of the valve timing as well as the wastegate actuator characteristics.

Including the wastegate spring stiffness (GRAD) and preload (PRESET) into the optimisation the variables were increased to six, namely: IVO, IVC, EVO, EVC, GRAD and PRESET. The same simplification on valve lift was made as in the full factorial search, it was kept constant.

Considering these facts, the following strategy for valve optimisation was developed:

1. Set initial values of IVO, IVC, EVO, EVC, GRAD, PRESET;
2. Determine initial wastegate area;
3. Run wave simulation;
4. Calculate new wastegate area based on boost pressure developed;
5. Adjust wastegate area to actuator characteristics;
6. Repeat steps 3 to 5 until all operating points correspond to actuator characteristics;
7. Evaluate torque curve;
8. Calculate new values for variables;
9. Repeat steps 3 to 5 until all operating points are on desired line;
10. Repeat steps 7 to 9 until no further improvement is found.

When the torque curve is evaluated it is actually compared to the target torque curve that the user specified. The optimisation program was programmed in such a way that a specific torque can be specified at each speed and also a weighing factor indicating its importance. The error that the optimisation program minimises can be expressed in Eq 4-2. Including the boost pressure in the error will have the result that the optimisation seeks the minimum boost pressure.

$$Error = \sum_{i=1}^n [|Tt_i - Tp_i| C_i P_{boost_i}] \quad \text{Eq 4-2}$$

Where:
 Tt_i = target torque
 Tp_i = predicted torque
 C_i = weighing factor
 P_{boost_i} = boost pressure
 n = number of speeds evaluated in simulation.

The initial values as well as the optimised results after 30 iterations on a model with exhaust manifold concept #1 are shown in Table 4-3; it took about three weeks to complete 30 iterations. The torque curves for the standard and optimised results can be compared in Figure 4-6 with the ideal torque curve.

Table 4-3 Simplex Optimisation Results (30 iterations)

Variable	Initial	Optimised
IVO	328	329
IVC	614	621.8
EVO	112	112.4
EVC	398	390.7
GRAD	20	19.1
PRESET	-25	-26.7
ERROR	63.4	24.7

Further investigation into the torque limit on the gearbox proved that 150 N·m was not the limit. Therefore the restriction of a torque limitation was removed. Since 6366 rev/min was above the standard engine's rev limiter (6250 rev/min), it was decided to lower the engine speed at which peak power would be developed. The target torque curve was constructed by calculating the required torque to deliver 100 kW from 5000 rev/min up to 5500 rev/min. This resulted in 191 N·m and 174 N·m respectively. Thus 191 N·m was then assumed from 2500 rev/min to 5000 rev/min and 174 N·m for both 2000 rev/min and 5500 rev/min and each point were given the same weighing factor.

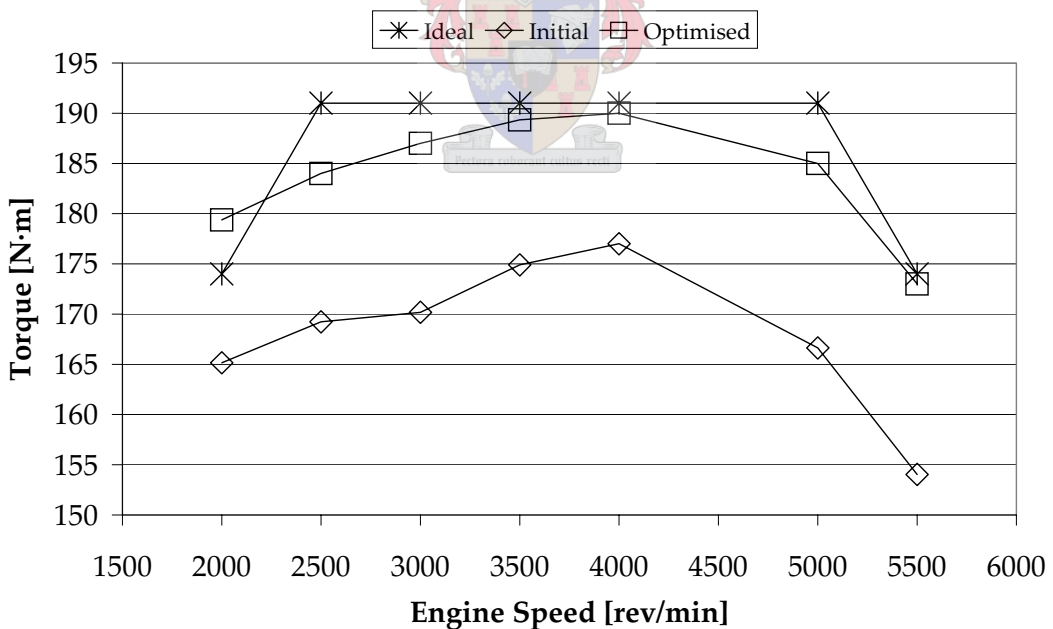


Figure 4-6 Effect of Optimised Valve and Wastegate Settings on Torque

It can be seen that with only 30 iterations the improvement was considerable. This improvement would not have been possible if only the valve timing was altered without adjusting the wastegate settings. This optimisation tool enables the user to specify any torque curve and the simulation will iterate until the best possible solution using minimal boost pressure is found given the constraints.

To simplify the optimisation and to speed it up, one or more of the variables can be made constant. Since the magnitude of the different variables in the optimisation varies between -20 and 600, scaling these parameters to the same magnitude also benefited the optimisation. See APPENDIX A for the Nelder-Mead simplex method algorithm that was implemented in the optimisation program as well as the scaling procedure.

4.3. Exhaust Manifold Concept Evaluation

As mentioned previously (section 4.2.2) the focus of the exhaust concept evaluation is the breathing characteristics of the engine, pressure difference across the engine and turbine and compressor performance. These were all compared using the same wastegate actuator settings to control the boost pressure.

Two exhaust manifold concepts were designed, one with easy manufacturing and assembly as the highest priority and is referred to as concept 1. The second concept was designed for optimal utilisation of the pulse energy in the exhaust gas and making use of simple pulse converters to limit the amount of pulse interference. This design is referred to as concept 2.

In Figure 4-7 it can be seen that the relationship between wastegate area and boost pressure for both concepts fell exactly on the same line, thus the actual actuator appears to have been simulated correctly in both cases. It is important to note that the individual points are not exactly coincident. It can be seen that concept 1 (C1) developed a higher boost pressure and thus the wastegate area is proportionally bigger. But when considering the torque developed as shown in Figure 4-8, concept 2 (C2) developed about 1 N·m more torque, which is a relatively small difference.

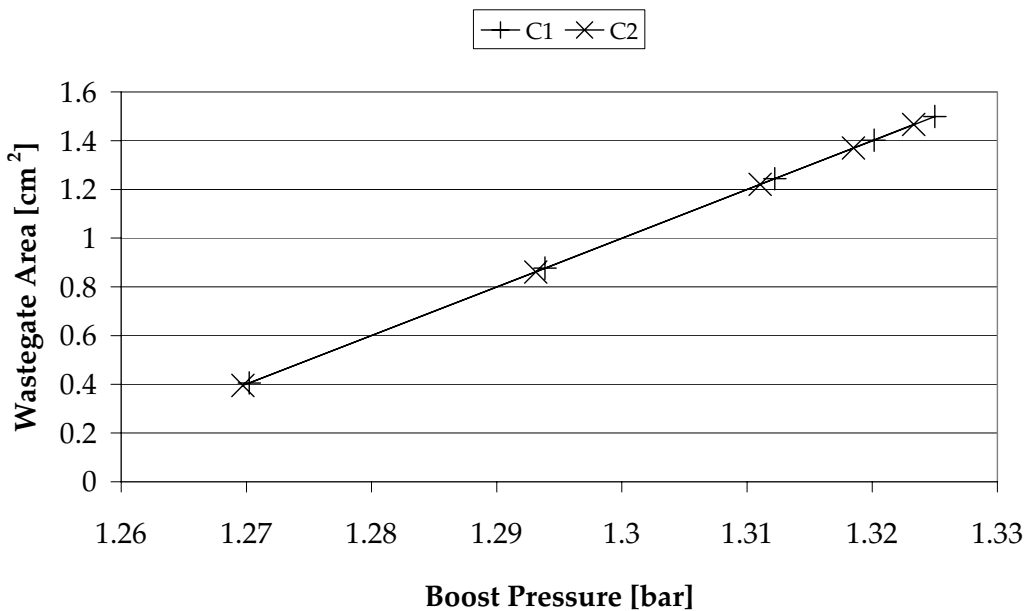


Figure 4-7 Exhaust Concept Evaluation: Wastegate Area

As can be seen from Figure 4-8 the difference in torque developed varies between 0.6 N·m and nearly 1 N·m and that C2 develops more torque than C1. If the boost pressure developed by C2 was lower, while the torque developed by C2 was greater, C2 must have a higher volumetric efficiency. This is illustrated in Figure 4-9, which compares the volumetric efficiency.

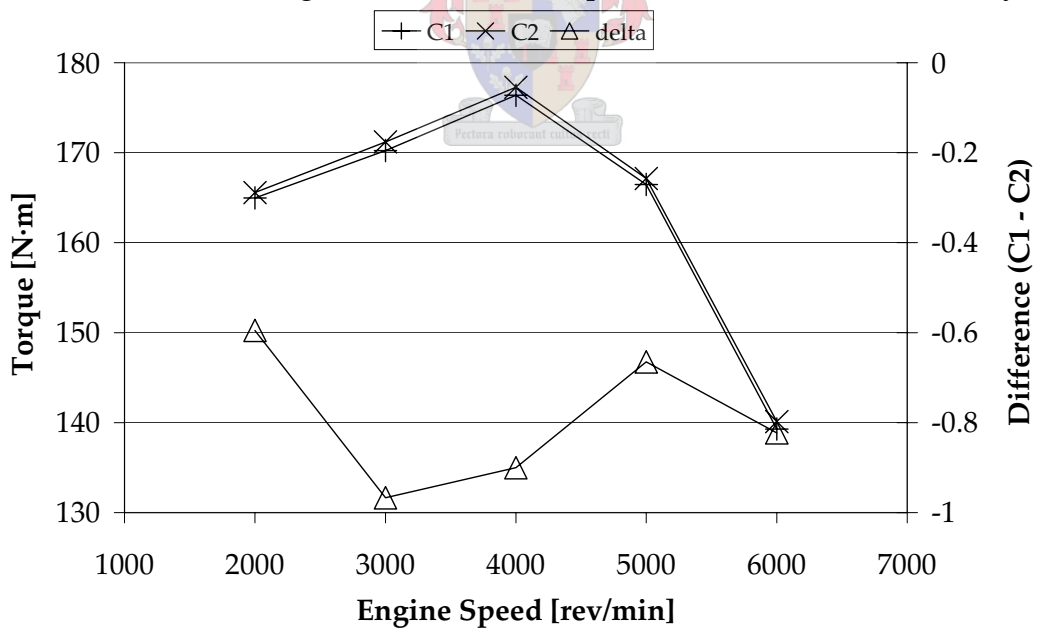


Figure 4-8 Exhaust Concept Evaluation: Torque

The difference in volumetric efficiency is small - less than 0.53%. The slightly higher volumetric efficiency can directly be translated into a higher airflow (Figure 4-10) through the engine.

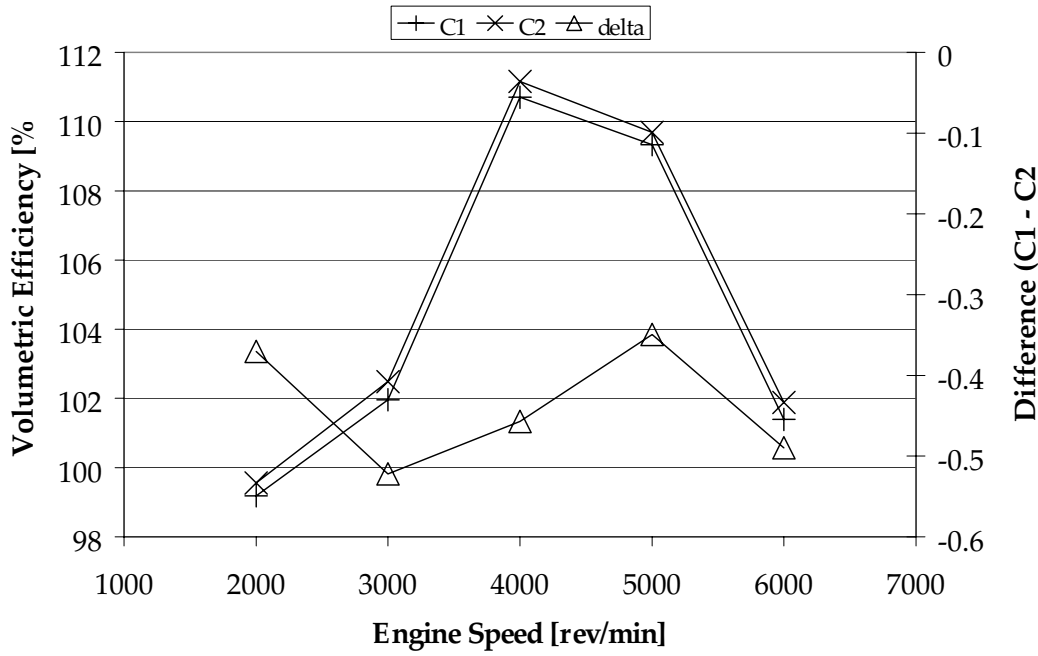


Figure 4-9 Exhaust Concept Evaluation: Volumetric Efficiency

At 6000 rev/min the difference in airflow is 1.24 kg/hr, which is a small difference but is significant enough to make a 1 N·m difference.

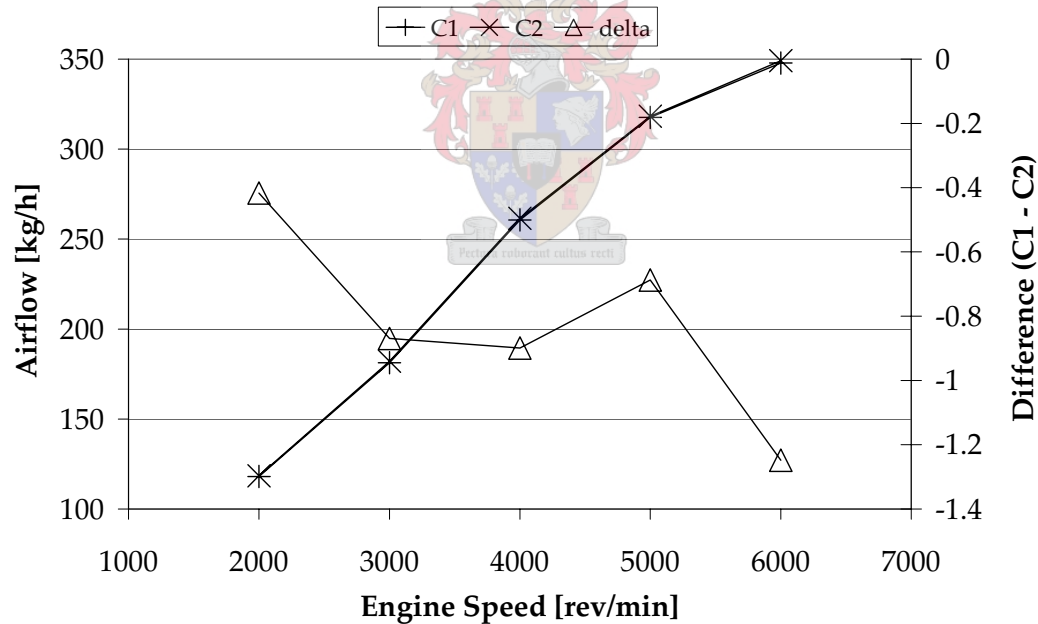


Figure 4-10 Exhaust Concept Evaluation: Airflow

When comparing the compressor and turbine efficiency, they were all within 0.5% of each other; thus it is too small to be significant. When comparing the average residual mass (Figure 4-11) in all 4 cylinders, it is clear why C2 develops more torque than C1. C2 has less residual mass inside its cylinders; thus it has more space for a fresh mixture of air and fuel and can therefore develop more torque. This is also the reason why the volumetric efficiency was higher for C2.

It is evident from Figure 4-7 that C1 develops a higher boost pressure than C2 and when comparing the average turbine inlet pressures the difference is less than 0.2 %, thus extremely small. Thus it is assumed that the higher residual mass of C1 could be attributed to the effect of pulse interference, causing reverse flow over the exhaust valve before closure or reverse flow over the inlet valve during valve overlap. In order to prove this assumption the mass flow over the valves should have been examined.

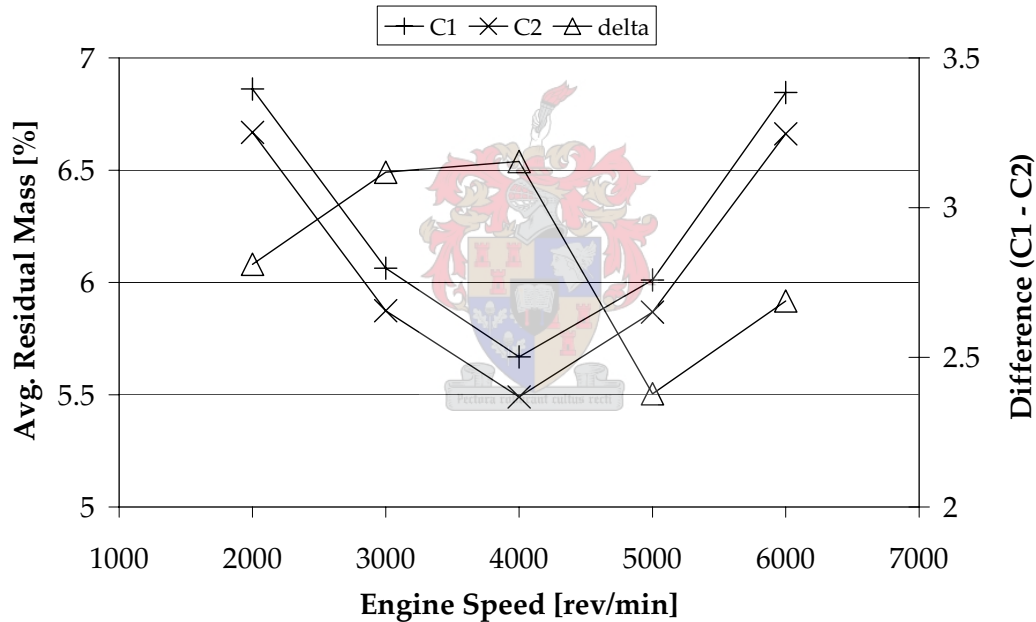
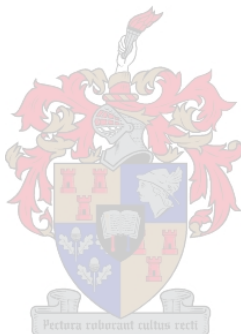


Figure 4-11 Exhaust Concept Evaluation: Average Residual Mass

Considering the above results, C2 is the better concept of the two, but it is only marginally better. Optimisation could be used to optimise the nozzles of the pulse converters, but optimisation might also be used to optimise C1 for pipe diameters and junction specifics. The optimisation of C2 or C1 might not be worth the effort.

When considering the advantages and disadvantages of each concept, simplicity, performance and practicality need to be taken into account. C1 was the obvious choice, since its performance is only slightly less than C2, and it was very much simpler and easier to manufacture than C2. The location of the bolts on the turbine inlet would interfere with C2, making assembly nearly impossible. C1 was thus manufactured for physical engine tests.



5. EXPERIMENTAL APPARATUS

Keeping in mind that the engine with a turbocharger and all the modifications must still fit into the engine bay of the original vehicle without modifications to the firewall, packaging is a significant challenge.

In this section all designed modifications are discussed in detail. The design process followed will not be discussed in detail, but only the final concepts and relevant manufacturing details will be highlighted. The difference between the standard and turbocharged engine is summarised in Table 2-1.

5.1. Exhaust Manifold Design

Designing an exhaust manifold that would fit in the engine bay, make use of the exhaust energy in the most efficient way and be easy to manufacture is an optimisation problem that has to satisfy very challenging criteria. On the basis of simulation results, which indicated small differences in performance between different concepts, it was decided that the manifold that was easiest to manufacture and that would fit was the solution that would be used. It may not be the most efficient manifold, but it would work satisfactorily. Thus fitting the turbocharger became a packaging challenge.

The spatial constraints are very tight, since no space can be wasted in a passenger car. The fact that the engine is of the cross-flow type with the inlet manifold on one side and the exhaust manifold on the other side complicates matter further. The engine is transversely mounted, with the exhaust to the firewall. The original equipment manufacturer (OEM) specifies that there must at least be a space of 25 mm between the engine and its attachments, e.g. exhaust manifold or turbocharger and the firewall. A CAD model of the complete engine bay was not available to the researcher, thus position measuring had to be done on the actual car.

A positioning rig (Figure 5-1) was designed and manufactured to enable the researcher to position the turbocharger, and then measure the position relative to the engine. These measurements were then entered into CAD and paths for the exhaust runners constructed from standard available pipe sizes and bends. If a solution could not be found, the position of the turbocharger had to be altered. This required that the new position had to be checked in the actual engine bay, before it could be finalised. Two exhaust manifold concepts were modelled and evaluated with the aid of simulation as discussed in the previous section.

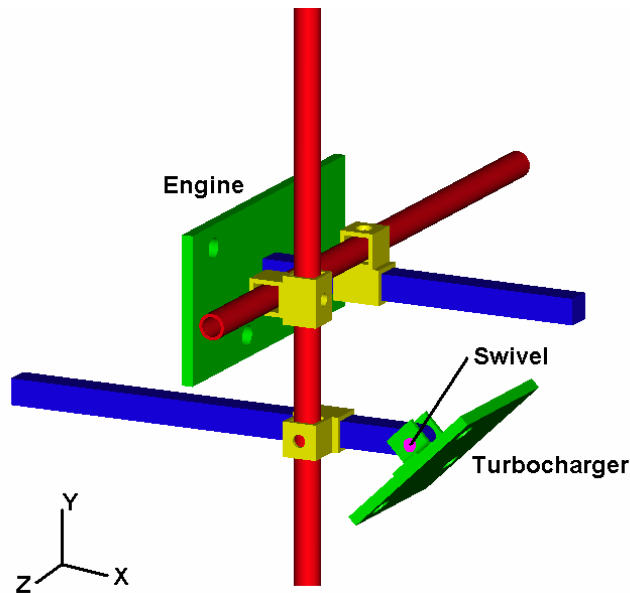


Figure 5-1 Positioning Rig

The positioning rig was bolted to the engine with the exhaust manifold studs. It then had three sliders with locknuts to make adjustment in the x, y and z-direction possible. The turbocharger was also bolted to the rig and could be rotated about the z-axis in order to correctly position the turbocharger. The position of the turbocharger was then easily measured by measuring the distances along the three axes and the rotation about the z-axis. These measurements could then be entered into CAD.

The strength calculations that were of interest were whether the manifold would be able to withstand the pressures and be structurally strong enough to support the turbocharger when operating at high temperatures.

Before analysing the two concepts for the exhaust manifold layout, pulse interference and how its disadvantages can be limited will be discussed. Pulse interference can seriously compromise the gas exchange process, by causing reverse flow into the cylinder just before EVC.

5.1.1. Pulse interference

When using a single turbine with a single entry, on an engine with more than 3 cylinders, it is inevitable that pulse interference will occur. Pulse interference occurs when the exhaust valve of a cylinder is nearing its closing and the exhaust valve of another cylinder opens. The pressure in the latter cylinder is much higher than in the manifold. This will cause a pressure wave travelling at sonic speed to travel towards the exhaust valves of the other cylinders. If the former cylinder's exhaust valve is still open, reverse flow can be induced and the cylinder will be filled with exhaust gases. Interference is likely to occur between: 1-3, 3-4, 4-2 and 2-1, where the first digit denotes the cylinder nearing closure and the second denotes the cylinder whose exhaust valve opens. These combinations are characteristic of a 4-stroke four-cylinder engine with firing order: 1-3-4-2. This can be clearly seen on the valve-timing diagram in Figure 5-2. It is also possible that a pressure wave travels toward the turbine entry and gets reflected at the nozzle. It then runs back to the cylinder where it came from. These kinds of reflections are called second-order reflected waves. There are even higher-order reflections, but their significance are usually negligible (Watson & Janota, 1984).

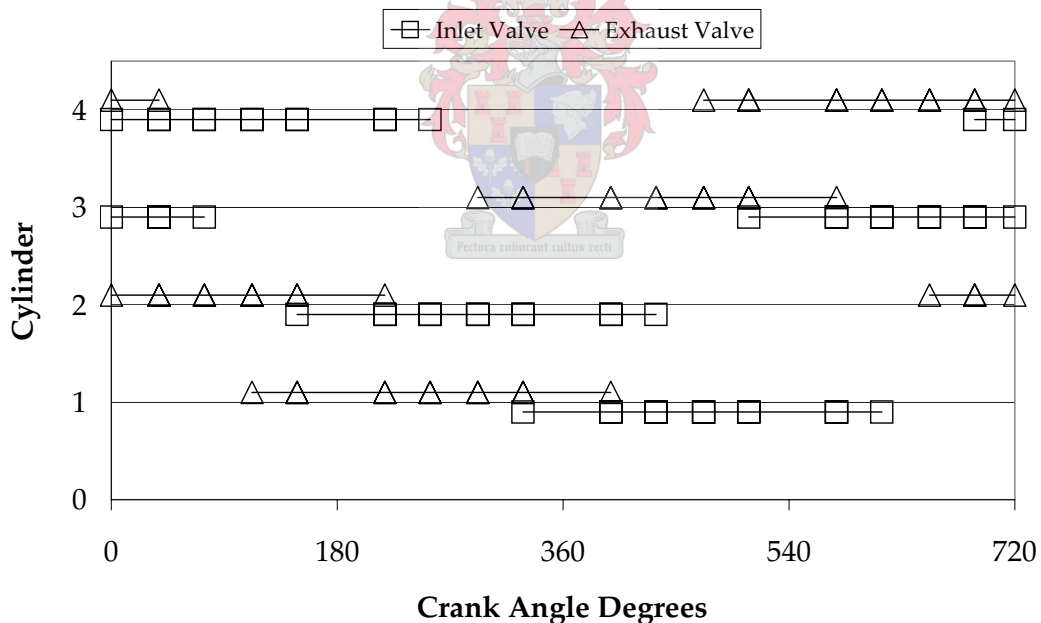


Figure 5-2 Four-cylinder engine's valve timing (firing order 1-3-4-2)

The question may arise: how is pulse interference overcome? The most obvious way is by making sure that the exhaust valve overlap period is shorter than the time needed for a pressure wave to travel from one exhaust port to the next. This means that a very short valve open time must be used or very long exhaust runners must be used. Both cases could cause serious restriction to the breathing ability of the engine.

Another way of overcoming pulse interference is by grouping the cylinders together in such a manner that there is no exhaust valve overlap on the grouped cylinders. From Figure 5-2 it can be seen that there is no exhaust overlap between cylinders 1-4 and 2-3. Thus the best way would be by grouping these cylinders together. Joining the two groups of 1-4 and 2-3 together might again result in interference, but if a twin-entry turbine is used pulse interference can be substantially reduced or even eliminated. The disadvantages of twin-entry turbines are that they are more expensive and, due to the lower frequency at which the pulses arrive at the entries, they usually operate at a slightly lower efficiency than a single-entry turbine.

5.1.2. Exhaust Manifold: Concept 1

Concept 1 shown in Figure 5-3 is the manifold that is the easiest to manufacture, simple to model, easy to assemble and it fits in the confined space. The manifold volume is small, but with short bends and sharp corners, it is not the ideal pulse system. Owing to the small volume, one will be able to harness some of the pulse energy. The disadvantage of such a manifold is that pulse interference is unavoidable. The flow path from cylinder #4 to the turbine entry makes a very sharp turn and a collector is absent at the transition from the three-into-one junction.

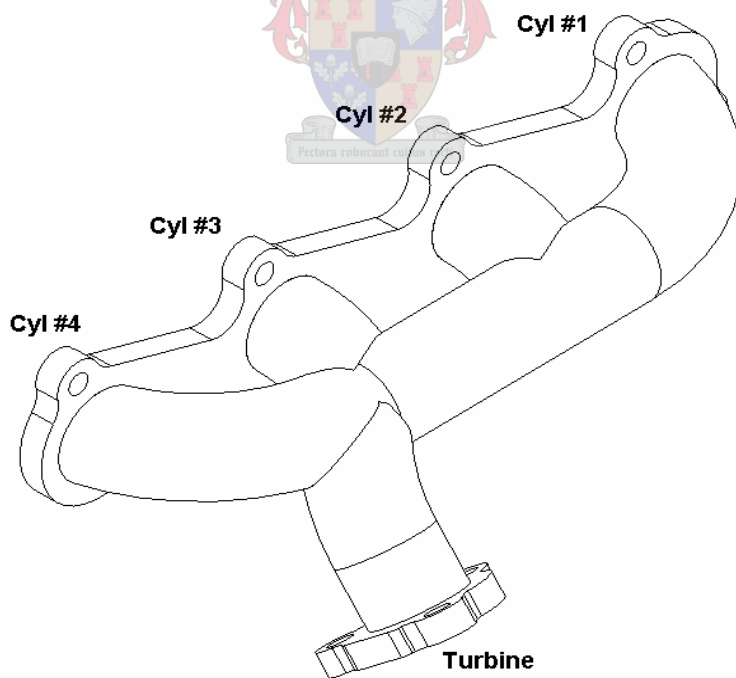


Figure 5-3 Exhaust manifold: Concept 1, CAD model

The pipes used to make up concept 1 are mild steel, have an inside diameter of 34.9 mm and a wall thickness of 1.6 mm. This was a standard pipe size for exhausts. The shortest centreline radius available on bends was 75 mm. The flange that fitted against the engine was laser-cut from mild steel and is 10 mm thick. The flange that fitted against the turbine was also made from 10 mm mild steel, but was hand cut. Both flanges were skimmed after welding to ensure flatness.

The strength calculations were based on an internal peak pressure of 2.5 bar absolute, the turbocharger weighs 5 kg and the exhaust manifold temperature was assumed to be 700 °C. A safety factor of 4 was implemented due to the fact that the exact temperatures and instantaneous pressures were not known. Material properties of mild steel at high temperatures can be found in Table 5-1.

Table 5-1 Material Properties of Mild Steel at High Temperatures (British Iron and Steel Research Association Metallurgy, 1953)

Temperature [°C]	Yield Strength [MPa]	Young's Modulus [GPa]
600	80	36
700	37	16.5
800	18	8
900	7	3

The manifold could be simplified by considering a thin-walled pressure vessel with internal pressure P_i , which is clamped in on the one side and a force on the other similar to the classic cantilever example (Figure 5-4).

The stresses for each case (pressure vessel and cantilever) were calculated using Eq 5-1 and Eq 5-2 and then added to give the total stress in the Z-direction.

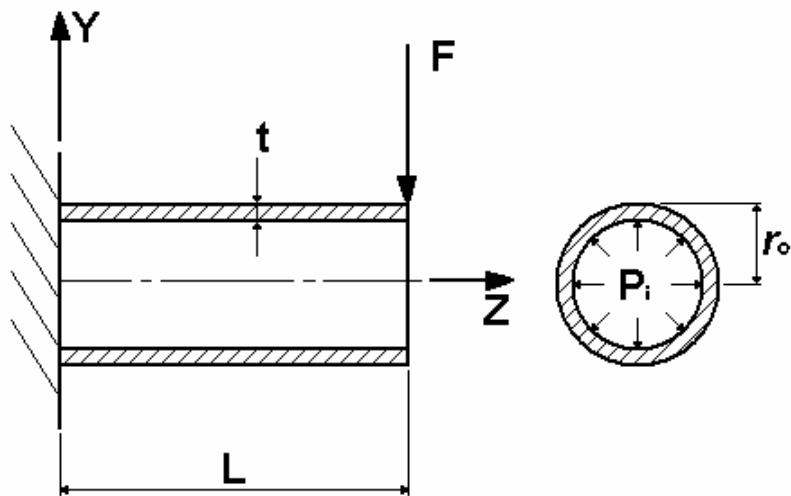


Figure 5-4 Exhaust Manifold Force Diagram

The yield strength in Table 5-1 was then divided by the total stress calculated to give the safety factor.

$$\sigma_{z,P} = \frac{P_i \cdot (r_o - t)}{2t} \quad \text{Eq 5-1}$$

$$\sigma_{z,F} = \frac{F \cdot L \cdot r_o}{I} \quad \text{Eq 5-2}$$

Where:
 P_i is the internal pressure (2.5 bar)
 r_o is the outside radius (19.05 mm)
 t is the wall thickness (1.6 mm)
 F is weight of the turbocharger (5 kg \approx 50 N)
 L is the distance from the clamped edge of manifold to the centre of mass of the turbocharger (103 mm)
 I is the second moment of area of the cylinder about an axis through the centre.

The safety factor was found to be 9; this was larger than what was considered to acceptable for a temperature of 700°C. Thus higher temperatures were also considered. For a temperature of 800°C the safety factor was calculated to be 4 and for a temperature of 900°C the safety factor was found to be 2. Due to the engine durability criteria, exhaust temperatures above 900°C are avoided during the calibration of the engine. Thus assuming a 200°C difference between the gas and the wall temperature it can be concluded that this manifold will be strong enough.

5.1.3. Exhaust Manifold: Concept 2

Concept 2 (Figure 5-5) may initially appear simpler, but is actually much more complex. Simple pulse converters are used at each 2-1 junction, thus totalling 3 pulse converters. The advantage of such a manifold is that short runners are used; thus the manifold volume is smaller than that of concept 1 and consequently more of the pulse energy could be harnessed. The disadvantages of concept 2 are that it is more complex, thus more difficult to manufacture, and assembly would be complicated due to the placement of the bolts at the turbine entry.

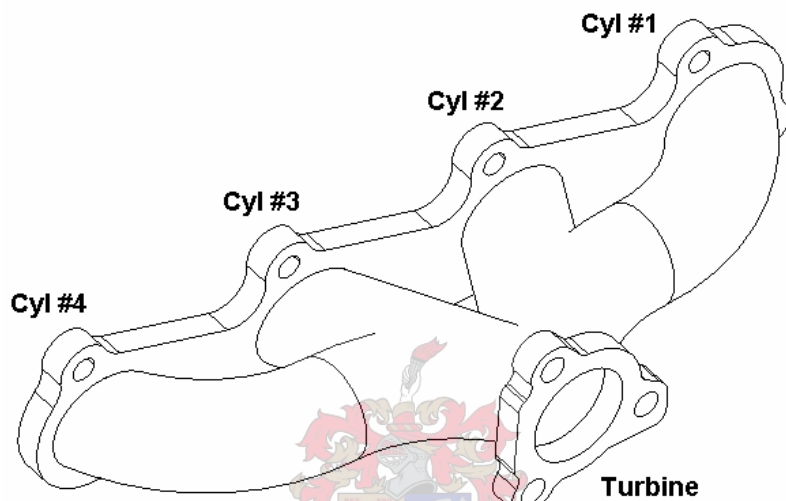


Figure 5-5 Exhaust Manifold: Concept 2, CAD model

The simple pulse converters were based on a nozzle area ratio of 0.65 and the throat area ratio 0.68. This combination was chosen so that the minimum nozzle area specified by Watson and Janota (1984) was used and the throat area was the same as the turbine entry. Strength calculations were not done on this concept, because it would not be manufactured. It was, however, also modelled in WAVE to compare its performance with concept 1 and the results are presented in 4.2.2.

5.2. Intake Piping Design

The intake piping includes all the pipes from the air-cleaner to the compressor and from the compressor to the intake manifold. The major challenge was packaging and the strength of these pipes was never a concern, thus no strength calculations will be shown.

5.2.1. Pre-Compressor Pipe

It was decided that the standard air-cleaner would be used, since it gets fresh air from the front of the engine bay, thus it would be the coolest air. Packaging was mainly done on the actual car by building a prototype with cardboard and then altering as was necessary. Due to the complexity and packaging of the whole engine and where the pipe fits into the engine bay, it cannot be shown on a photograph, but the CAD model can be seen in Figure 5-6. The pipe sizes were pre-determined, since the pipe that comes from the air-cleaner is fixed and the compressor intake diameter is fixed, thus a connection pipe that would fit into the engine bay and have the above-mentioned diameters needed to be designed.

After fitting and measuring different combination and configurations the best and easiest solution was found. It was made up of a straight section with a 60 mm outside diameter (OD), a short radius 90° bend, and a reducer to 40 mm OD, since that is the inlet diameter of the compressor. The short radius bend was only available in stainless steel, with an OD of 63 mm and centreline radius of 100 mm. The straight pipe had to be flared to join properly to the bend. A suitable standard reducer could not be found, thus it had to be made from a solid round bar, thus reducing from 63 mm to 40 mm. All the parts were welded together and painted for protection against corrosion.

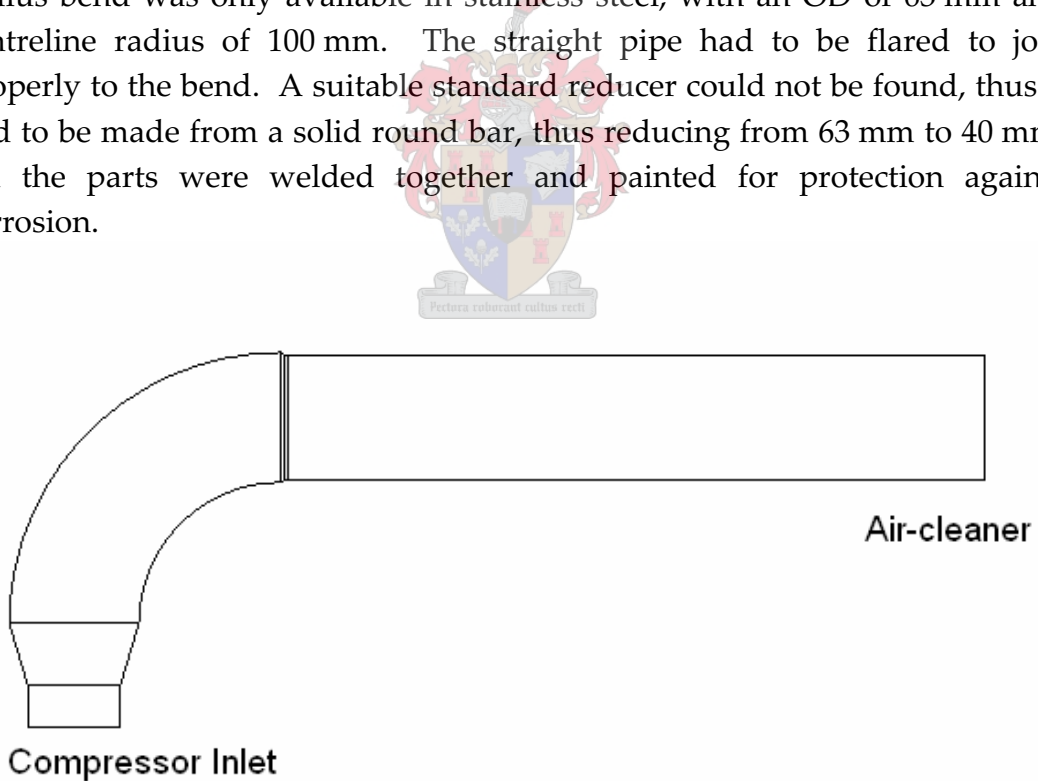


Figure 5-6 Pre-Compressor Pipe

5.2.2. Post-Compressor Pipe

The post-compressor pipe extends from the compressor outlet to the intake manifold, where it joins up with the throttle body. Since the compressor outlet is very near to the exhaust manifold, rubber hose that could withstand the pressure would not be able to withstand the temperature. Thus the second choice of material for the pipe was mild steel. The outlet diameter of the compressor is 50 mm OD and the throttle body has an OD of 60 mm. To keep the pressure drop over the post-compressor pipe as small as possible, it was decided to use the biggest diameter (60 mm) for as much as possible of the pipe.

On the compressor side it was necessary for a very sharp bend to clear and get as far as possible away from the exhaust manifold. The only option was to cut two 50 mm pipes at an angle and then weld these two together. This, however, leaves a very sharp bend with sharp corners. Therefore it was decided to put 3 guide vanes in the bend to direct the flow. Guidelines on calculating the pressure drop for such bends were found in Kröger (1998), but no guidelines for the design were available. Van der Spuy (2004), a specialist in turbomachinery and compressible flow, was consulted. He suggested the layout and size of the guide vanes. A cross-section of this bend is shown in Figure 5-7.

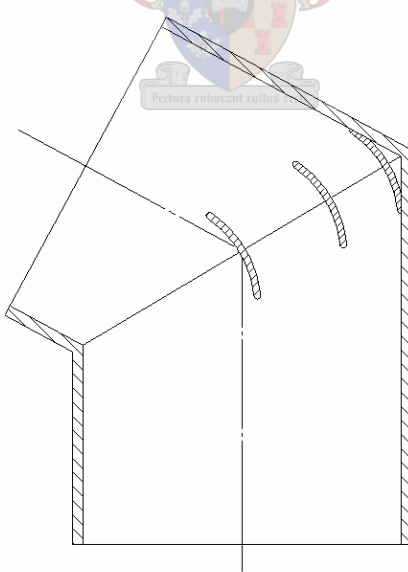


Figure 5-7 Guide Vanes in a Sharp Bend

The complete pipe is composed of the sharp bend followed directly by a diffuser from 50 mm to 60 mm OD. The diffuser follows into a 90° bend, then a straight section and is completed with another 90° bend which fits against the throttle body. The CAD model of the complete post-compressor pipe is shown in Figure 5-8.

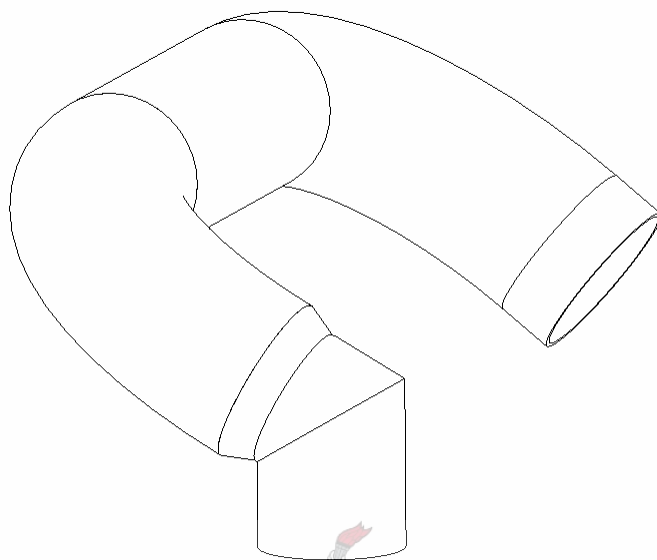


Figure 5-8 Post-Compressor Pipe

Special high-temperature silicon hose with inside diameter (ID) 50 mm and 60 mm respectively was used to connect the compressor outlet to the post-compressor pipe and the post-compressor pipe to the throttle body. The hoses were secured with hose clamps on each side.

The post-compressor pipe had to withstand the boost temperatures and pressures. In this case the boost pressure was never above 1 bar and the boost temperature never above 100°C. Thus it was clear that a mild steel pipe with wall thickness of 1.6 mm would never operate anyway near its yield strength.

5.3. Variable Wastegate Actuator Design

Since electronic boost control is a complex matter on its own, the need for an actuator that can easily be adjusted to accomplish different boost pressures was identified. The requirements of such a variable wastegate actuator (VWA) were that both the spring stiffness and pre-load on the spring must be independently adjustable.

Different concepts were evaluated and the final concept is shown in Figure 5-9. The spring stiffness can be adjusted by adjusting the number of active coils and the preload can be adjusted by adjusting the locknuts on the rack as on a normal turbocharger with a wastegate configuration.

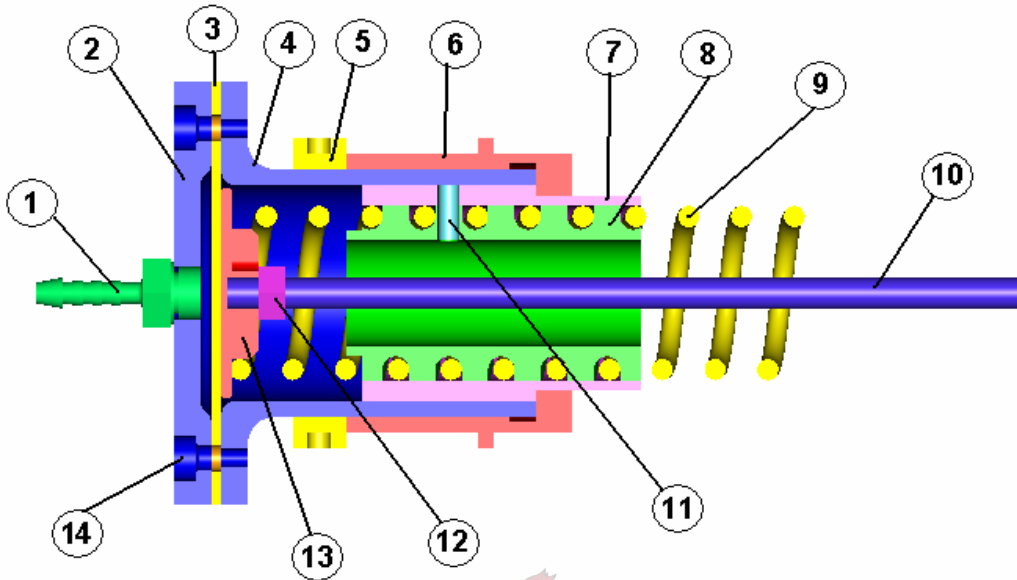


Figure 5-9 Variable Wastegate Actuator

The working and function of the parts are discussed with reference to Figure 5-9. Pressure is supplied to the actuator via the hose tail (1) and acts as the input to the actuator. Part 2 forms a lid for the pressure chamber. Part 3 is the diaphragm, which deflects to push the plunger (13) that is connected to the rack (10), which acts as the output and opens the wastegate. The rack screws into the plunger and is locked with a locknut (12). The spring (9) was ground flat on the plunger's side and the tip was turned radially inward to form a tip that fits into a slot in the plunger. This stops the spring from turning independently of the plunger. The combination of parts 7 and 8 locked together with a grubscrew (11) forms an adjusting mechanism to adjust the number of active spring coils. Parts 4 and 6 screw into each other to adjust the distance between the diaphragm and part 8. This adjustment allows independent setting of the number active coils and the amount of preload on the spring. Parts 4 and 6 are locked together with a locknut (5). The lid (2), diaphragm (3) and part 4 were all held together by six cap screws.

The VWA was tested with different diaphragms. Since the diaphragm must deform to push the plunger and wastegate open, it is necessary for it to have a high level of elasticity, withstand gasoline fumes and be able to withstand high temperatures. This implies that the opening characteristic of the wastegate is not only dependent on the spring stiffness, but also on the characteristics of the diaphragm. The combined characteristics of the spring and diaphragm caused the relation of rack travel against pressure to be non-linear as can be seen in Figure 5-10. The diaphragm was made of rubber. This rubber was made from a mixture of natural and synthetic rubber. This rubber diaphragm was not resistant to gasoline; however, the little that it would be exposed to would not harm it for the duration of a test. The wastegate actuator was tested with two different rubber compounds. Compound 1 was red and 3 mm thick while compound 2 was black and about 1.5 mm thick.. The data presented in Figure 5-10 were measured with a very stiff spring. Actual testing was done using compound 1.

Commercially available wastegate actuators that are supplied with the turbocharger do not rely on the diaphragm to deform. In fact, the diaphragm is non-elastic. The diaphragm is preformed and looks like a woven material coated with some kind of rubber to make it airtight. The actuator's construction is such that the diaphragm moves without elastic deformation.

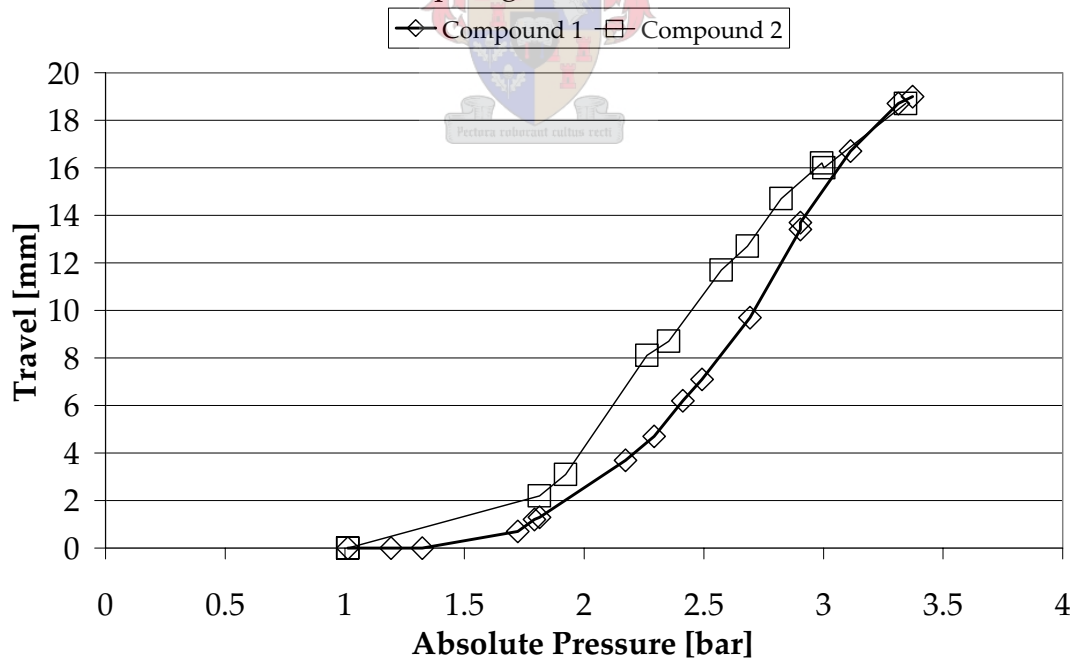


Figure 5-10 VWA Diaphragm Test

5.4. Oil Feed and Return lines

Oil must be supplied to the turbocharger's bearings and then be returned to the engine's sump. The return line must be free flowing and rely on gravity only, since any back pressure could result in a situation where the oil is forced past the turbine and compressor's seals. This could cause permanent damage to the seals and the oil is then burned in the turbine or induced into the engine intake system.

On CI engines this situation could result in engine runaway, which could cause serious damage or even total destruction of the engine. The oil induced into the intake would be burned, because there is always excess air in the combustion chamber and the combustion pressures would be much higher than in SI engines. If more oil is burned in the combustion chamber, the power extracted by the turbine increases and the developed boost pressure will increase, causing even more air to be induced, leading to runaway. The engine could keep on running on engine oil, even if the fuel supply is shut-off. The only way of stopping this is by cutting off the air supply to the engine. This risk does not apply to SI engines where oil ingestion leads to engine fouling and excessive smoke emission.

According to the turbocharger manufacturer's specifications (APPENDIX B), the maximum oil flow through the bearings is 1.8 litres per minute if 20W-20 oil is used at 4 bar and 100°C, while the turbocharger spins at 150 000 rev/min. Adding a safety factor of 1.5, the system that had to be designed must be able to deliver 2.7 litres of oil per minute to the bearings and return it to the sump.

The thread in the hole for the oil supply on the turbocharger is M10 parallel thread. Using a double ferrule fitting, the biggest steel pipe that would fit into this fitting is 6 mm OD (4 mm ID). This pipe has a pressure rating that is much higher than the operating oil pressure of the engine. The oil supply was taken from the clean oil side on the oil filter adapter. An aluminium bush was welded onto the adapter and threaded to accept the same fitting as on the turbocharger. The oil filter adapter is on the opposite side of the engine as the turbocharger, thus the supply line was routed around the engine. The pipe was bent by hand with the help of a pipe bender. The shortest path was from the adaptor, against the engine block behind the intake manifold around the back (gearbox's side) of the engine to the turbocharger. The pipe was secured to the engine with two specially made pipe clamps and the ends were secured into the fittings. This configuration was secure and there were no long pieces of unsupported pipe that could vibrate and result in a fatigue failure.

The return line was a little more complicated, since back pressure build-up could have significant consequences as described earlier. There were two options for returning the oil to the sump. The first was through the drain plug of the sump and the second was to return it above the oil level via a hole in the sump. The problem with the first configuration was that the oil was returned below the level of oil inside the sump. Thus the head (h_1) of oil build-up in the return line is proportional to the resistance to flow through the connection at the drain plug. A schematic of the situation is shown in Figure 5-11.

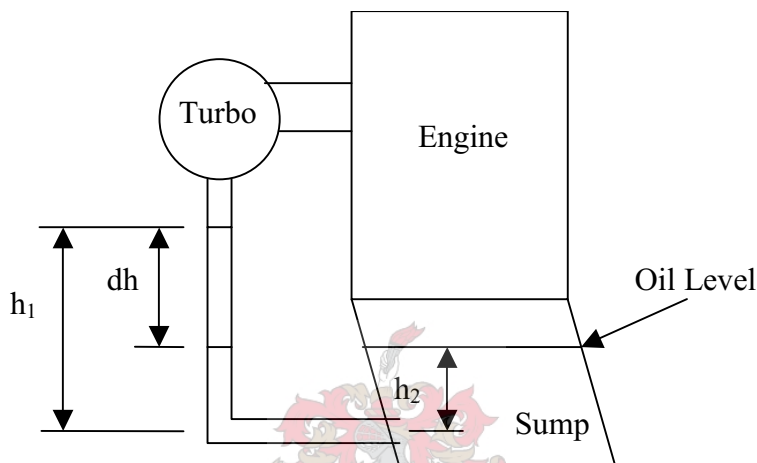


Figure 5-11 Oil Return Schematic

An experiment was done with the connection as it would be on the actual engine and water was used as the fluid. The height of build-up (dh) was measured for different flow rates. The build-up height (dh) could be related to the volume flow rate by Eq 5-3 and assuming that the system was in equilibrium.

$$dh = h_1 - h_2 - \frac{1}{2g} \left[\frac{\dot{Q}}{A} \right]^2 \quad \text{Eq 5-3}$$

Where: \dot{Q} = Volume flow rate [m^3/s]

A = area of the pipe [m^2]

The flow rate for oil was then calculated by assuming that the Reynolds number must be the same. Thus the flow rate for oil can be calculated according to Eq 5-4.

$$\dot{Q}_{oil} = V_{H_2O} \cdot \frac{\rho_{H_2O} \cdot \mu_{oil}}{\rho_{oil} \cdot \mu_{H_2O}} \quad \text{Eq 5-4}$$

The build-up height for oil could therefore be calculated by using Eq 5-3. It was found that there was sufficient space for build-up when the oil was hot, but when the oil was cold the viscosity was too high and the height (dh) was larger than the height of the turbocharger above the oil level, there would be a pressure build-up in the bearing housing.

Therefore the second option of returning the oil to the sump via a hole above the oil level was the most appropriate solution. The sump had to be taken off in order to weld a bush to the sump, after which it was drilled and tapped. These operations could not be done on the engine, since the drilling and tapping process would cause burrs to fall into the sump. Removing the sump from this specific engine involved separating the engine and gearbox in order to remove two of the bolts securing the sump to the engine block.

The size of the oil outlet on the turbocharger is 10 mm. Thus it was decided to use a pipe with connections that have a minimum diameter of 10 mm. A custom fitting was made up from a hose-tail connection welded to a flat piece of mild steel to form a flange. This connection could then be bolted to the turbocharger and connected to a pipe. The other end of the pipe was then connected to the fitting on the sump. This pipe was braided hydraulic hose with ID 13 mm, which could withstand up to 10 bar at a temperature of 200°C. This hydraulic hose was secured at each end with a hose clamp. The fittings used had a minimum inside diameter of 11 mm, thus the smallest opening was that of the turbocharger's oil outlet. The system would therefore be safe and would not cause back pressure on the bearing housing.

5.5. Fuel System Upgrade

The standard injectors on the engine are rated at 110 gram per minute at a working pressure of 2.7 bar. From initial calculation of target power, required fuel and necessary airflow, it became evident that bigger injectors were needed. The local suppliers of BOSCH equipment were contacted and 4 injectors of 160 gram per minute at 3 bar were made available. The standard fuel pressure regulator was also replaced with a 3 bar regulator. This upgrade was able to fulfil the engine's fuel requirement.

5.6. Exhaust System Upgrade

The initial idea was to use the standard exhaust system, since the package was designed in such a way that the coupling from the turbocharger is exactly where the connection on the standard engine is between the manifold and the exhaust system. After the first tests with minimal boost it was found that the exhaust back pressure went above 50 kPa, which was deemed to be too high, thus it was decided to use a bigger exhaust. A free flow exhaust was available, which has been used in a previous project. This exhaust was fitted without any modification being necessary. With the free flow exhaust the back pressure never went above 35 kPa.

5.7. Experimental Set-up

The engine was set up on a test bed in a test cell with an Eddy-current dynamometer to absorb energy from the engine. The calibration of the load cell on the dynamometer was checked before and after each test. The fuel consumption was measured with an AVL gravimetric fuel-flow meter. The airflow through the engine was measured with a Ricardo flow meter. Two calibrated orifice flow meters were used to measure the mass flow of coolant and water through the engine and oil cooler respectively. All temperatures that are above 300°C were measured with type-K thermocouples and all below 300°C with type-J. The reason for using type-J thermocouples is their higher sensitivity at low temperatures.

The engine was fitted with a calibration ECU, thus the calibration maps could be adjusted from a computer with the ECU calibration software installed. All measuring channels were fed into a programmable logic controller (PLC) that was connected to another computer with ETA (Engine Test Automation) software installed. ETA is a software package that can display and save the measured channels as well as control everything from coolant temperature, air temperature to the engine's torque and speed according to user-defined set points.

All engine tests were carried out at steady-state conditions. The engine speed or torque was adjusted and readings were only taken after a stabilisation period, when all temperatures and pressures had reached equilibrium. This usually took about two to five minutes depending on engine operating conditions. Data were then saved at one-second intervals for a duration of 30 seconds. These 30 data points were then averaged to give one result at a single engine speed or load.

5.7.1. Combustion Analysis

In order to calculate the combustion heat release and burn duration, the cylinder pressure history must be known. Cylinder pressure is usually measured with a piezoelectric pressure transducer. This type of transducer contains a quartz crystal. One end of the crystal is exposed through a diaphragm to the cylinder pressure; as the cylinder pressure increases, the crystal is compressed and it generates an electric charge, which is proportional to the cylinder pressure. A charge amplifier is then used to produce a voltage proportional to this charge. Accurate pressure versus crank angle data can be obtained with these systems provided the following steps are adhered to:

1. The correct reference pressure is used to convert the measured pressure signal to absolute pressure;
2. The pressure versus crank angle, or volume, phasing is accurate to within about 0.2° crank angle (CA);
3. The clearance volume is estimated with sufficient accuracy;
4. Transducer temperature variations, which can change the transducer's calibration factor, due to variation in wall heat flux during the engine cycle are held to a minimum (Heywood, 1988).

In this project a special spark plug fitted with piezoelectric pressure transducer was used. These transducers are known to have a limited accuracy and are not recommended for very accurate thermodynamic analyses. Given the lack of an available instrumented cylinder head and related transducers, the spark plug transducer was the only option for this study. For the purposes of this study, where cylinder pressure and burn rates for the substantially different NA and turbocharged versions of the engine were measured and compared, the spark plug transducer was adequate to indicate major differences. However the spark plug transducer would not be adequate to indicate minor differences in pressure or burn rates.

A variety of indexing systems for the measuring of the position of the crankshaft are available. The actual system comprised of an inductive pick-up and a toothed wheel. The toothed wheel had 60 equally spaced teeth, but 2 teeth were removed to create a reference mark on the wheel. A USB (Universal Serial Bus) MicroDAQ was used as data-acquisitioning system together with WaveView™ for Microsoft® Windows™. The maximum sampling frequency was 250 kHz on one channel. Thus, sampling two channels effectively halved the maximum sampling speed. It was decided that the same sampling speed in terms of degree CA would be used at all engine speeds, given the maximum sampling frequency of 125 kHz per channel the fastest possible would be three samples per degree CA and the sampling time was adapted to capture at least 300 engine cycles.

A dedicated software program post-processed this data to provide a crank angle referenced pressure curve. This program called PostWave was developed by Van der Weshuizen, H J (2003). The offset between the true TDC and the reference mark on the indexing wheel was determined by plotting the logarithm of the measured cylinder pressure versus the logarithm of the cylinder volume for a motored trace. The lines must be straight with no curvature, and have as little area as possible between them, but there must be no cross-over between the two lines. A graph with the correct offset can be seen in Figure 5-12. This motored test was done at low MAP and by nature of the logarithm, the pumping loop appears exaggerated.

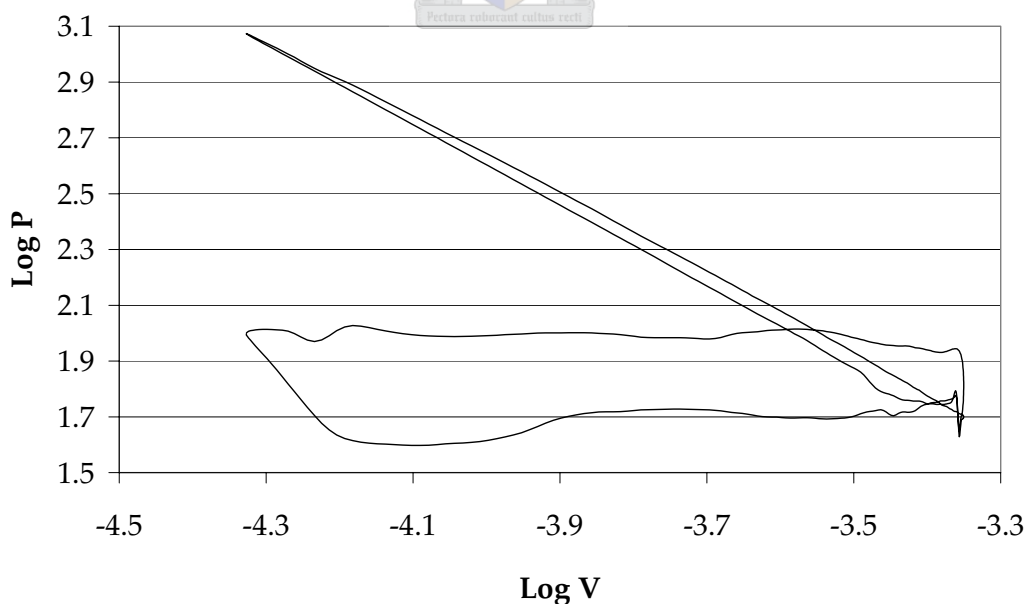


Figure 5-12 LogP-LogV of motored test

RACER, a program implementing a simple single-zone, fully mixed model, type of heat-release analysis, as described by Gatowski, Balles, Chun, Nelson, Ekchain and Heywood (1984) and Heywood (1988) and programmed by Moran, D P, *et al* (1997), was used for the determination of the combustion heat release from the measured pressure data. The basic analysis calculates a rate of combustion, which is in units of rate of energy release (Joule/ $^{\circ}$ CA). From this other useful quantities can be calculated which aid the description and comparisons of combustion processes. Two such quantities, namely burn duration and the 50% burn point, were of interest since they are needed in the WAVE simulations as described in section 3.4.2.

The burn duration used in the simulation is 10% to 90%, which can be defined as the angle through which the crank turns from the point when 10% of the mass was burned until 90% of the mass was burned. The 10% to 90% burn duration was preferred because it eliminates the uncertainty which results from the asymptotic nature of the departure and approach to the horizontal, where zero heat release occurs, on the burned mass fraction curve. Other popular groups are 2% to 98% and 5% to 95%. The 50% burn point is the crank angle when 50% of the mass was burned. This gives an indication of the combined effect of ignition timing and burn duration.

In Figure 5-13 the calculated cumulative combustion heat release is compared to that predicted by WAVE simulation ("Sim"). The curve designated "RAW" is that calculated by RACER. As can be seen, there is an increasing offset from zero before actual ignition in the calculated heat released until about 10° after TDC. This was due to an offset error that exists on the burn rate curve. This offset is then integrated and thus continues to increase. This phenomenon was witnessed at all speeds and can be attributed to the specific heat ratios and conduction constants in the heat release model. This did not affect the results of RACER, since RACER's model takes into account that no heat can be released before ignition. Thus burn rate can be scaled in such a way that the combustion and hence heat released only starts after ignition. Integrating the burn rate from ignition onwards, the "Scaled" curve is obtained as shown in Figure 5-13. This was only done for the purpose of illustration and does not affect the burn duration and 50% burn point values calculated by RACER.

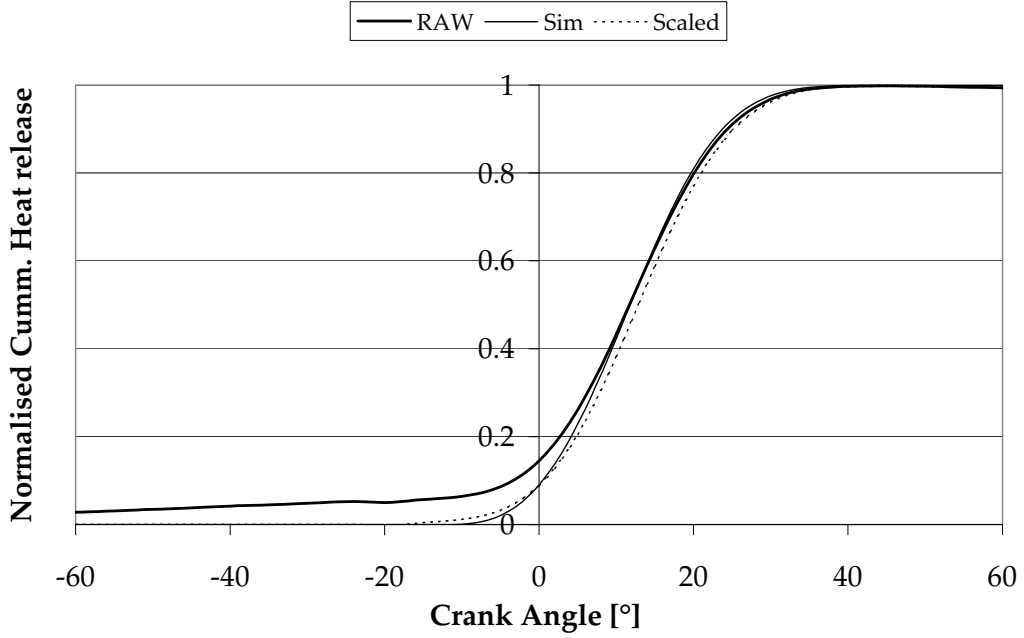


Figure 5-13 Normalised Cumulative Heat Release (NA engine, WOT at 4000 rev/min)

Thus it can be seen that, if the Wiebe exponent with the value of 2 as proposed by Heywood (1988) is used, the correlation between the cumulative heat released as calculated by RACER and that simulated with WAVE is good (see Figure 3-15 for simulation with different Wiebe exponents).

5.7.2. Power Correction

The measurement of the power output from internal-combustion engines and the correction for atmospheric conditions is a broad matter as there are many different standards. The most common standards are the ECE, SABS, SAE and DIN. The differences between these standards are highlighted and discussed by Kingwill (2000). See APPENDIX C for the reference values and correction formulae of the ECE standard that is applied throughout this thesis.

The air during testing had a relative humidity ranging from 28% to 68%. The torque and power measured were adjusted and the corrected values are presented for the NA engine tests. However, the standards do not apply to turbocharged SI engines, thus the uncorrected values are presented when comparing turbocharged results. Since the simulations were run at the reference conditions no correction were applied to the simulated results.

5.7.3. Exhaust Gas Measurement

A thermocouple placed in a pipe with gas flowing as shown in Figure 5-14 does not directly measure gas temperature. The temperature of the tip of the probe is at an equilibrium point between the gas temperature and the wall temperature which depends on the convective heat transfer from the gas, radiation heat transfer to the (cooler) walls and conduction along the thermocouple axis to the walls.

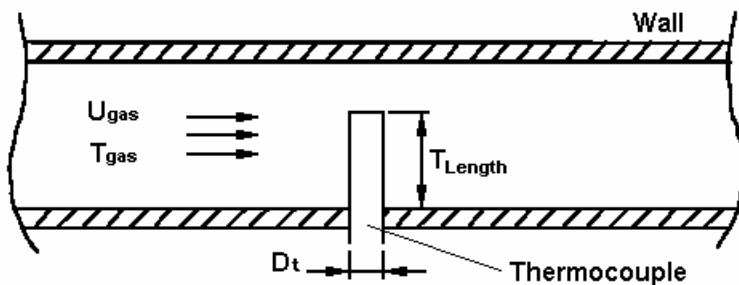


Figure 5-14 Thermocouple Set-up (Ricardo, 2002)

The contribution of conduction to the heat transfer is usually small and can be neglected. The different components of heat transfer from the probe are given by (Ricardo, 2002):

$$Q_{conv} = h \cdot A_{tip} (T_{gas} - T_{tip}) \quad \text{Eq 5-5}$$

$$Q_{rad} = \varepsilon \cdot \sigma \cdot F \cdot A_{tip} (T_{tip} - T_{wall})^4 \quad \text{Eq 5-6}$$

Where: h = convective heat transfer coefficient [W/m²·K]

A_{tip} = area of thermocouple tip [m²]

T_{gas} = gas temperature [K]

T_{tip} = thermocouple tip temperature [K]

T_{wall} = wall temperature [K]

ε = emissivity ($\gg 0.8$)

σ = Stefan-Boltzmann constant (5.669E-08 W/m²·K⁴)

F = radiation view factor to walls (1.0)

An energy balance between convection and radiation shows that heat radiation can produce errors in exhaust gas measurements of up to 50 K (Ricardo, 2002), therefore the thermocouple temperature will read too low. In unsteady flows there is a further problem, especially in comparisons between measurements and simulation. The simulation prints out cycle-averaged values of mass flow-averaged temperatures in the ducts. However, the thermocouple reading, which is also an average value, represents a different average, defined by the averaging of the above equations. This produces even larger differences between the simulated predictions and measurements. The thermocouple model available in WAVE allows the radiation and convection to the thermocouple to be modelled to enable better comparison with test results.

This thermocouple model was used to verify the phenomenon witnessed in testing where the thermocouples in the exhaust ports measure a lower temperature than further downstream in the exhaust, where all four exhaust runners joined. An initial possibility was that this might be due to the effect of post-combustion, which is combustion taking place in the exhaust, but tests with a very lean air-fuel mixture showed exactly the same phenomenon. Therefore post-combustion could not be the cause.

The results shown in Figure 5-15 are the averaged exhaust port temperatures compared to the downstream (ds) temperature for both simulated and actual tests. These data were recorded during a power curve on the NA engine with an exhaust manifold which had surface mount thermocouples to measure the actual wall temperature.

As can be seen, the difference between the average port and downstream temperatures is smaller at low engine speeds. The frequency of pulses downstream of the 4 into 1 junction is four times higher than in the ports. Thus at high engine speeds the thermocouple in the port measures a lower average temperature due to convection and radiation heat loss to the cooler walls as it is exposed to hot exhaust gas pulses for a shorter period of time than the downstream thermocouple that is basically in a continuous flow of exhaust gas. At low engine speeds, on the other hand, the heat loss to the exhaust pipe as the gas flow from the port to the downstream thermocouple, plays a bigger role than the convection and radiation losses at the port thermocouple and that is why the downstream measurement is closer to that measured in the port.

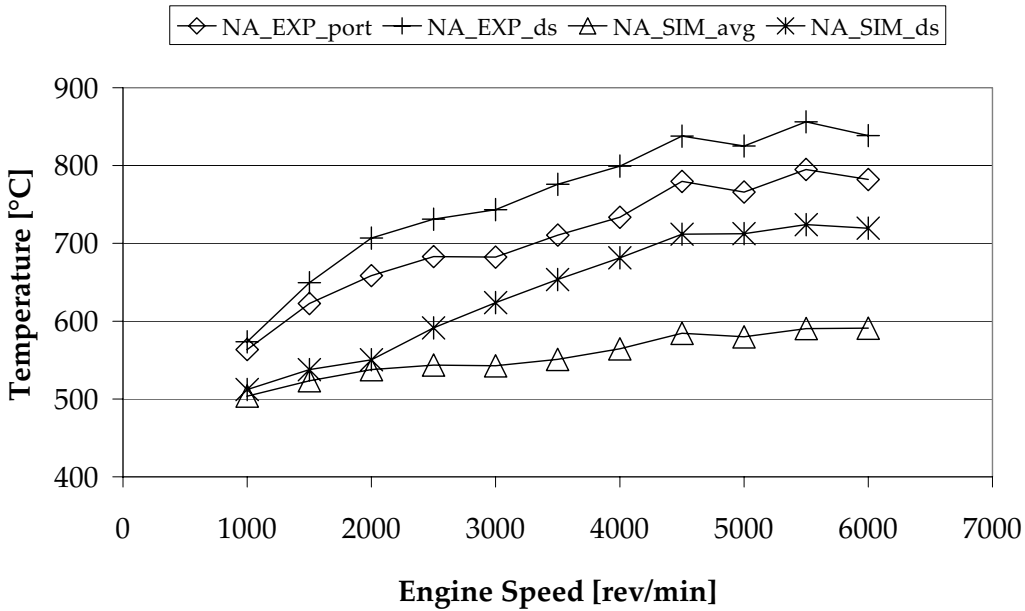


Figure 5-15 Exhaust Port versus Downstream Temperatures

In reality, measuring actual exhaust gas temperature would require that a long piece of exhaust is perfectly insulated and enough time must be allowed for the wall temperature to reach the same temperature as the gas. Only then can the thermocouple measure accurately.

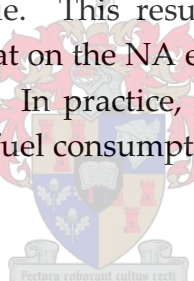
In practice it is unnecessary to measure the exact temperature of the exhaust gas, but one rather uses the same method of measuring to enable one to have results that are reliable and repeatable, but not absolute in terms of quantity. For this reason the thermocouples were always inserted deeper than halfway into the pipe, in order to eliminate conduction along the axis of the thermocouple.

This thermocouple model was not implemented in all the simulations, because the wall temperature was not measured in all tests and the accuracy of this thermocouple model relies on reliable wall temperature data. A wall temperature could be estimated, but using an estimate of the wall temperature together with the added complexity, which increased the simulation time, had no real significance. Instead the actual gas temperature values are presented and should therefore be higher than the measured results by an amount illustrated in Figure 5-15.

5.7.4. Engine Calibration

At WOT for the turbocharged engine, fuel loop and timing swing experiments were conducted to find the optimum timing and fuelling for maximum power at WOT. The experimental engine was fitted with a knock sensor. The ignition timing was advanced until the ECU detected knock and then it was retarded two steps. The step sizes in timing maps of the ECU software were roughly 1.25 degrees. The fuelling was then enriched if the exhaust temperatures were above 815°C, or if the exhaust temperature was below 815°C it was made leaner, until knock was detected or the limit on exhaust temperature was reached. This iterative procedure ensured that the optimum engine settings were attained, given the constraints of knock and exhaust port temperature. The NA engine data is presented as taken from a power curve run using the production ECU and settings.

During part load, the NA engine's lambda values were used for the turbocharged engine, if it was possible to reach these values subject to limiting the exhaust temperature below 815°C. The ignition timing was optimised for maximum torque. This resulted in ignition timing settings slightly more advanced than that on the NA engine, since the high octane fuel had a higher knock resistance. In practice, the lambda and ignition timing would be optimised for lowest fuel consumption at part load.



6. RESEARCH RESULTS

The objective of this thesis is to compare the developed turbocharged engine to the standard NA engine, but also to compare the simulated results against the actual measured results in order to answer the question as to whether 1-D flow simulation is adequate to predict engine performance for turbocharged engines.

The results presented in this chapter will firstly be concerned with the correlation between simulated and measured NA engine performance. Secondly, the turbocharged simulation results and actual turbocharged performance will be discussed and, thirdly, the turbocharged results will be compared to those of the NA engine.

6.1. NA Results: Simulation versus Experiments

When simulating and predicting engine performance, one can force the model to get the desired output, but then the input might not represent the actual set-up. A base model was available for the test engine. This model was used as a starting point and it was modified and refined to better represent the actual engine. It was found that the valve sizes were larger than on the actual engine. Changing the valve size directly affects the gas exchange process. A better correlation for volumetric efficiency could not be found thus the valve sizes in the base model were not altered. The proper way to calibrate the model would be to measure the actual flow coefficients on a flow bench, but it was not available for this study.

The base model was set up such that the throttle body is closest to cylinder #1 instead of #4, which was corrected. Other adjustments to the model included: updating the complete exhaust system, adjusting the air-fuel ratio to represent the actual measured data and setting the combustion parameters to that measure on the actual engine. The combustion is modelled based on the Wiebe correlation as presented in section 3.4.2. The input parameters are the 50% burn point and the burn duration (10% - 90%). These two parameters were calculated from measured data as explained in section 5.7.1.

Engine parameters, which were measured, are compared to the simulated predictions of brake torque, volumetric efficiency, airflow, maximum combustion pressure, motored in-cylinder pressure, exhaust backpressure, specific fuel consumption (SFC), intake MAP and intake manifold air temperature.

As can be seen in Figure 6-1 the predicted torque curve is nearly the same; however, the simulation predicts peak torque at 4000 rev/min as opposed to the actual torque peak at 2500 rev/min. Another aspect is that the dip in the actual torque curve is not evident in the simulation, where instead a hump is predicted. The maximum difference in torque prediction was 6 N·m which translates to an error of 4.6%.

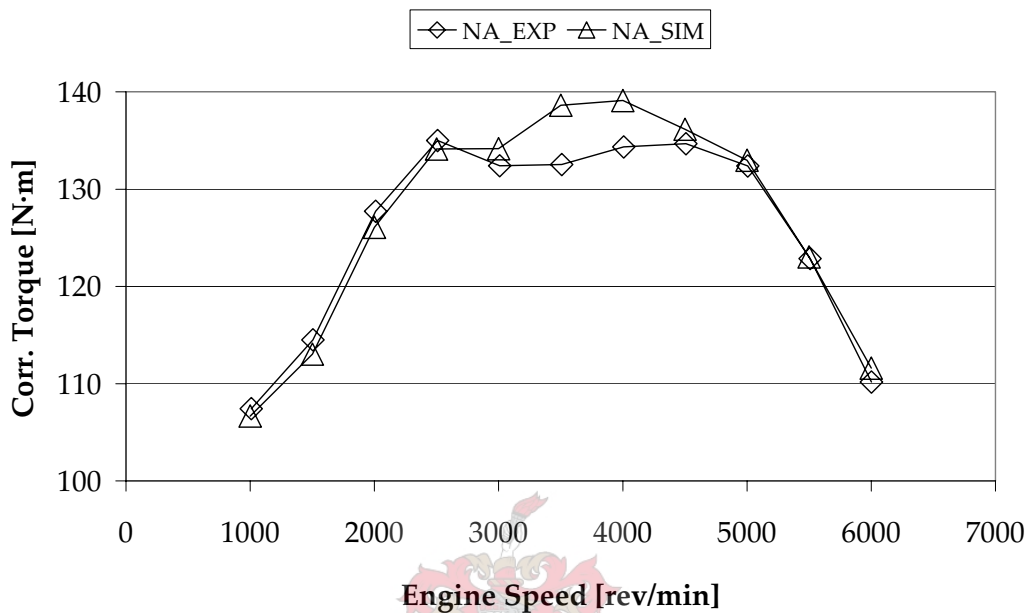


Figure 6-1 NA Simulation vs Experiment: Torque

This difference in torque can be explained by looking at Figure 6-2 and Figure 6-3, where the volumetric efficiency and air flow respectively are compared. The predicted volumetric efficiency and air flow is nearly the same as the measurements on the actual engine in the range from 3000 rev/min to 4000 rev/min, which is exactly the range where the torque hump is predicted. The simulation predicts more torque than is actually developed with similar airflow or volumetric efficiency.

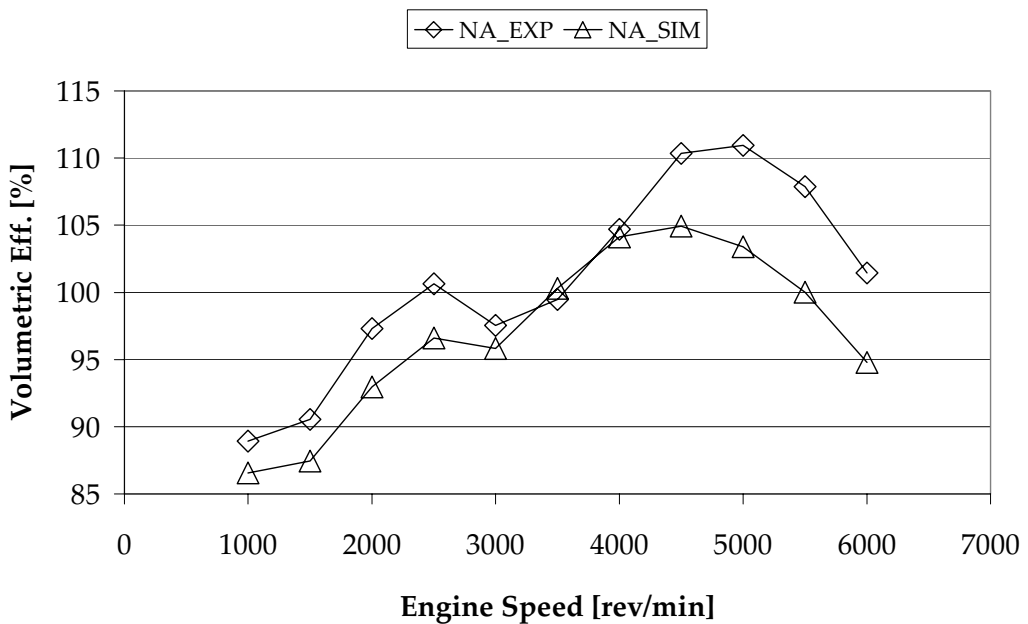


Figure 6-2 NA Simulation vs Experiment: Volumetric Efficiency

When considering the airflow, shown in Figure 6-3, in the same speed range, 3000 rev/min-4000 rev/min, it can be seen to be very much the same as opposed to the bigger offset at higher engine speeds. The difference at high engine speeds is again believed to be due to the valve flow coefficients that might not be representative of those on the actual engine. Thus the same trends are witnessed for both volumetric efficiency and air flow.

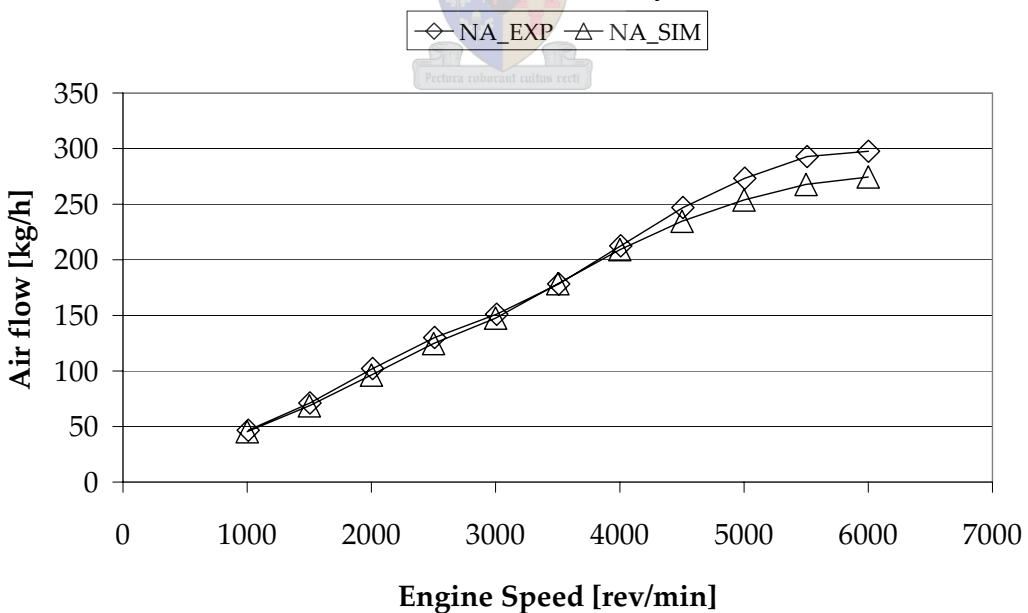


Figure 6-3 NA Simulation vs Experiment: Airflow

The fact that the engine simulation predicts more power from the same amount of airflow could be due to the fact that the simulation does not take blow-by into account. Blow-by may not only influence indicated performance, but also the gas pressure on the rings, which influences the friction and wear characteristics as well as the hydrocarbon emissions (Ferguson, 1986). Mass loss due to blow-by could then be used to explain the difference in peak combustion pressures as shown in Figure 6-4. The maximum difference in peak pressure is 15.4% at 1000 rev/min, with 14.8% at 3500 rev/min.

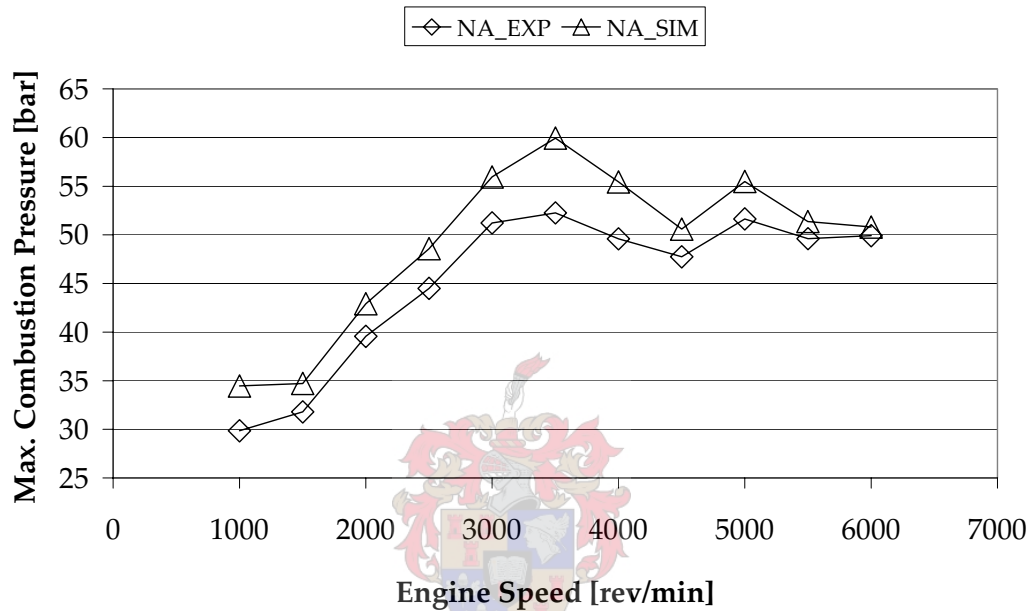


Figure 6-4 NA Simulation vs Experiment: Maximum Combustion Pressure

To try and illustrate the effect of blow-by, a measured pressure curve for a motored case is compared in Figure 6-5 to that predicted by simulation. The difference in peak pressure in the motored case can only be due to blow-by (assuming no measuring error was made), since the air intake pressure, temperature and airflow through the engine match those of the actual engine. The difference in motored peak pressure is 14.8%. Using the polytropic relation Eq 6-1 between volume, pressure and temperature and assuming isentropic compression with no heat transferred to the gas as it is compressed, the mass lost due to blow-by is 10%. Heywood (1988) states that mass lost due to blow-by is in the order of 1%.

$$\frac{T_2}{T_1} = \left(\frac{P_2}{P_1} \right)^{\frac{\gamma-1}{\gamma}} = \left(\frac{V_1}{V_2} \right)^{\frac{\gamma-1}{\gamma}} \quad \text{Eq 6-1}$$

Using the initial pressure, displacement volume and clearance volume and assuming no heat transfer from or to the gas, the actual peak pressure for the motored case is 13.3% lower and the simulation peak pressure is 1.7% higher than the pressure based on the polytropic relation respectively. The lower pressure measured in the actual engine can be justified by assuming the cylinder walls and piston to be at the same temperature as the engine coolant, thus 90°C, there would certainly be heat loss to the cylinder walls and piston. The polytropic relation predicts a gas temperature of 425°C at the end of compression. Thus it is expected that the gas temperature would be lower at the end of compression due to heat loss and thus resulting in a lower pressure.

The higher pressure predicted by the simulation can be attributed to the use of the same boundary conditions as for a fired case. Thus the cylinder walls and piston would be at a higher temperature than during a motored case and would cause heat transfer to the gas resulting in a higher temperature and pressure at the end of compression.

Therefore the discrepancy between the measured and simulated cylinder pressure could be attributed to a combination of heat addition and measurement error.

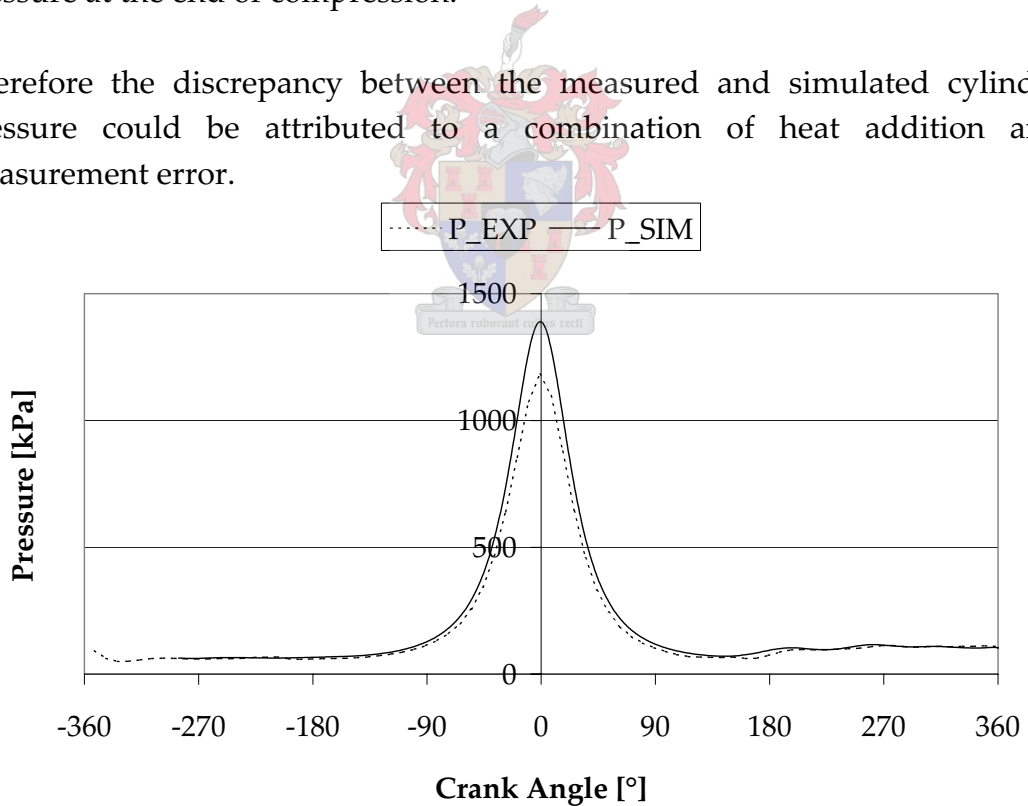


Figure 6-5 NA Simulation vs Experiment: Motored in-cylinder Pressure (1500 rev/min)

Since the exhaust system is not a complete model representing the actual exhaust, the orifice can be adjusted in order to give a good correlation between the exhaust backpressure as predicted and the actual measured data. This correlation is shown in Figure 6-6.

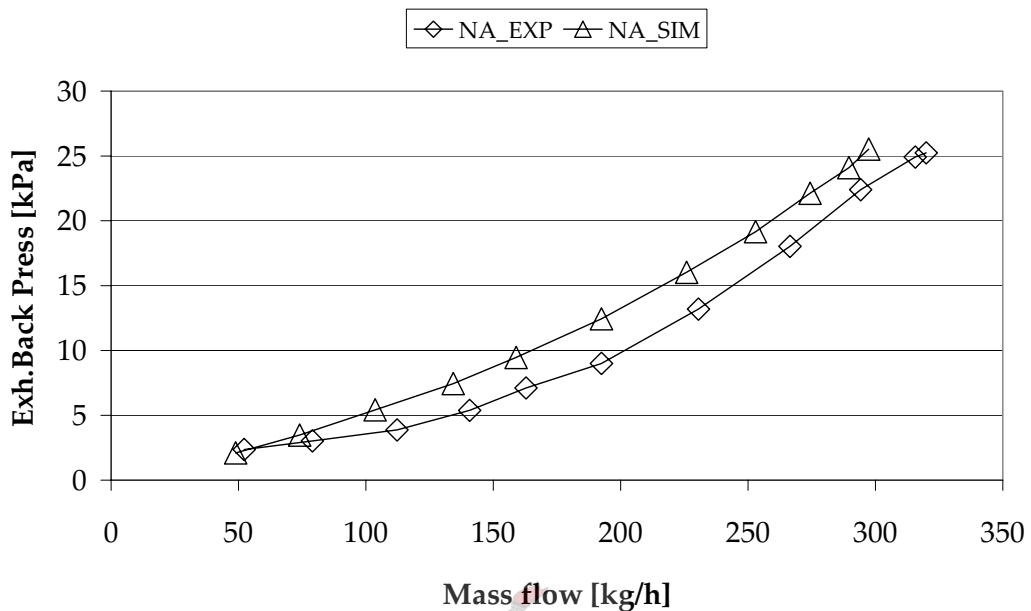


Figure 6-6 NA Simulation vs Experiment: Exhaust Backpressure

The trend of SFC shown in Figure 6-7 is very much the same; however the correlation at low engine speeds is better than at high engine speeds. This could be explained by the combined effect of torque and airflow. At low and high engine speeds the torque was accurately simulated, but the airflow at high engine speeds was less accurate than at low and medium engine speeds. Thus given nearly the same torque at high engine speeds combined with the lower air flow and thus also lower fuel flow, it directly translates into a lower SFC.

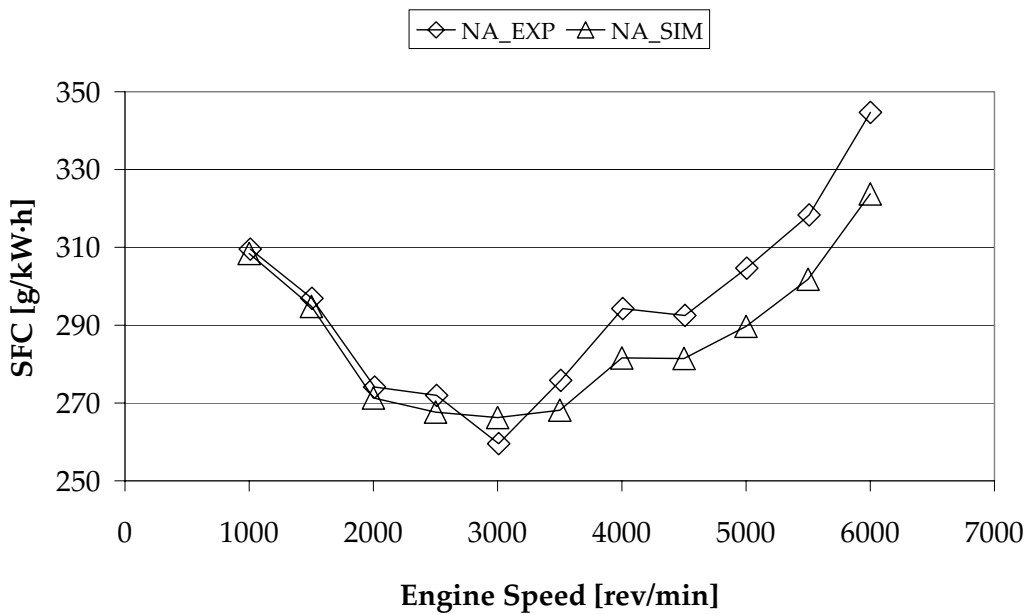


Figure 6-7 NA Simulation vs Experiment: Specific Fuel Consumption

MAP was measured using the engine's T-map sensor. This sensor is used to measure this engine's MAP and intake air temperature on the engine. The data were logged in ETA but were imported from the ECU calibration software. The resolution of the MAP in the ECU calibration software is very coarse, which could explain the roughness of the MAP curve in Figure 6-8.

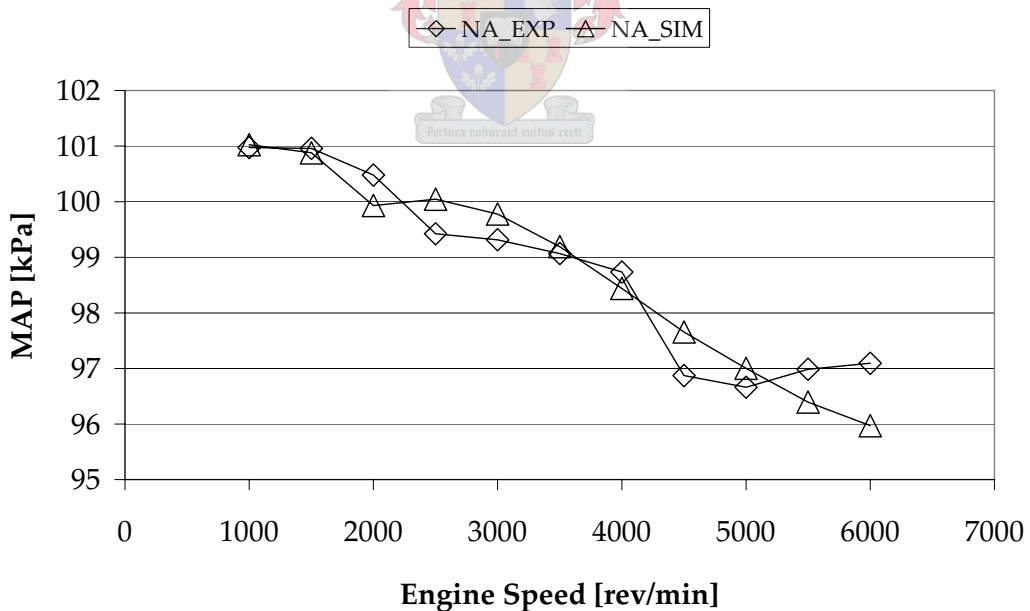


Figure 6-8 NA Simulation vs Experiment: Manifold Absolute Pressure

The air temperature inside the intake manifold was measured with the T-map sensor. The air temperature in the manifold is not only dependent on the atmospheric air temperature, but also on the heat transfer from the manifold itself to the air inside the manifold. The air inside the manifold could heat up due to radiation and convection from the manifold walls. The effect of this heating would be more significant at lower engine speeds, when the airflow is lower and the flow velocity is slower. The air spends more time inside the manifold before it is induced into the cylinders. This could explain why the predicted air temperature inside the manifold is much higher than actually measured at low engine speeds, whereas at higher engine speeds the correlation is better as is shown in Figure 6-9.

The manifold wall temperature was estimated for the simulations and it was assumed to be independent of engine speed. Considering the engine is in a thermal equilibrium condition, it radiates the same amount of heat energy because it has the same area and the operating temperature should be nearly the same, because the coolant temperature is controlled to be constant. Therefore it is assumed that the engine block is at a constant temperature; this assumption could hold for the intake manifold as well.

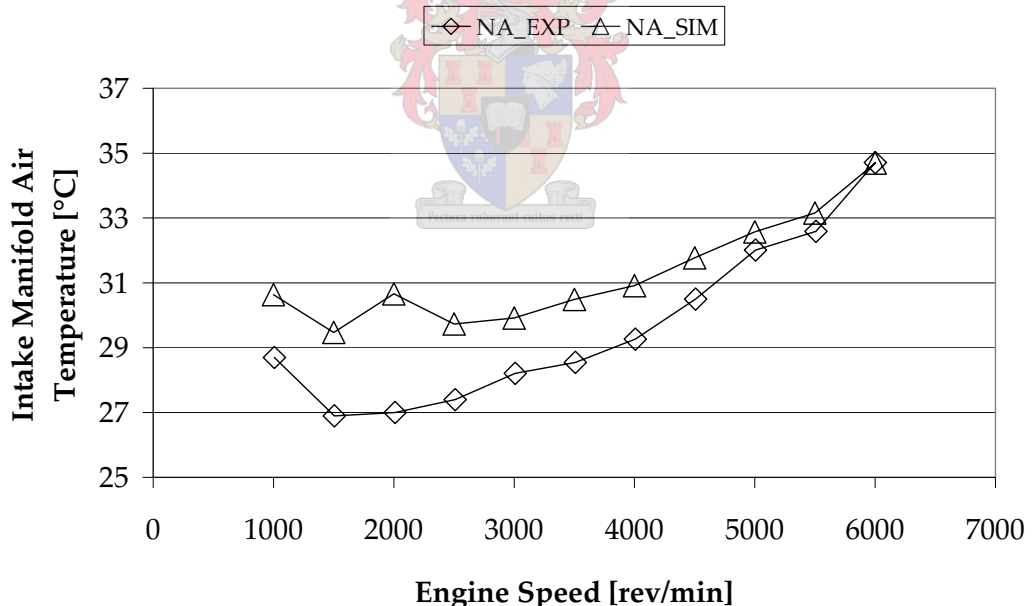


Figure 6-9 NA Simulation vs Experiment: Intake Manifold Air Temperature

This concludes the comparison between the simulated and actual test results of the NA engine. In general the simulation could predict the trends accurately, thus the influence that one factor could have on another could be investigated with the aid of simulations. The maximum error on brake torque prediction is $8 \text{ N}\cdot\text{m}$ on $131 \text{ N}\cdot\text{m}$, which equates to 6%. Thus the general conclusion can be drawn that 1-D flow simulation could be used with confidence for NA engine performance prediction.

6.2. Turbocharged Results: Simulation versus Experiments

Comparing turbocharged results is not as simple as comparing the naturally aspirated results, since there are many more factors playing a role and complicating the comparison. There are various ways of simulating a turbocharged engine. The way the wastegate is controlled is the main variant. The wastegate can be operated as a pneumatic valve, opening proportionally to the boost pressure developed; this method is used on most cars not equipped with electronic boost control. This proportional control method was not available in simulation, but by combining a programmed algorithm with the simulation package it was possible. The other options are specifying a target BMEP value or boost pressure value that the simulation then tries to match by opening or closing the wastegate.

For comparison the actual test results will be presented against these three options: PROP (opening proportional to boost pressure), BMP (target BMEP value), BP (target boost pressure value). In the proportional case the wastegate area versus boost pressure in the simulation was adjusted until it corresponded exactly with that relationship measured on the actual engine.

The torque and power presented for the turbocharged engine are not corrected, since there is not a standard for correcting the power developed by a turbocharged SI engine.

The largest error in predicting the torque as shown in Figure 6-10 was the case where the boost pressure was the same; the predicted torque was more than the actual with a maximum difference of $17 \text{ N}\cdot\text{m}$ or 9%. The second most accurate was the proportional control and BMP was exactly the same, which is expected since the target BMEP was specified for this case. The trends in torque prediction for all the cases correspond very well.

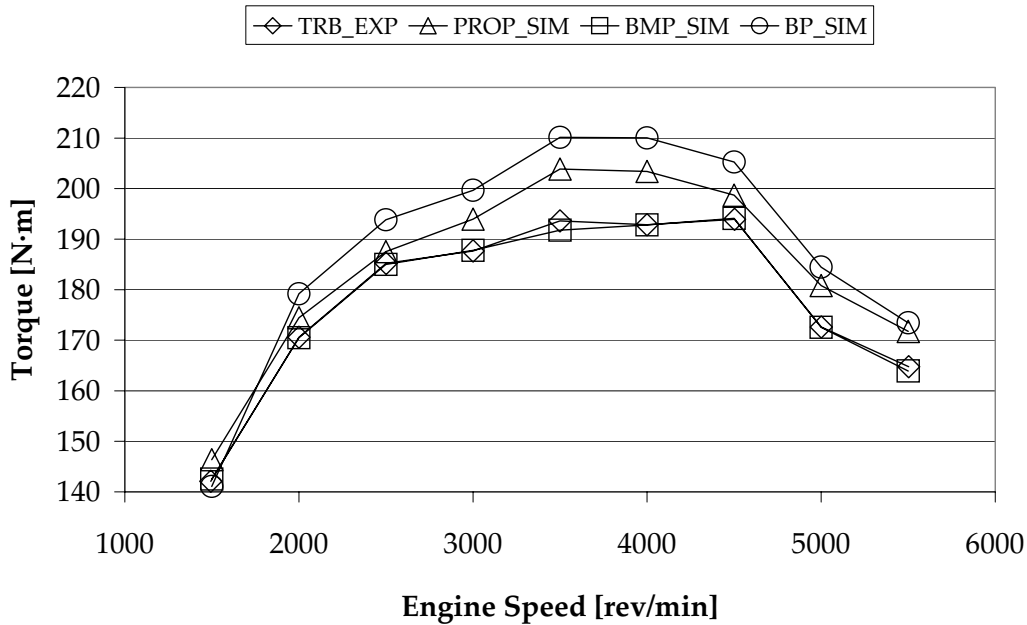


Figure 6-10 Turbocharged Simulation versus Experiment: Torque

However, when the boost pressures as shown in Figure 6-11 for the different cases are compared, the worst prediction was the case where the BMEP was matched to that of the actual engine. Thus the simulation predicts the same power output with lower boost pressure or a higher power output with the same boost pressure. This tendency of the simulation performing better than the actual engine was witnessed in the NA engine simulation as well especially between 3000 rev/min and 4500 rev/min where the simulated air flow was nearly equal to the measured air flow.

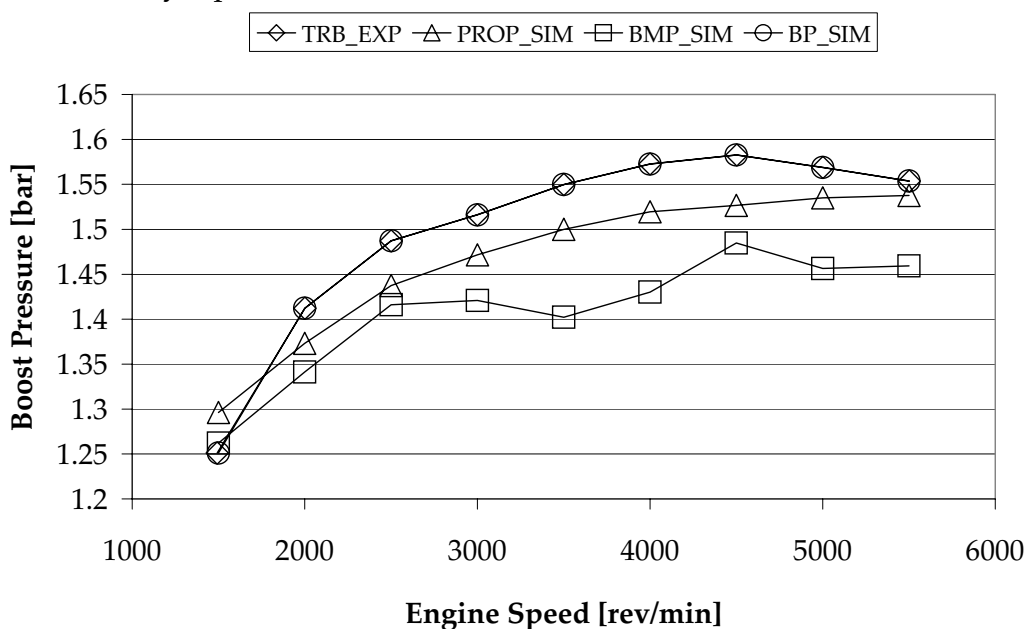


Figure 6-11 Turbocharged Simulation versus Experiment: Absolute Boost Pressure

Comparing the volumetric efficiencies based on the density in the manifold it is clear why the actual engine under performs with regards to the torque developed. It is only at 1500 rev/min and above 4500 rev/min where the actual engine comes close to the simulation in terms of volumetric efficiency. At 5000 rev/min and 5500 rev/min the actual engine performs better than the simulation. As can be seen in Figure 6-13 the actual air flow at 5000 and 5500 rev/min is very similar to the simulation with the same boost pressure. Thus the actual engine has the same or better volumetric efficiency if the air flow is similar to that of the simulations.

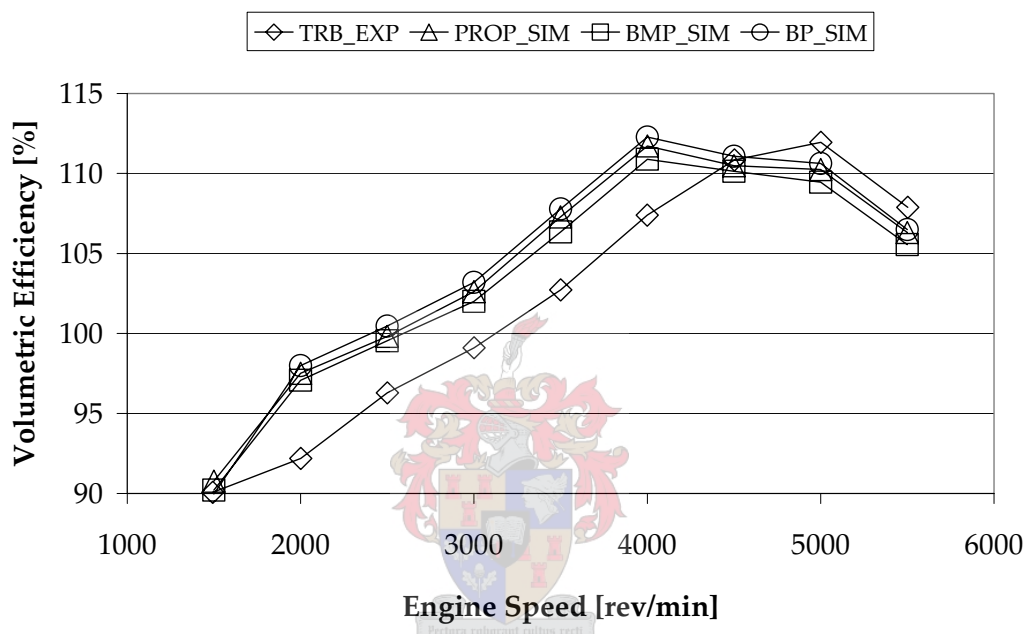


Figure 6-12 Turbocharged Simulation vs Experiment: Volumetric Efficiency

When comparing the turbocharged and predicted airflow as shown in Figure 6-13, it can be seen that the airflow is lowest in the BMP case. This is the same as in the case when comparing the naturally aspirated simulation and test results; the airflow was lower while developing the same power output. The PROP case matched the airflow fairly well, but then the predicted torque was more than the actual torque. In the case where the boost pressure was matched, the simulation predicted higher airflow than was actually measured. Thus it can be assumed that the breathing characteristics of the actual engine and the model used in the simulations are not exactly the same and this could be attributed to the valve flow coefficients.

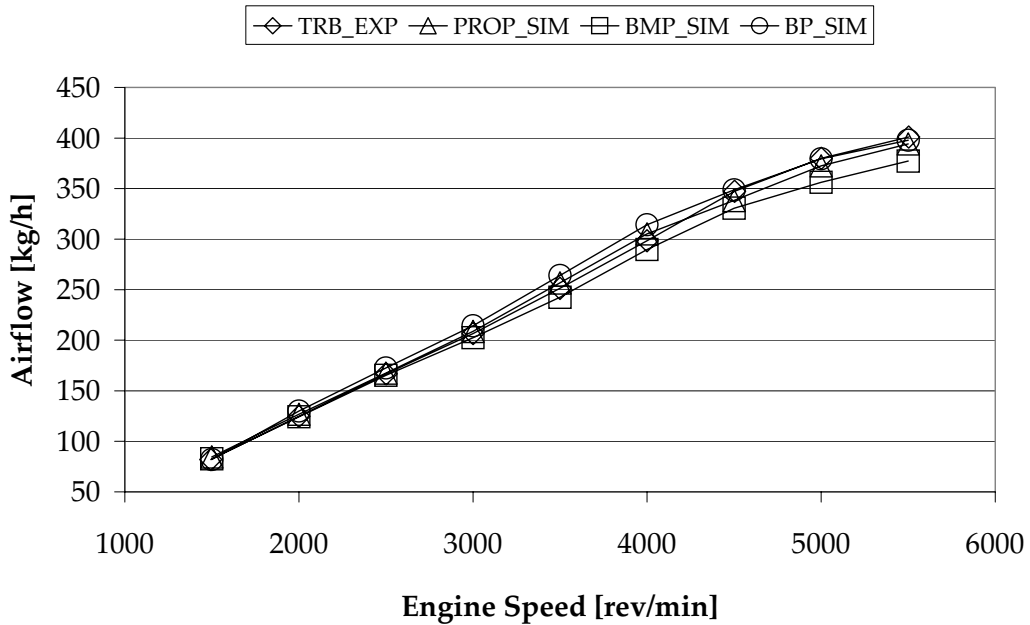


Figure 6-13 Turbocharged Simulation versus Experiment: Airflow

The discrepancy between airflow and power developed could partially be due to blow-by, the same as in the naturally aspirated case. The simulation does not take blow-by into account and therefore predicts lower airflow but higher torque. This could also be used to explain why the predicted maximum combustion pressures in Figure 6-14 were higher than the actual results, although the mass lost due to blow-by is not significant enough to result in such a big difference in peak combustion pressure. Therefore factors such as the accuracy of the spark plug pressure transducer and heat transfer from the gas inside the cylinder to the cylinder walls could have a significant effect on the peak combustion pressure.

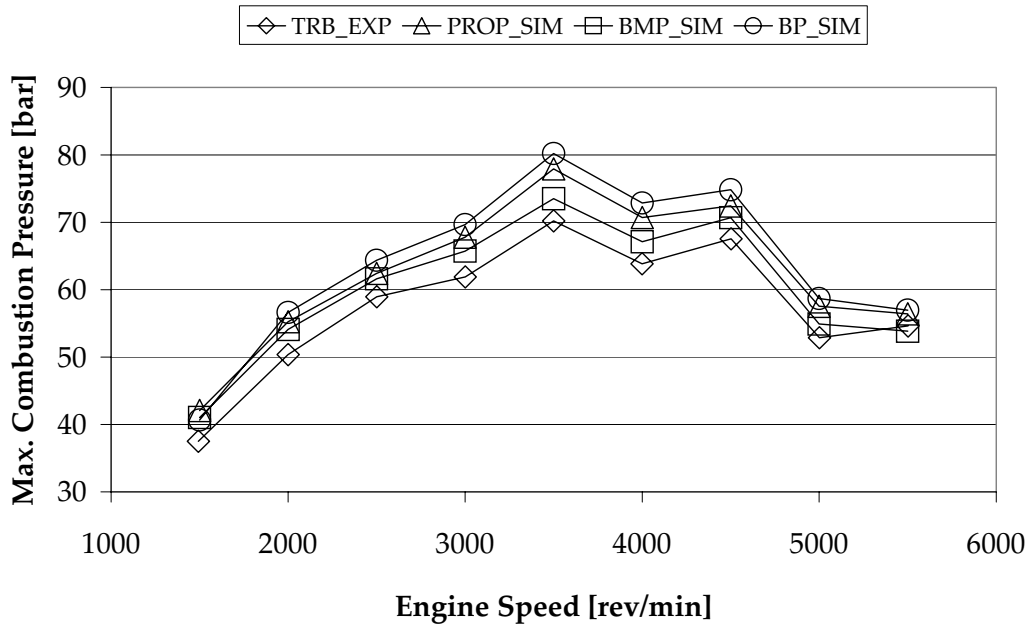


Figure 6-14 Turbocharged Simulation versus Experiment: Max. Combustion Pressure

The case where the boost pressure was matched, the maximum combustion pressure is the highest, but it is also the case where the highest airflow was predicted. Thus it makes sense that, if a higher mass of air is present in the combustion chamber, the maximum pressure will also be higher.

However, when comparing the SFC as shown in Figure 6-15, it is interesting to note the trends of all the different cases are similar and that despite the difference in boost pressure and developed torque the simulations all predict the same SFC. The simulated results predicted higher SFC than the actual engine at low engine speeds and lower SFC at high engine speeds.

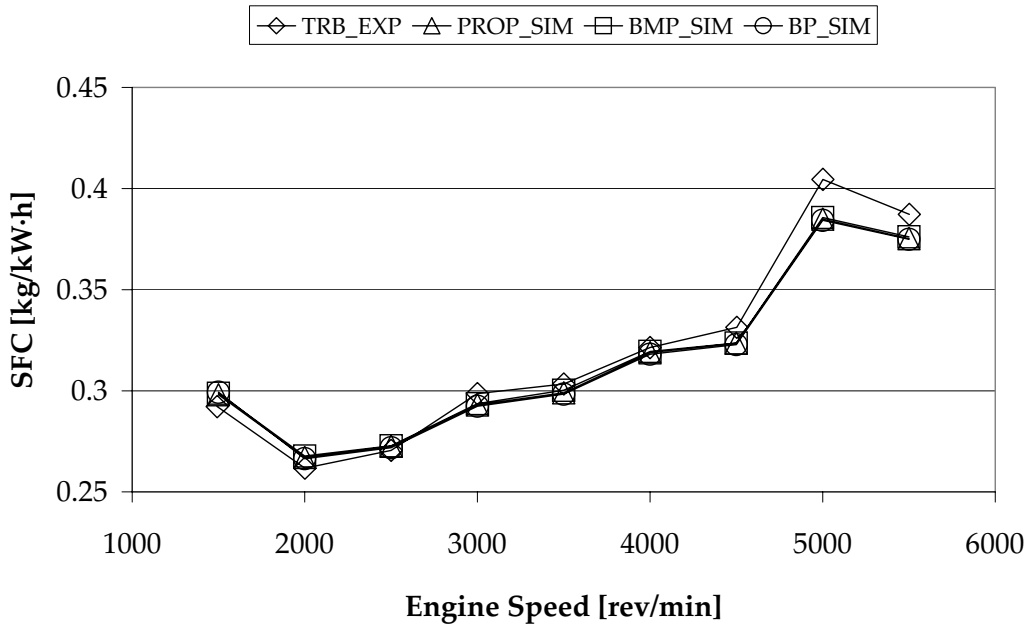


Figure 6-15 Turbocharged Simulation versus Experiment: SFC

The intake manifold pressure as shown in Figure 6-16 is dependent on the boost pressure, but also includes the pressure drop across the intake piping and throttle. The smallest error was predicted by the BP case, where the boost pressure was matched exactly. This shows that the flow losses from the compressor outlet to the intake manifold are representative of the reality. The largest under-prediction was in the case of matching the BMEP, where the simulation predicted the same power output with a lower boost pressure than was actually required.

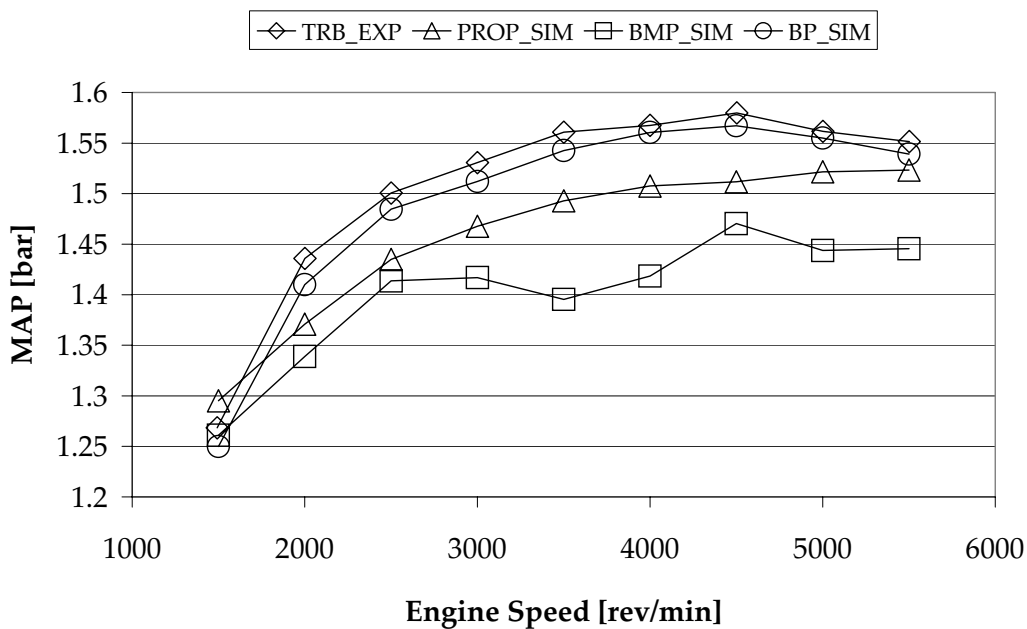


Figure 6-16 Turbocharged Simulation versus Experiment: MAP

Predicting the intake manifold air temperature as shown Figure 6-17, all the simulations predicted lower temperatures than were actually measured. This could be due to the fact that the wall temperatures that were used in the simulations were lower than in reality; thus the air was actually cooled by the cooler manifold walls.

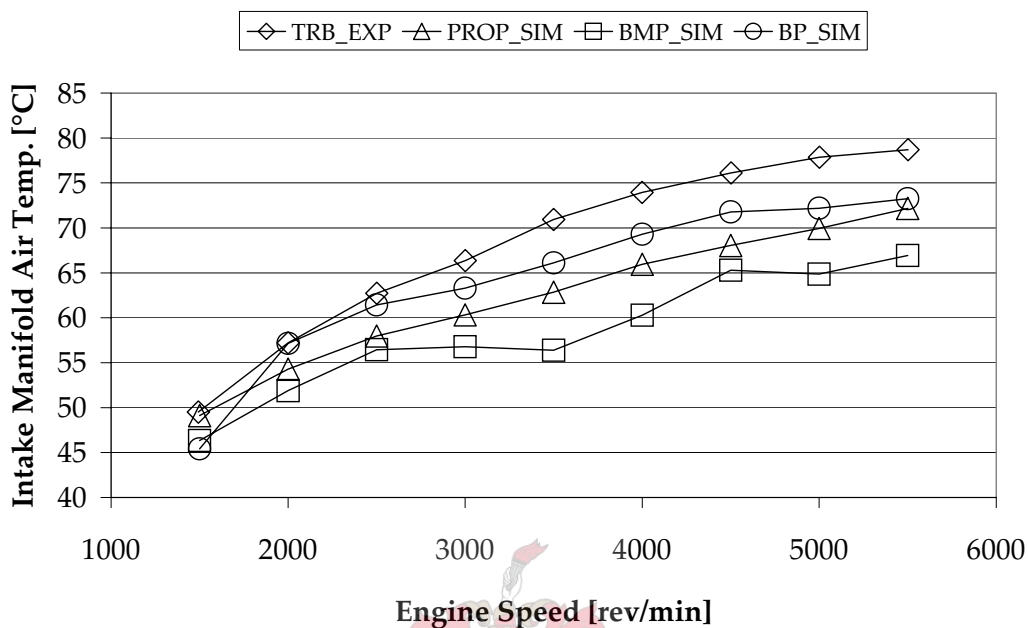


Figure 6-17 Turbocharged Simulation versus Experiment: Intake Manifold Air Temperature

When comparing the compressor outlet air temperature as shown in Figure 6-18, it is evident that BP was the best prediction. Thus the same increase in pressure resulted in similar increase in air temperature; therefore the predicted compressor efficiency should be very close to reality. This indicates that the simulation interpreted the compressor map correctly and is representative of the reality. The lower boost pressure as in the case of BMP results in a lower air temperature; this is further confirmation that the compressor map and efficiency have been interpreted correctly.

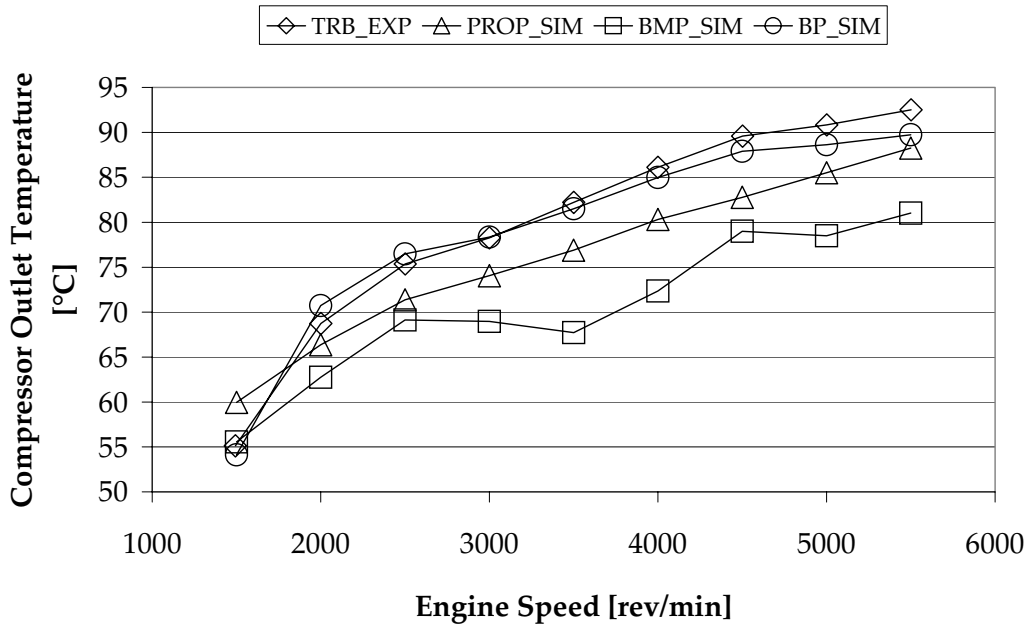


Figure 6-18 Turbocharged Simulation versus Experiment: Compressor Outlet Temperature

The amount of boost pressure developed is proportional to the amount of energy that can be extracted out of the exhaust gas by the turbine. Thus the relationship between the wastegate area and boost pressure can be compared in Figure 6-19 for both the actual and the simulated conditions. It can be seen that the relationship between the wastegate area and boost pressure is much more sensitive in the simulated case and therefore the maximum area predicted is much smaller than was actually measured. It can be seen that the wastegate area for the PROP case falls on the measured line and thus it was simulated correctly.

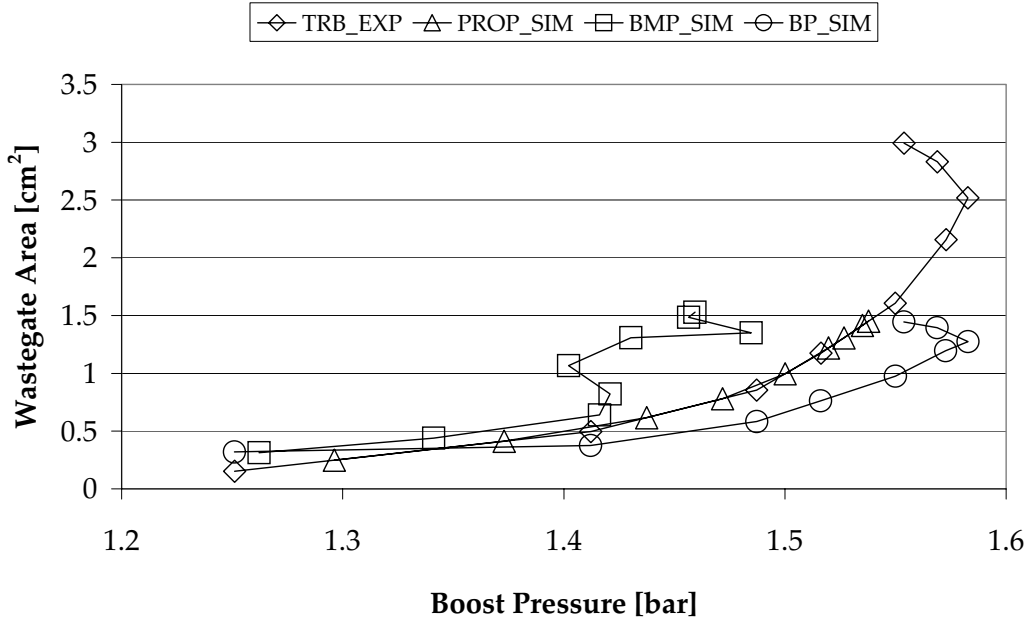


Figure 6-19 Turbocharged Simulation versus Experiment: Wastegate Area

What is not obvious immediately when considering Figure 6-19 is why the wastegate area curves back and thus for the same boost pressure there are two corresponding area values. This phenomenon occurred in reality as well as in the simulations. In reality it is impossible to achieve this with the standard wastegate actuator; since it consist only of a diaphragm and spring, the opening area must be proportional to the boost pressure. The cause of this effect is the force on the wastegate valve itself due to the large pressure difference between the turbine entry and outlet. Thus the force experienced by the spring is the sum of the force on the diaphragm caused by the boost pressure and the force on the wastegate valve caused by the pressure difference across it. Thus the force on the wastegate valve causes the wastegate to open more than is predicted by using purely the boost pressure.

When considering the wastegate area versus exhaust mass flow, as shown in Figure 6-20, it is interesting to note that it is a near linear relationship. The gradient of the actual results is totally different from that predicted by the simulation. Thus it can be concluded that the wastegate area and or its flow characteristics were not simulated correctly or the calculation of the wastegate area from the measured rack travel is inaccurate.

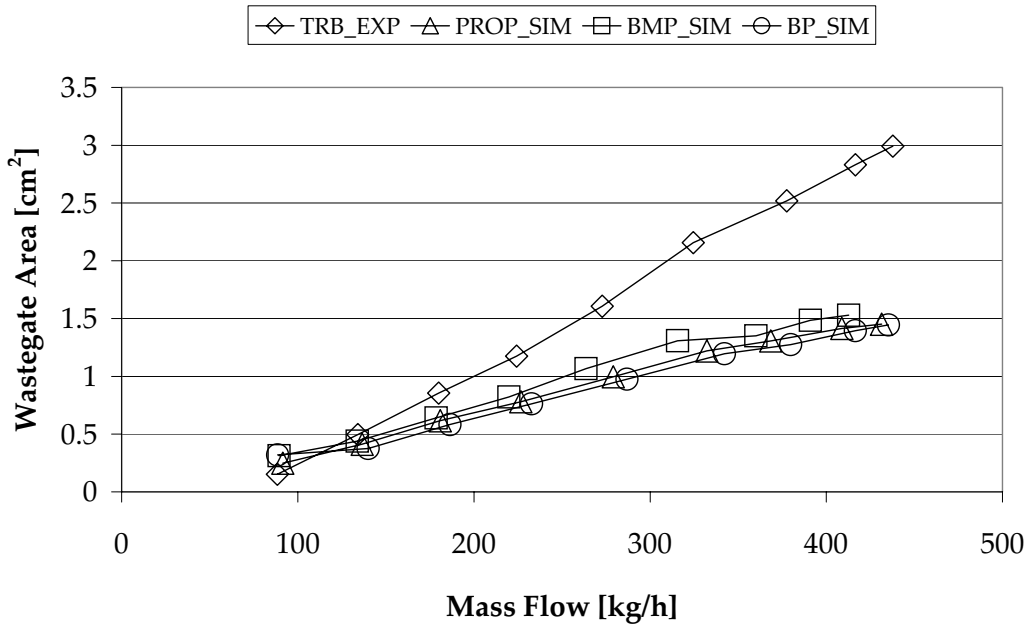


Figure 6-20 Turbocharged Simulation versus Experiment: Wastegate Area as function of mass flow

In Figure 6-21 the turbine pressure ratio which best resembles the actual results is that of the BMP case. The pressure ratios for the other cases were both higher. This is due to the fact that the predicted turbine inlet pressure was higher for the same mass flow than the actual results indicated. This complements the assumption that the flow characteristic of the simulated turbine does not correspond to the actual tests.

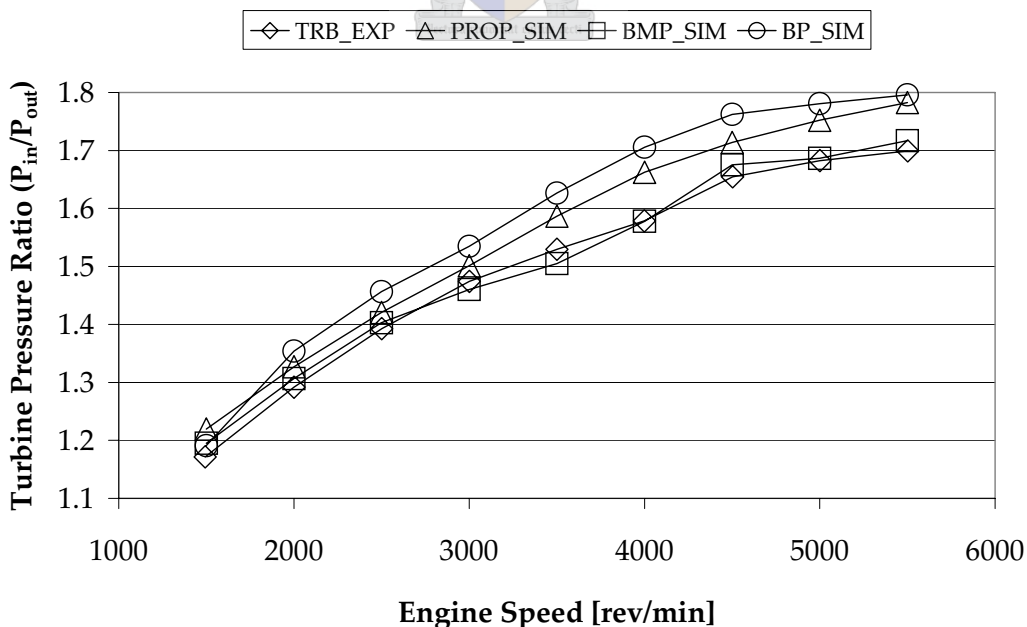


Figure 6-21 Turbocharged Simulation versus Experiment: Turbine Pressure Ratio

The predicted turbine inlet temperature as shown in Figure 6-22 correlated fairly well. The temperatures are predicted well inside the range of the 50°C error, which is the sort of error that can be expected when measuring exhaust temperatures as is done in practice (see section 5.7.3). What is a matter of concern is that the predicted temperatures are lower than the actual results. The measuring error would cause thermocouple readings that are lower than the actual values. Thus the predicted result should have been higher.

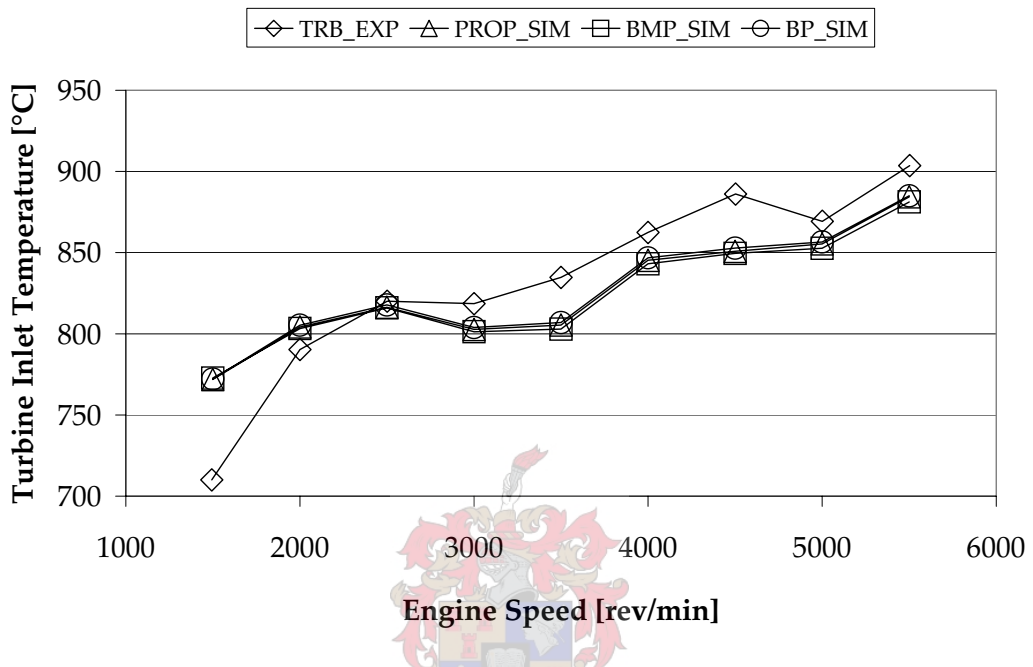


Figure 6-22 Turbocharged Simulation versus Experiment: Turbine Inlet Temperature

However, the fact that the simulation predicts lower temperatures only at speeds above 2500 rev/min could be linked to the fact that very rich mixtures were used at speeds above 2500 rev/min. Thus the simulation predicts lower exhaust temperatures than the actual temperatures, especially when very rich mixtures were used. A possible reason for this is the simulation's inability to accurately predict exhaust temperature with very rich mixtures. Another possibility could be that there might have been combustion in the exhaust manifold if air was leaking into the exhaust manifold. The air could be introduced into the exhaust manifold, although the exhaust manifold pressure was nominally higher than the atmospheric pressure; due to the pulsation effects in the exhaust manifold.

It can be concluded that the simulated results showed the same trends as were measured on the actual engine. The compressor modelling seems to be of a high standard, but there is concern about turbine modelling and map interpretation as well as the wastegate area predicted. The engine power output is highly dependent on the boost pressure, which is in turn dependent on the energy extracted from the exhaust gas. Thus both the compressor and turbine modelling should be accurate in order to predict the same boost pressure, turbine inlet pressure as well as wastegate area.

6.3. Comparison of the NA and Turbocharged Results

When comparing the turbocharged engine to the NA engine, not only are the same aspects considered as in the previous two sections, but the forces on the bearings and the energy balance were also compared. The forces are an important factor, because if the forces developed exceed the functional limit of the components, then durability will be compromised. The energy balance can be used to audit the modifications made to the engine in order to make an objective engineering judgement whether it is worthwhile.

The CR of the turbocharged engine was the same as that of the NA engine and the turbocharged engine did not have an intercooler. Thus the compressor would increase both the initial charge pressure and temperature and knock could result. Therefore a fuel with a higher octane was used during the turbocharged engine tests. The fuel used was Shell 102.6 octane racing fuel. This fuel contains more than 0.05% lead and can therefore be classified as leaded. The fuel used during testing of the NA engine was unleaded with a 95 RON.

6.3.1. Comparison of Turbocharged Boost Settings

Different wastegate actuator settings were tested in order to find the best solution that would give a torque curve as flat as possible while producing a maximum of 100 kW. The experiments were started at low boost and the boost pressure was gradually increased until the 100 kW target was reached. In this section only the different boost pressures, lambda settings, ignition timing, compressor operating points and the resulting torque curves will be compared to the NA engine. A detailed comparison involving only the optimum boost setting and the NA engine results will follow in the next section.

The boost pressures (gauge) developed are shown in Figure 6-23. The NA engine has no boost pressure and is therefore 0 bar. The lowest boost curve, 0.21 bar, was run with the NA engine's standard exhaust pipe. This caused a very high exhaust backpressure and it was then replaced with a free flow exhaust. A peak boost pressure of 0.21 bar was achieved with no preload on the spring in the variable wastegate actuator. Due to the stiffness of the diaphragm, the same spring stiffness was used in all the tests. The standard wastegate actuator was used in the 0.36 bar STD experiment, and the preload was set so that the wastegate would start opening at 0.3 bar boost. As can be seen, this is the flattest boost curve, because this actuator opens linearly with boost pressure. The highest boost curve was the one that was actually used, since it met the target power output.

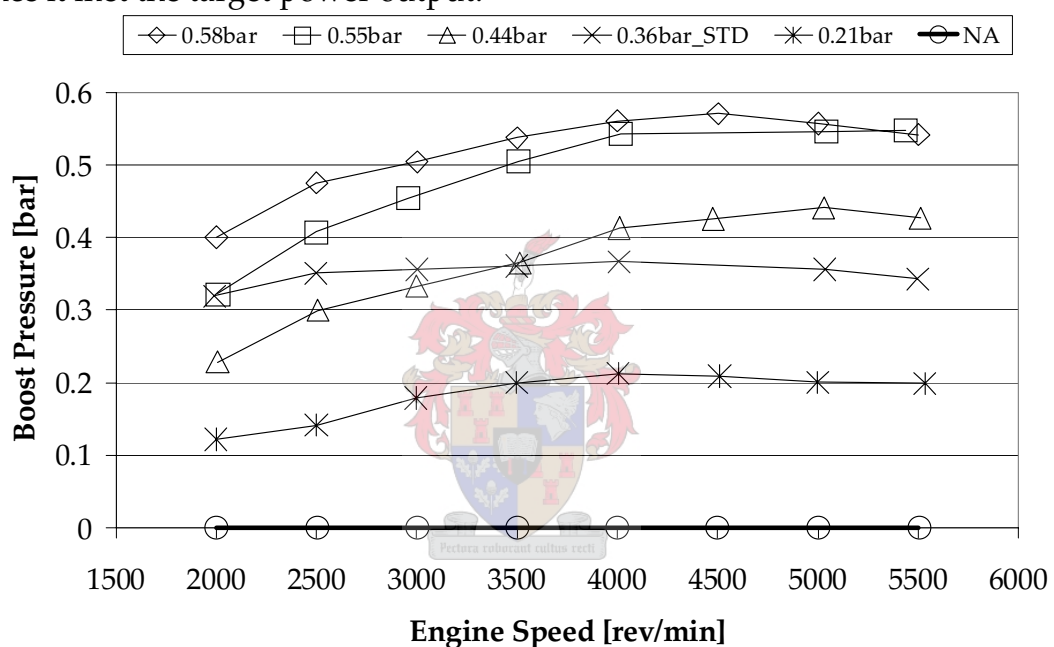


Figure 6-23 Turbocharged Boost Settings: Boost Pressure

The lambda settings for the experiments are shown in Figure 6-24. It is evident that the NA engine's lambda was the closest to stoichiometric. The turbocharged engine's exhaust temperatures were very high and therefore a very rich lambda was used to maintain port temperatures below the threshold of 830°C.

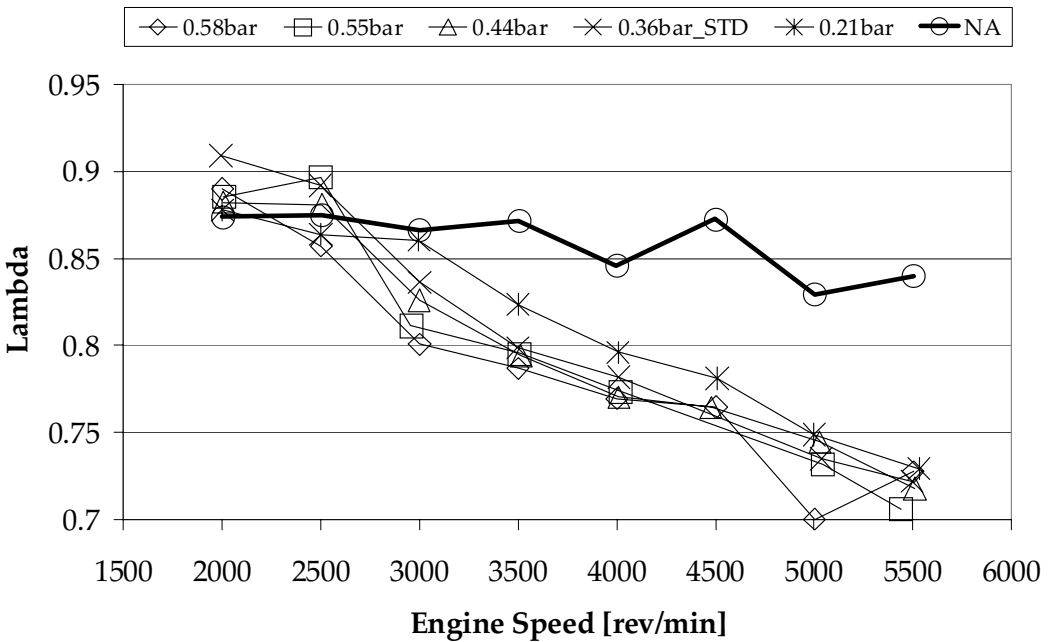


Figure 6-24 Turbocharged Boost Settings: Lambda

The ignition timing is compared in Figure 6-25. As can be seen, the ignition timing was most advanced in the 0.21 bar experiment. This was possible since the boost pressure was low and high-octane fuel was being used, therefore knock was not a limitation. As the boost pressure was increased, the ignition timing had to be retarded, since knock became a limitation.

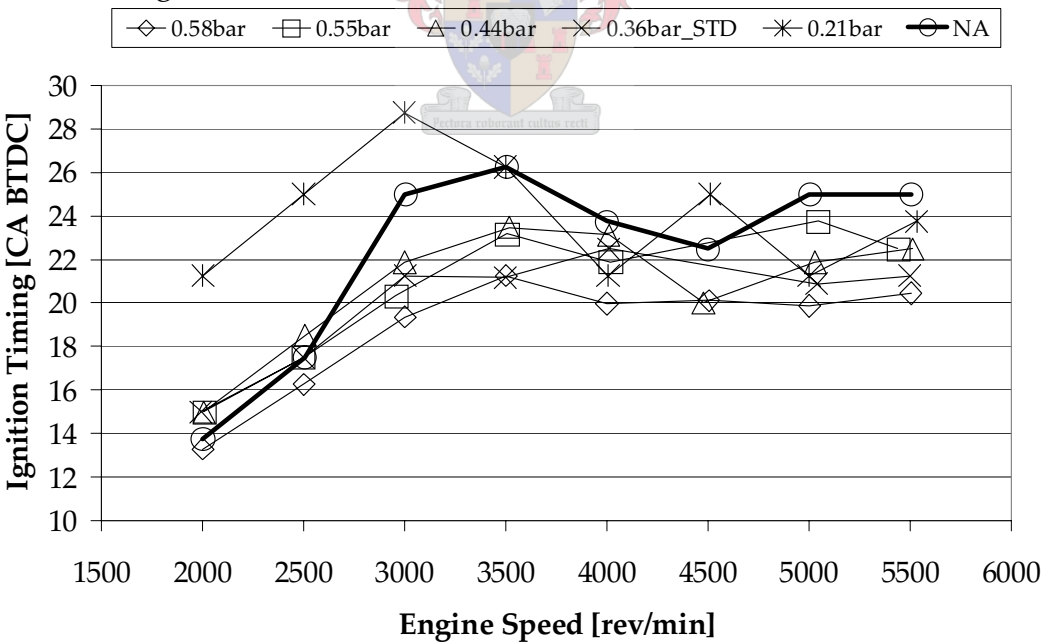


Figure 6-25 Turbocharged Boost Settings: Ignition Timing

The compressor operating points were superimposed on the compressor map and this compressor map is shown in Figure 6-26. Since the NA engine did not have a compressor, its operating points are only shown in order to see the difference in volume flow rates. It can be seen that 0.58 bar runs through the highest efficiency area of the compressor. Therefore the match between the compressor and this engine is very good.

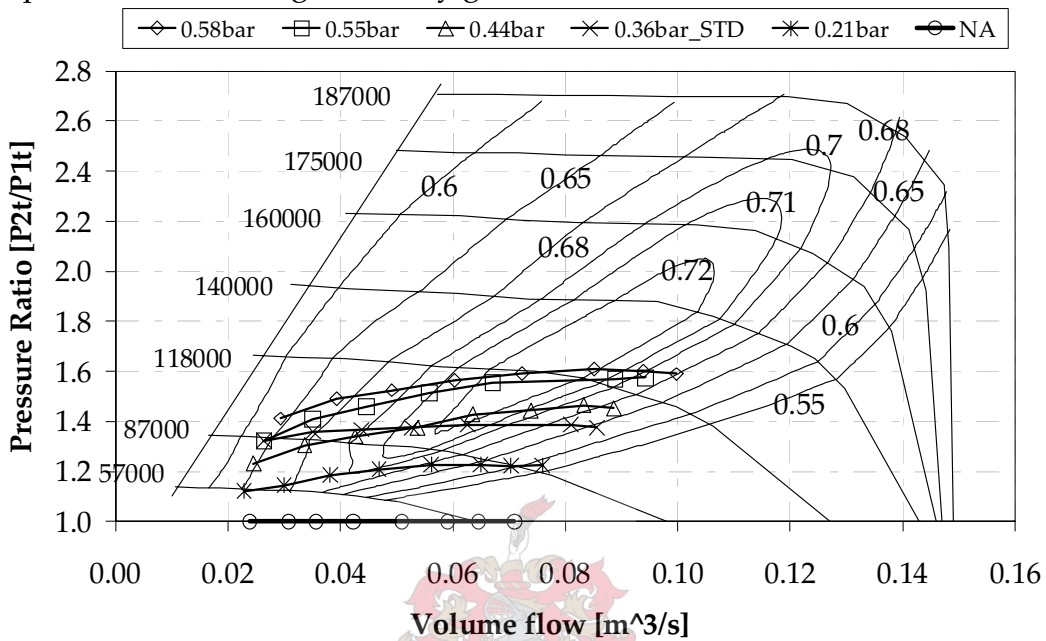


Figure 6-26 Turbocharged Boost Settings: Compressor Operating Points

The torque curves for the different boost settings are shown in Figure 6-27. The higher the boost pressure the higher the torque produced. It is evident from all the curves that the torque decreases considerably at engine speeds higher than 4000 rev/min. When considering the boost curve of 0.36 bar STD, it is nearly flat from 2000 rev/min up to 5500 rev/min. This boost curve resulted in a very flat torque curve from 2500 rev/min up to 4000 rev/min, after which it decreases significantly. Therefore more boost is needed at high engine speeds in order to maintain the same amount of torque.

This phenomenon of decreasing torque can partly be due to the fact that at 4000 rev/min the compressor is at its highest efficiency; thus at higher engine speeds the boost pressure drops and the boost temperature increases. Another factor that could cause the torque to decrease at engine speeds higher than 4000 rev/min is pulse interference. Pulse interference was discussed in a previous section (5.1.1) and it could be very engine-speed specific (Watson & Janota, 1984). It impedes the gas exchange process and causes higher residual mass in the combustion chamber. Therefore the torque produced would be less.

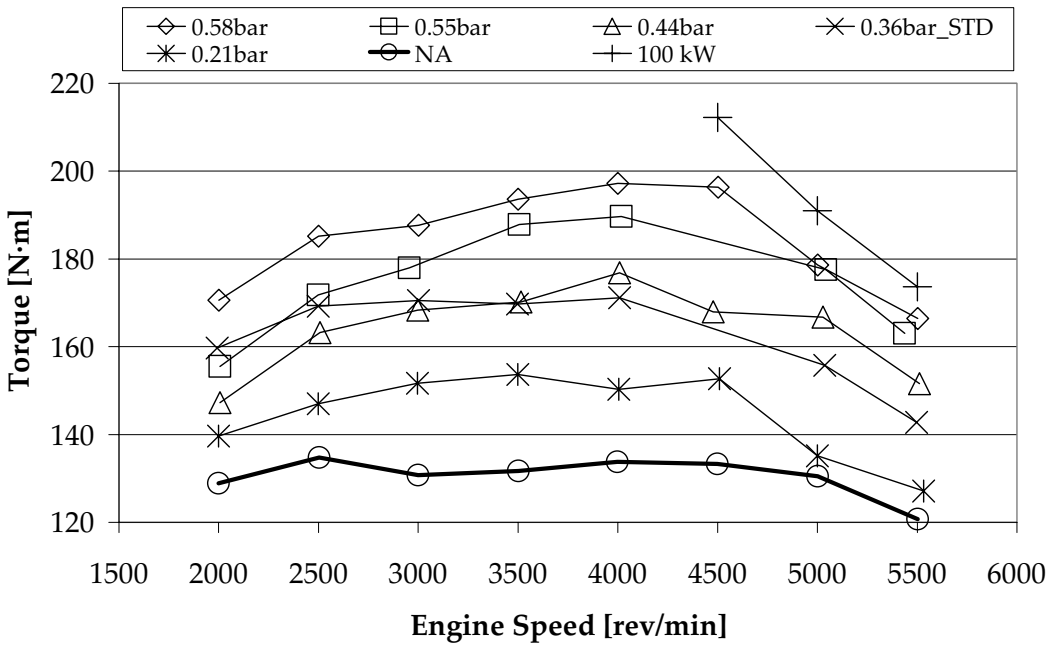


Figure 6-27 Turbocharged Boost Settings: Torque

Different boost settings were tested and the resulting torque curves were presented. The boost curve with the highest boost resulted in the highest power output and the 100 kW target was reached with this setting at 5000 rev/min. In the following discussions all the turbocharged results refer to the 0.58 bar boost setting.

6.3.2. Force Analysis

An important aspect of engine analysis is the loading on the bearings. Since the in-cylinder pressure was measured, the forces on the piston can be calculated. The acceleration forces, however, are not explicitly known, but assumptions can be made to make calculations simpler. The assumptions can be summarised as follows:

- The crankshaft is turning at a constant speed;
- The piston's centre of mass is at the centre of the small-end bearing;
- The connecting rod is composed of two point masses, one at each end, connected with a weightless rod;
- The crankshaft is perfectly balanced and it is assumed to be weightless;
- Friction is neglected in all joints as well as between the piston and cylinder wall.

The mass of a generic piston and connecting rod was used. Therefore the forces quoted in this comparison cannot be used as absolute values. The objective was to investigate the order of magnitude of the bearing forces that an increase in cylinder pressure would have.

A pure mathematical model was derived for the motion (displacement, velocity and acceleration) of the piston. The derived equations can be seen in APPENDIX D. The method of dynamically equivalent masses as described by Mabie, H H and Reinholtz, C F (1987) was used to account for the inertia of the connecting rod. The mass of the counter-weights was chosen so that they would perfectly balance the mass of the connecting rod at the big end bearing.

An elementary model of the crank, connecting rod and piston was also built in Adams-View to compare it to the mathematical model. The gas force on the piston, as a function of crank angle, and the rotational speed of the crankshaft was used as input to the simulation. The simulation then animates movement and calculates the accelerations and forces at the bearings. These accelerations can then be compared to those of the mathematical model for correlation. Figure 6-28 show the correlation between the piston's acceleration and velocity calculated by the derived mathematical equations and the simulation.

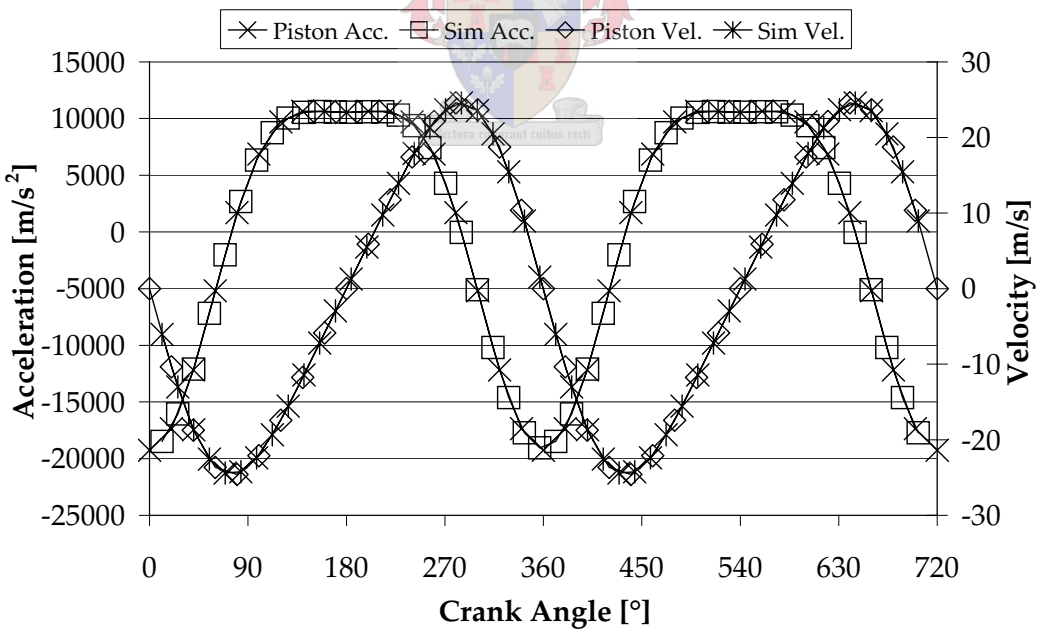


Figure 6-28 Piston Velocity and Acceleration Correlation

The correlation between the analytical and simulated magnitude of the force in the small- and big-end bearings of the NA engine at 3000 rev/min and WOT are presented in Figure 6-29 and Figure 6-30 respectively and the correlation was very good.

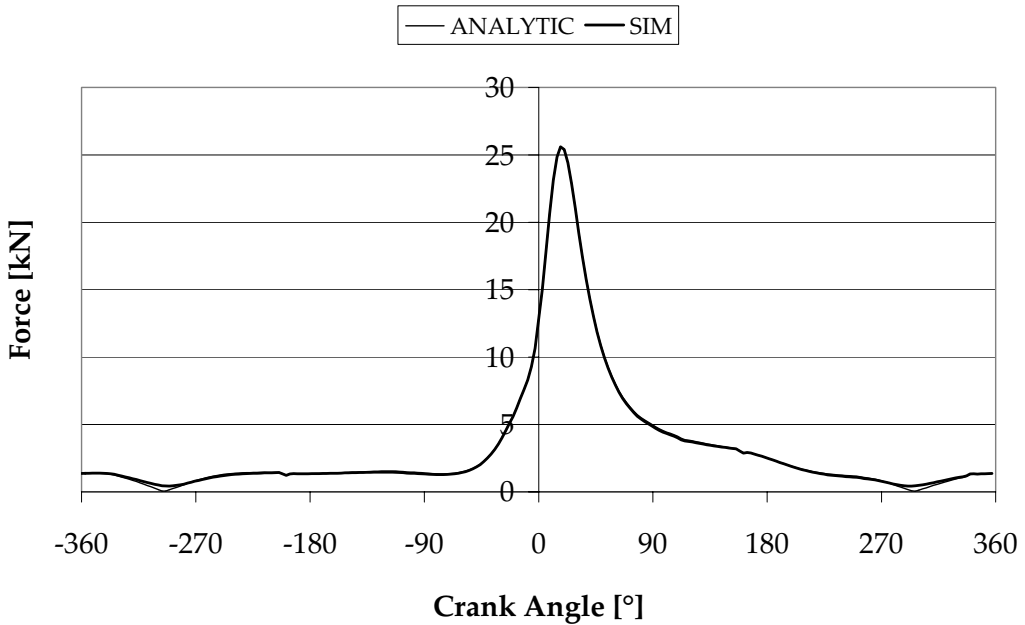


Figure 6-29 Small-End Bearing Force Comparison: Analytical versus Simulation

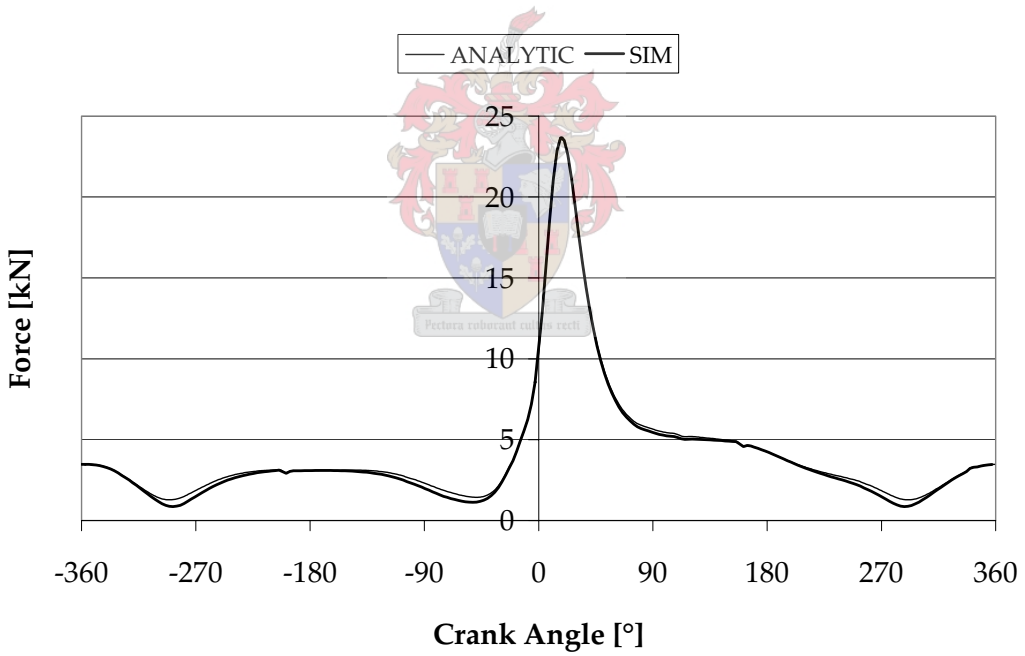


Figure 6-30 Big-End Bearing Force Comparison: Analytical versus Simulation

The analytical comparison between the forces is presented in Figure 6-31. As can be seen, the maximum force occurs in the small-end bearing. The big-end bearing force is the smallest of the three and can be attributed to the inertia of the piston and connecting rod.

The inertia force is always in the opposite direction to the acceleration, and therefore the inertia force acting on the big-end bearing can be subtracted from the gas force acting on the piston. This is the reason why the big-end bearing's maximum force is smaller than that of the small-end bearing. A similar reasoning can be used to explain the difference between the main bearing and small- and big-end bearing forces. The force on the main bearing is carried by two bearings in the case of a single cylinder engine. In the case of a multiple cylinder engine depending on engine configuration, the main bearing forces of two adjacent cylinders always cause negative interference and tend to cancel each other out.

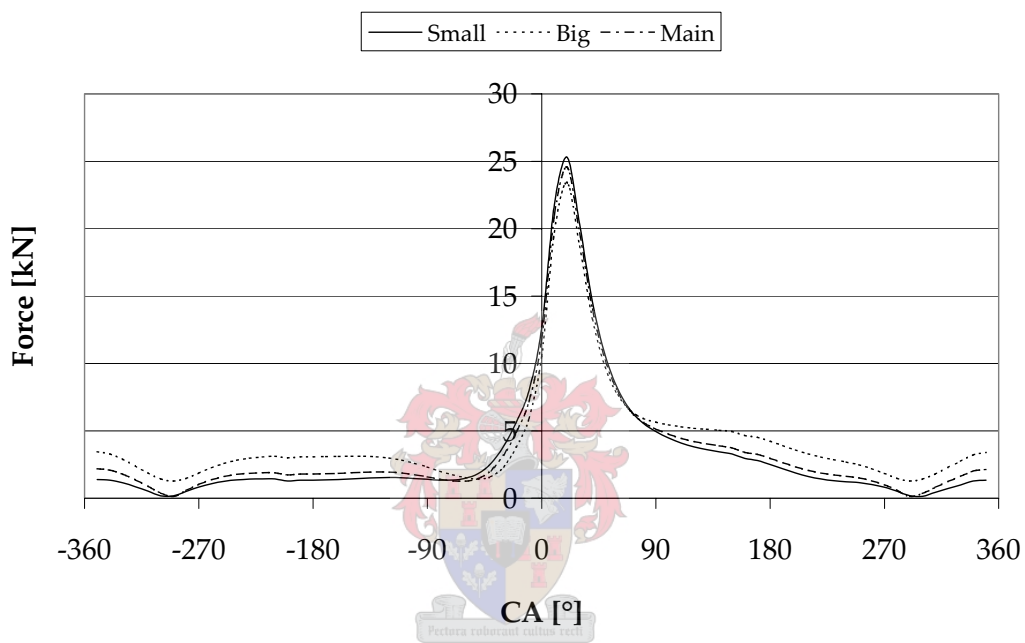


Figure 6-31 Analytically Determined Bearing Forces

The forces predicted by the simulation are only a magnitude (do not take the direction of action into account) and therefore only the maximum forces for the NA engine and turbocharged engine will be compared. The gas force that acts on top of the piston is presented in Figure 6-32. The drop in gas force at 5000 rev/min is due to the late ignition timing and longer burn duration. The maximum gas pressure for the turbocharged engine occurred 5°C A later at 5000 rev/min than at the other engine speeds. The burn rate at 5000 rev/min was also 5°C A slower than the average of other speeds.

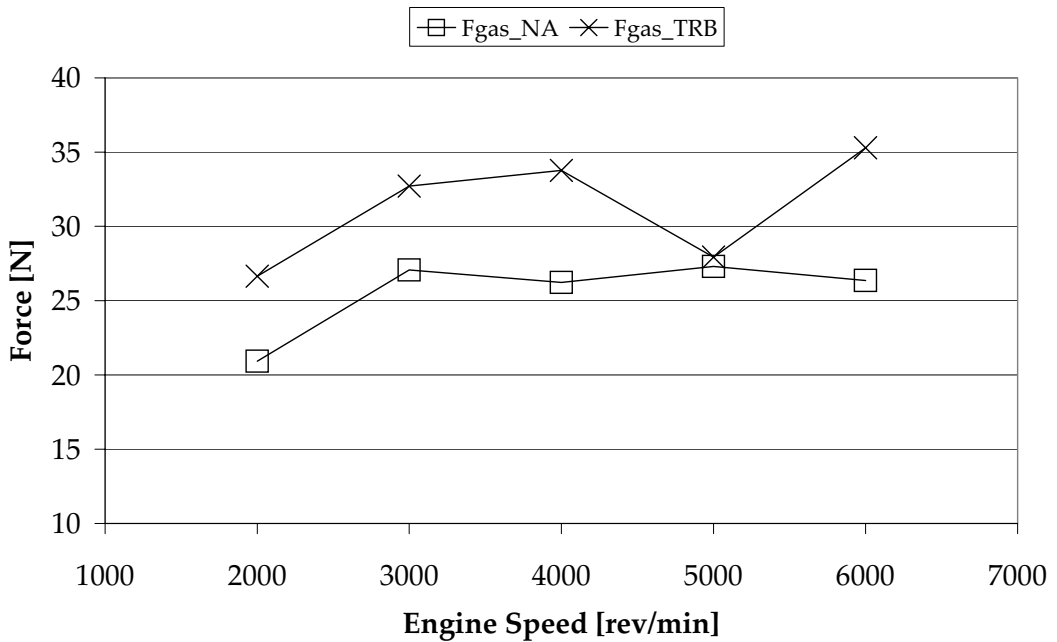


Figure 6-32 NA versus Turbocharged Results: Gas Force on Piston

The maximum forces on the small- and big-end bearings at different engine speeds are presented in Figure 6-33 and Figure 6-34 respectively. When considering the gas force in the NA engine, it is fairly constant from 3000 rev/min up to 6000 rev/min; however, the small- and big-end bearing forces decrease with an increase in engine speed. This is due to the fact that as the engine speed increases, the inertia force also increases and, as explained earlier, the inertia force tends to cancel out the gas force on the piston. Therefore the force on the bearings decreases as the engine speed increases and the gas pressure remains nearly constant.

The same reasoning can be followed for the turbocharged engine; however, the gas pressure does not decrease, but increases steadily with increased engine speeds, yet the bearing forces still decrease as the engine speed increases.

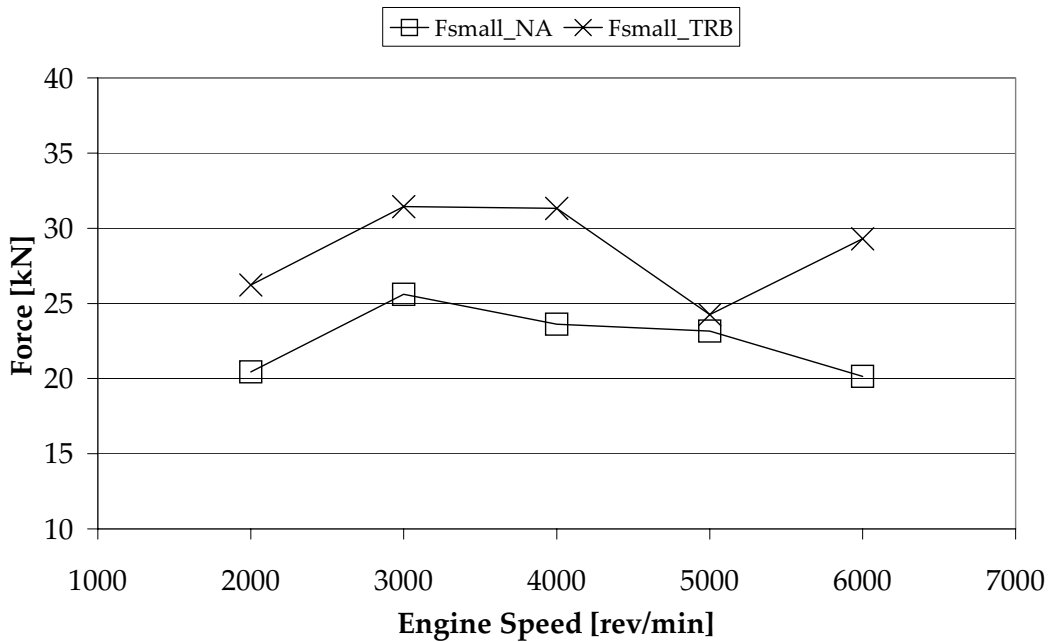


Figure 6-33 NA versus Turbocharged Results: Small-end Bearing Forces

The forces on the small-end bearings are higher than those on the big-end due to the mass and inertia of the connecting rod. Due to the simplification assumptions the forces predicted by simulation on the main bearings are exactly equal to those on the big-end bearings and are therefore not presented.

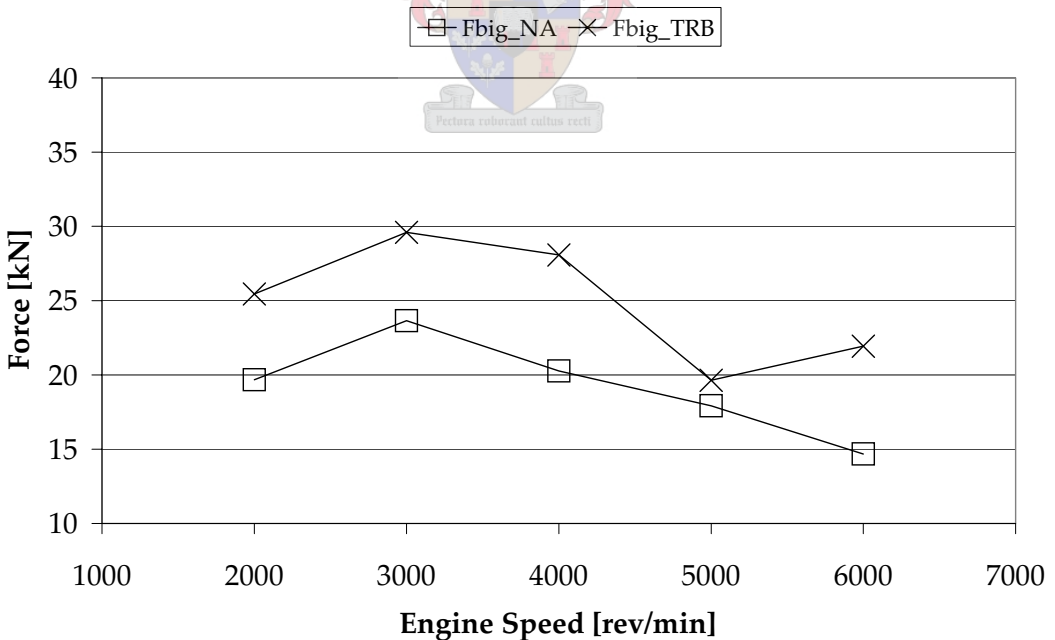


Figure 6-34 NA versus Turbocharged Results: Big-end Bearing Forces

The maximum forces on both the small- and big-end bearings were increased by 45% and 49% respectively as a result of turbocharging to yield 48% more torque and 37% more power. The area under the curves was also increased; thus it could be assumed that the turbocharged engine is more susceptible to failure due to fatigue as a result of the increased loading and thus a compromise on durability is inevitable.

6.3.3. Energy Balance

Energy cannot be created nor be destroyed; thus if energy enters a system, and the energy of the system does not increase, it must leave the system. Thus an energy balance is the sum of what enters, what leaves and what remains in the system. If the system is in a steady-state condition, its energy (or temperature) can be assumed to remain constant, and then it is only necessary to consider what enters and what leaves the system.

The simplification was made that air at atmospheric conditions has zero potential energy; thus the exhaust gases have a great deal of thermal energy. Thus the amount of energy input into the system in terms of fuel energy must be recovered as shaft energy, heat rejected to the cooling system, thermal energy in exhaust gas, chemical energy in the exhaust gas and radiation to the surroundings. The chemical energy in the exhaust is made up of partially and un-burnt hydrocarbons and carbon monoxide. The energy in the carbon monoxide can be accounted for with a relation presented by Heywood (1988). The hydrocarbons are unaccounted for and make up part of “other” energy. Due to the complicated measurement of radiation energy, it is also accounted for as “other” energy.

The heat rejection was measured by installing 2 orifice flow meters; one in the engine’s cooling system and the other in the facility water side that circulated through the oil cooler. The engine coolant was thus not routed through the oil cooler in order to measure the effect of the turbocharger on the oil separately from that of the cooling system. The pressure drop across the orifices was measured as well as the temperature difference across the engine and oil cooler. From these measurements the mass flow and thus the total energy removed could be calculated. The heat rejected to the cooling system, which uses a mixture of 50% water and 50% ethylene glycol can be calculated if the specific heat for the fluid are known. The specific heat value was extrapolated by fitting a second-order polynomial to the data found in Mills (1995), see Figure 6-35. The specific heat at 90°C was found to be 3786 J/kg·K compared to a specific heat value of 4128 J/kg·K for pure water.

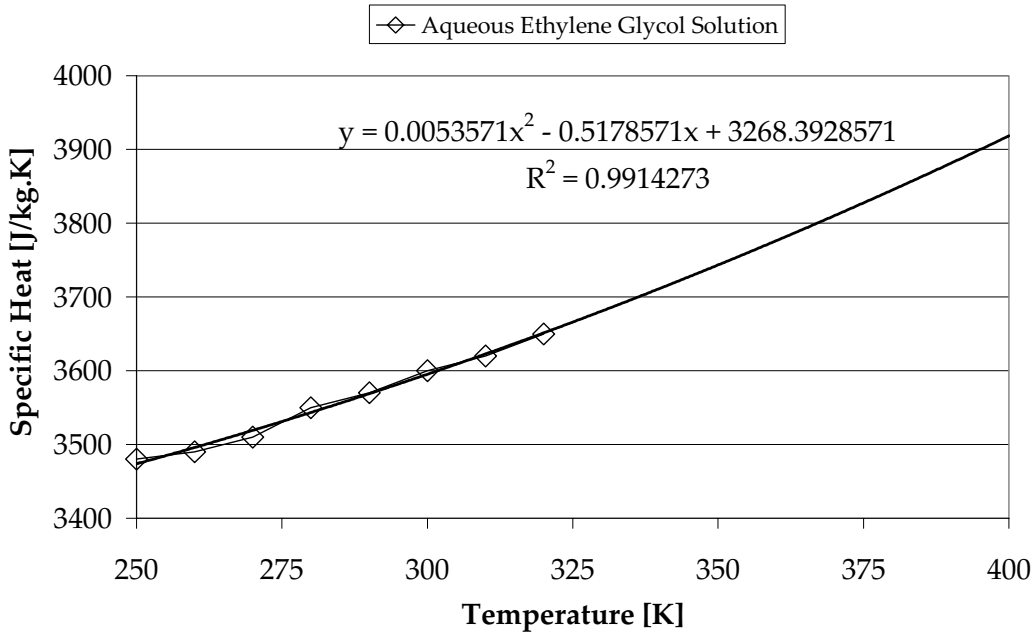


Figure 6-35 Extrapolation of Specific Heat

When comparing the heat rejected to the cooling system and the oil cooler as shown in Figure 6-36, the heat rejected to the cooling system is more in the case of the turbocharged engine, as can be expected, but what is of interest is that the heat removed by the oil cooler is nearly the same.

The maximum increase in heat rejected to the cooling system was 35% which is in the same order of magnitude as the 37% increase in maximum power output. Therefore it can be assumed that, if the power output of an SI engine is increased by $x\%$, the cooling system would have an $x\%$ increased loading and should be upgraded if it does not have enough spare capacity.

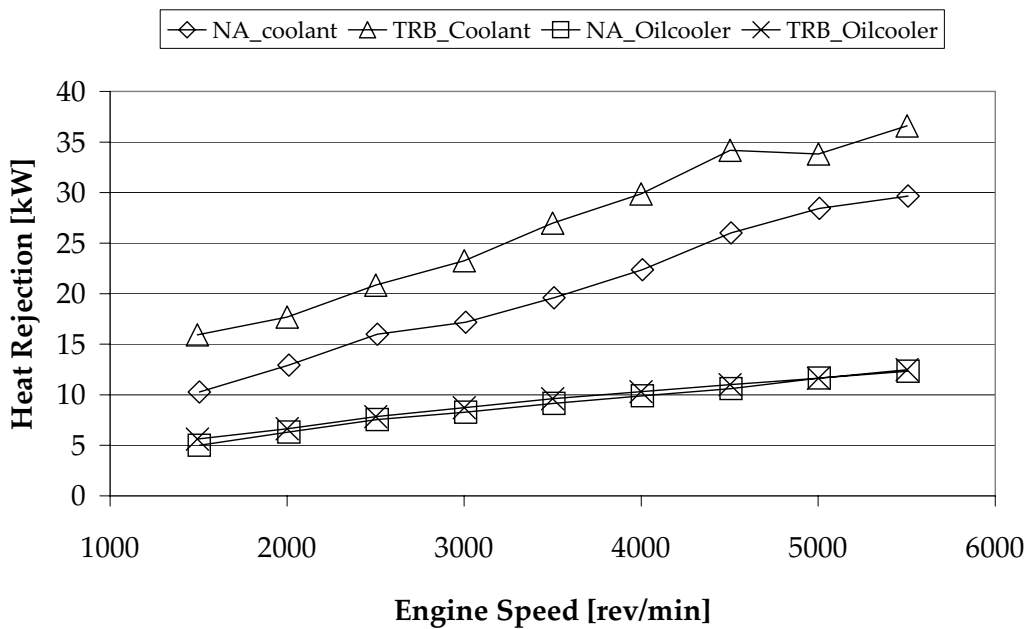


Figure 6-36 NA versus Turbocharged Results: Heat Rejection

It might be considered that the oil cooler is operating at its limit and therefore no more heat can be extracted, but when looking at the oil temperature as shown in Figure 6-37, it can be seen that the oil temperature of the turbocharged engine is actually lower than for the NA engine. This can be explained by the fact that the turbocharger's bearing housing is water-cooled. Thus most of the heat energy in the bearing housing is removed by the cooling system and not the oil; in fact some of the heat energy in the oil must be removed by the cooling system, because the oil temperature is lower for the turbocharged engine.

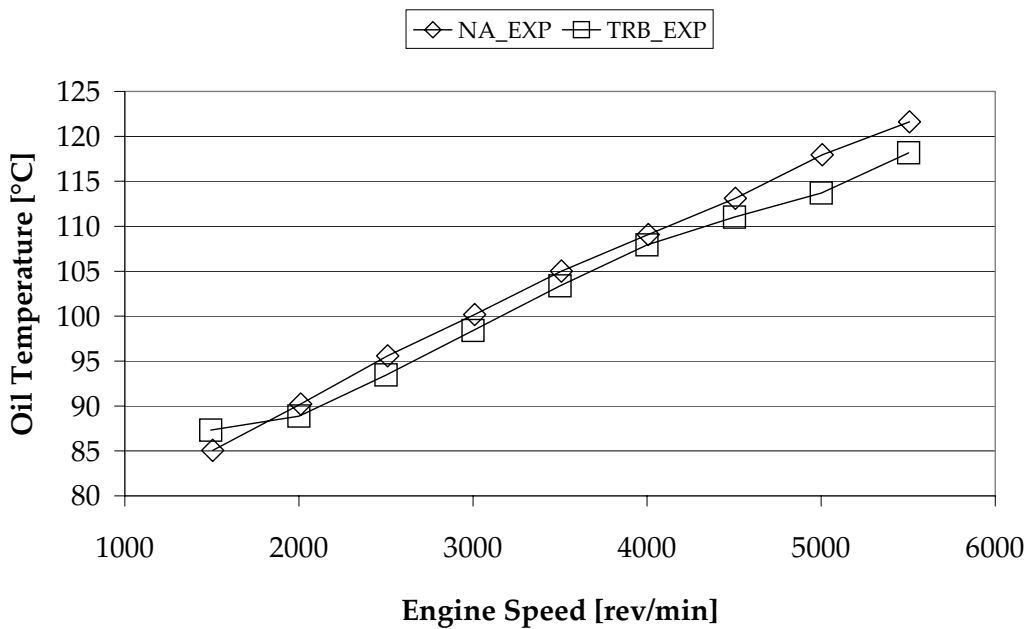


Figure 6-37 NA versus Turbocharged Results: Oil Temperature

When comparing the energy balance for the NA engine in Figure 6-38 to that of the turbocharged engine in Figure 6-39, it must be kept in mind that everything is in percentages and that 100% of the fuel energy for the NA engine is actually less than 100% for the turbocharged engine because of the different fuel quantities consumed.

It is interesting to note that the NA engine never converted less than 25% of the fuel energy into shaft energy, as opposed to the turbocharged engine, which at 5000 rev/min and 5500 rev/min is only converting 20% of the fuel into useful shaft energy. This is due to the fact that a very rich mixture was used to cool down the exhaust temperatures. What is a matter of concern is the fact that the “other” energy accounts for 38% to 46% of the fuel energy in the case of the turbocharged engine from 3000 rev/min to 5500 rev/min. This is due to the fact that unburned and partially burned fuel is leaving through the exhaust, which is unaccounted for in the energy balance. When operating at part load with lambda values near 1, the amount of “other” energy decreases drastically to about 6% to 10% of the fuel energy. This is shown and explained in section 6.3.5. The chemical energy contained in the carbon monoxide accounts for a maximum of 2% in the case of the NA engine and 3% for the turbocharged engine.

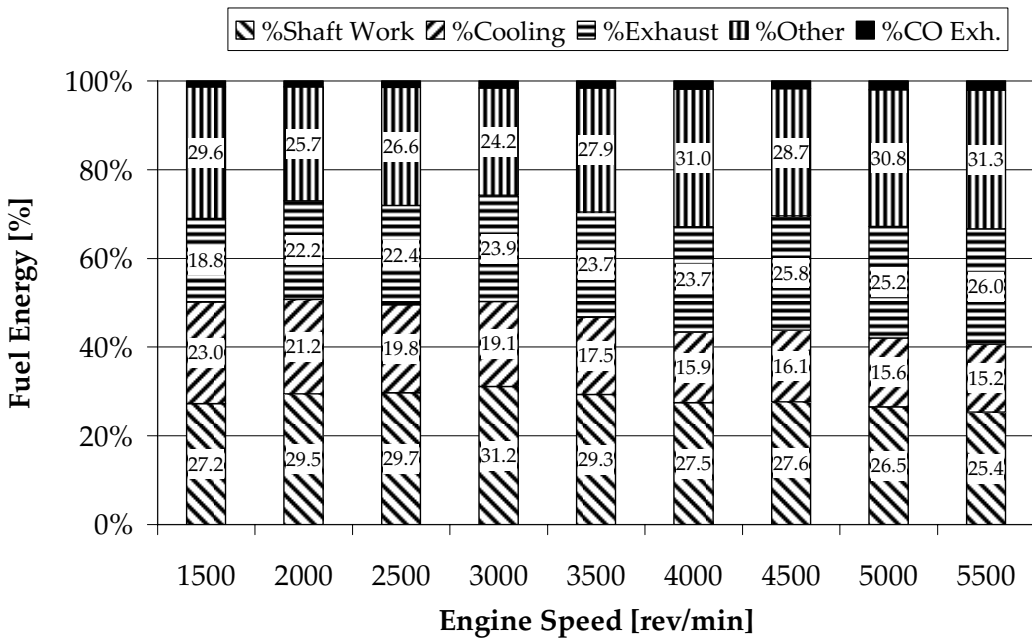


Figure 6-38 NA engine: Energy Balance at WOT

When comparing the percentage of energy leaving the exhaust, it can be seen that about 5% more goes to waste in the NA engine than in the turbocharged engine. This is where it is beneficial to have a turbine that utilises some of the energy that is available in the exhaust gas.

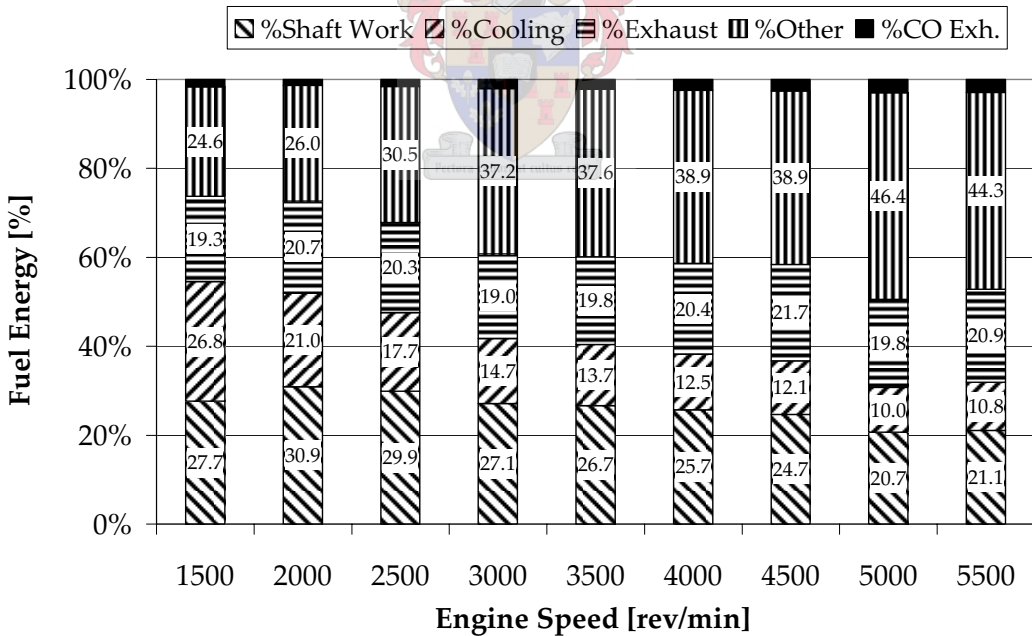


Figure 6-39 Turbocharged Engine: Energy Balance at WOT

6.3.4. Performance Comparison

Before the turbocharged conversion was done, the base engine was tested to have a baseline for comparison. After all the testing on the turbocharged engine was completed, the engine was built back to the original specification in order to see whether the engine sustained any damage or performance degradation. The torque measured before and after the conversion is presented in Figure 6-40. It can be seen that there are no major differences; thus it would be safe to assume that the engine has not suffered any damage because its performance is on par. This also gives an indication of the repeatability of the test procedure and reliability of the equipment used.

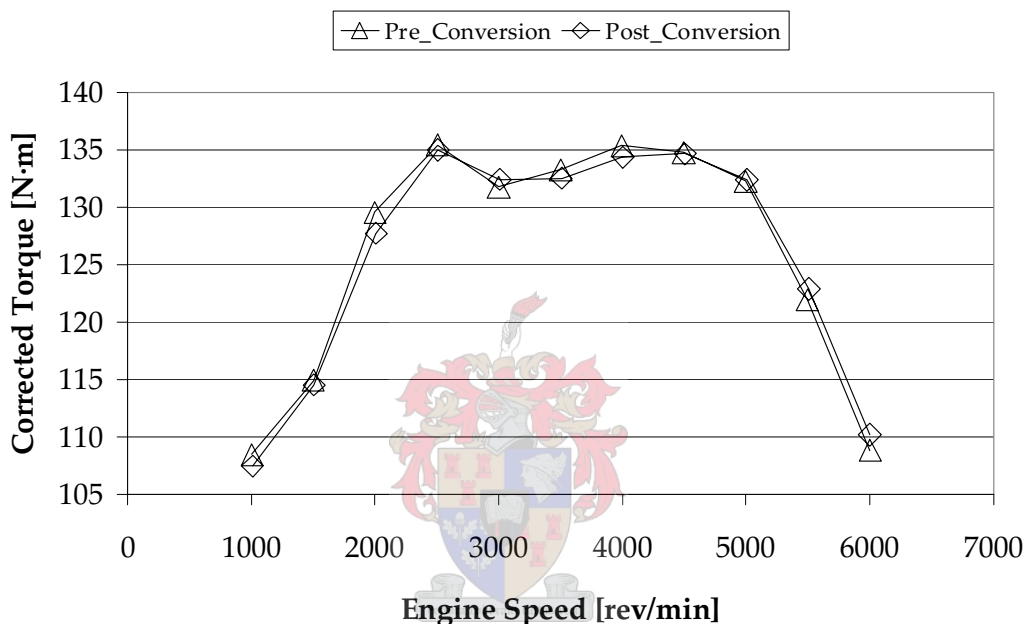


Figure 6-40 NA Engine Torque

The measured torque and power of the turbocharged and NA engine are shown in Figure 6-41. The torque was increased at 1500 rev/min with 27 N·m. The maximum increase in torque is at 4000 rev/min, where it is increased by 64 N·m, which translates to an increase of 48%. The maximum power output was increased by 37% to a maximum of 96 kW.

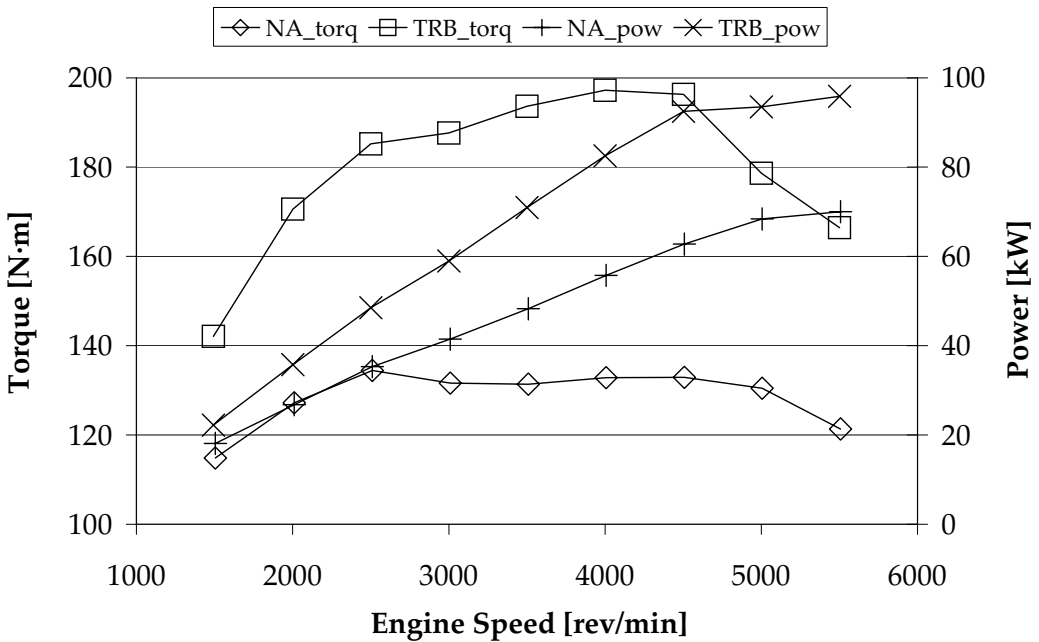


Figure 6-41 NA versus Turbocharged Results: Torque and Power

The target of 100 kW was thus not achieved on this power curve. This was due to the fact that the characteristics of the wastegate actuator were dependent on the diaphragm, which is temperature dependent. When the initial set-up was done, the wastegate was still relatively cold and thus the diaphragm was stiff. This caused the wastegate to open, but enough boost pressure was produced to obtain a maximum power of 100 kW at 5000 rev/min.

When the actual power curve was done, the measurement was started at low engine speeds and then increased by 500 rev/min steps. When the test has progressed to 5500 rev/min, the wastegate has warmed up and the diaphragm was not as stiff as when it was cold. This caused the wastegate to open more than during set-up and the necessary boost pressure was not obtained and the maximum power was thus less than obtained during the initial set-up.

The sharp decrease in torque at 5000 rev/min and 5500 rev/min could be due to the effect of retarded ignition timing, as shown in Figure 6-42, and the rich mixtures used, as shown in Figure 6-43. Due to the limitation of knock, the turbocharged engine could not use the same ignition timing as the NA engine, even though a fuel with a higher octane rating was used. The retarded ignition timing resulted in very high exhaust temperatures, thus a very rich mixture, as shown by the lambda values in Figure 6-43, had to be used to keep the exhaust temperature within reasonable limits.

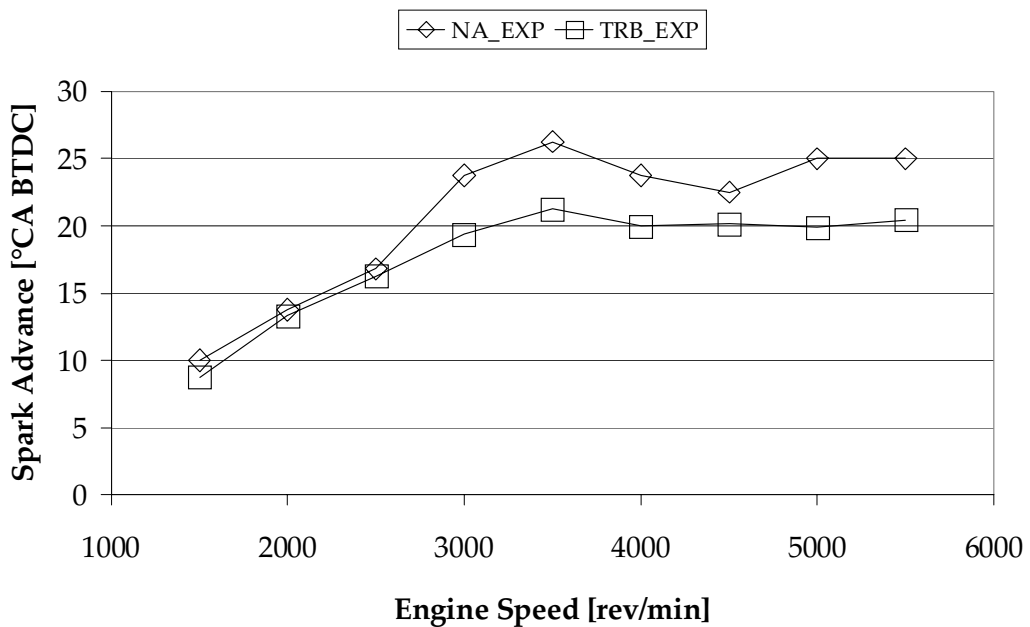


Figure 6-42 NA versus Turbocharged Results: Ignition Timing

During a telephonic interview with a calibration engineer, P Krabbendam (2004), who was involved with the initial calibration of the ECU on the standard production engine, the limit on exhaust port temperature was mentioned as 815 °C. This limit was due to the specific exhaust valves and valve seats being used in these engines.

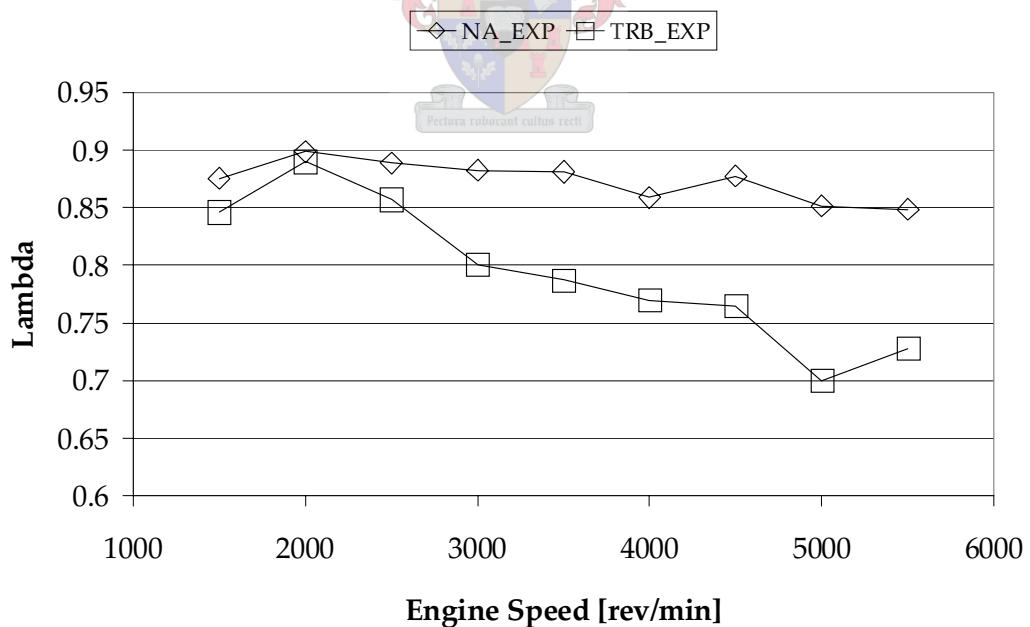


Figure 6-43 NA versus Turbocharged Results: Lambda

As a result of the retarded ignition timing and very rich mixtures, the turbocharged engine operated at a higher SFC than the NA engine, as shown in Figure 6-44. The lower the SFC the more efficient the engine. The highest SFC values were at 5000 rev/min and 5500 rev/min, where the lambda values were below 0.75. The turbocharged engine operated at lower SFC than the NA engine at engine speeds below 2500 rev/min. At these operating conditions the ignition timing was nearly the same, but the lambda was slightly richer than that of the NA engine. Thus the higher power output at these low engine speeds resulted in an SFC below that of the NA engine.

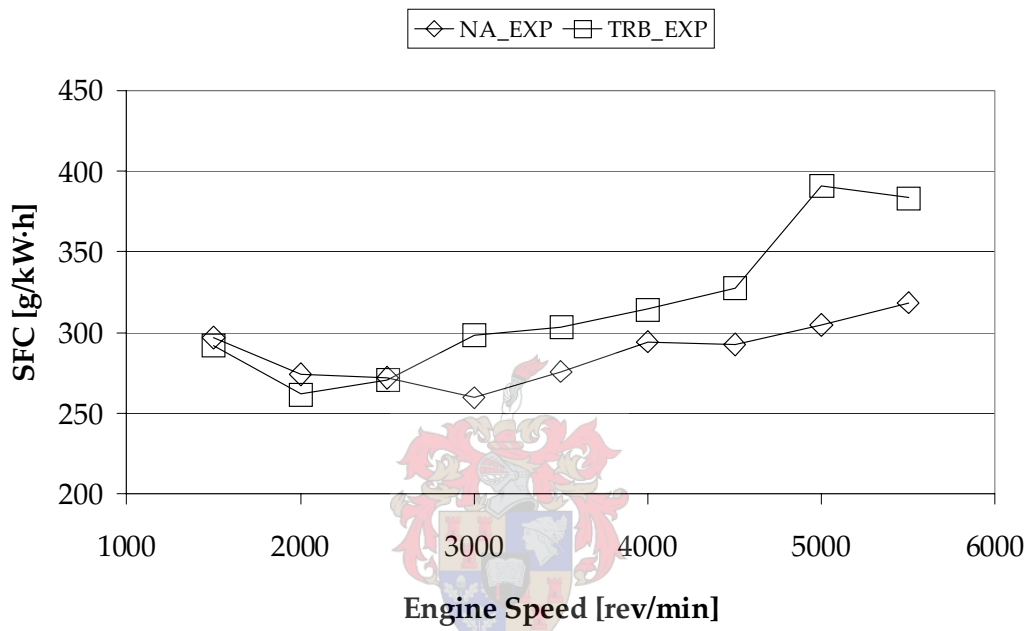


Figure 6-44 NA versus Turbocharged Results: SFC

The intake manifold absolute pressure, MAP, and intake manifold temperature, TMAP (measured with TMAP sensor), are shown in Figure 6-45. This indicates that the difference in MAP between the turbocharged and NA engine is nearly 60 kPa. The temperature difference between the two versions of the engine is about 50°C above 5000 rev/min. The boost pressure decreases slightly from 4000 rev/min and higher. This reduction in boost pressure can be attributed to the force on the wastegate valve caused by the pressure drop across the valve. Thus the wastegate opens more and less boost pressure is developed.

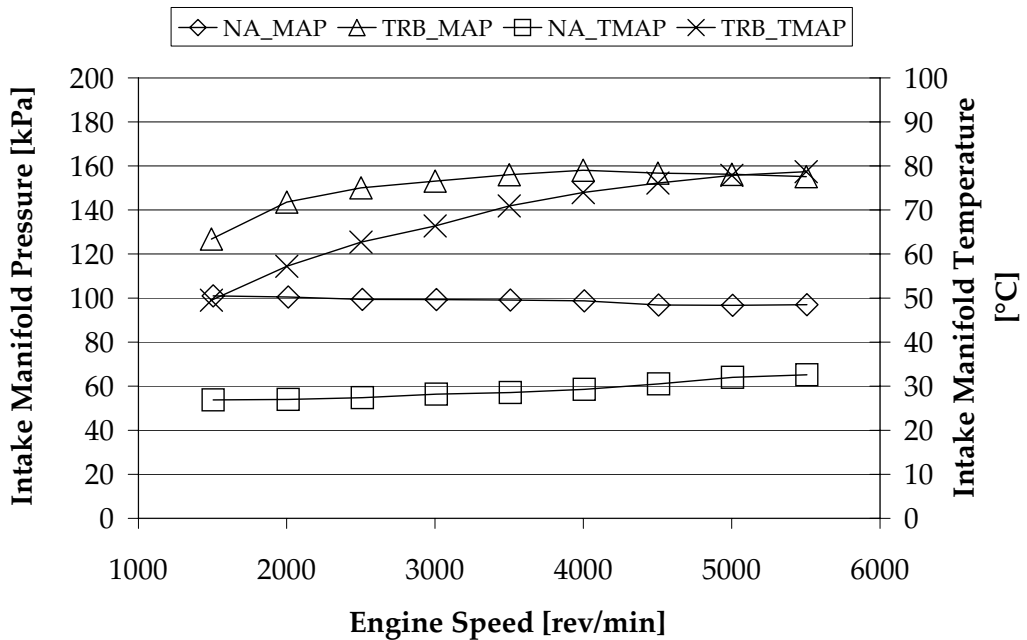


Figure 6-45 NA versus Turbocharged Results: MAP and TMAP

The boost pressure versus wastegate area is shown in Figure 6-46. It can be seen that the wastegate opens more for the same boost pressure when the area is bigger than 2.5 cm^2 . This was phenomenon was explained in a previous section (p 98).

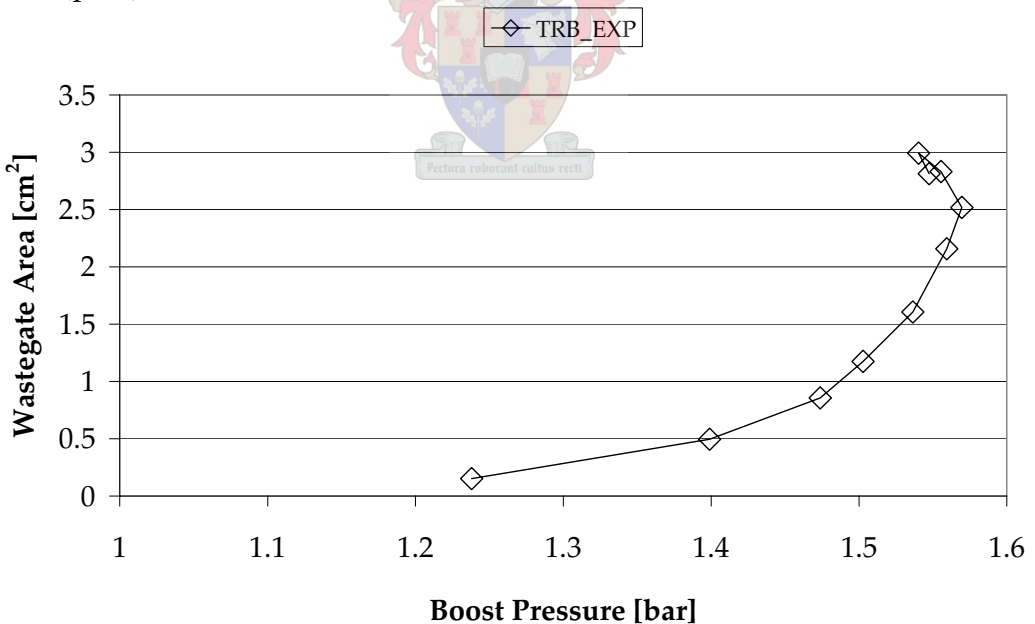


Figure 6-46 NA versus Turbocharged Results: Wastegate Area

The increased pressure in the manifold resulted in a higher density in the manifold, as shown in Figure 6-47. The effect of decreasing boost pressure and increasing temperature is clearly visible on the air density inside the intake manifold of the turbocharged engine for engine speeds above 4000 rev/min. On the NA engine a similar phenomenon is witnessed, and this is due to the increase in temperature and the decrease in MAP. MAP drops as speed increases due to the upstream restrictions including the clean air system (filter, pipes and throttle body).

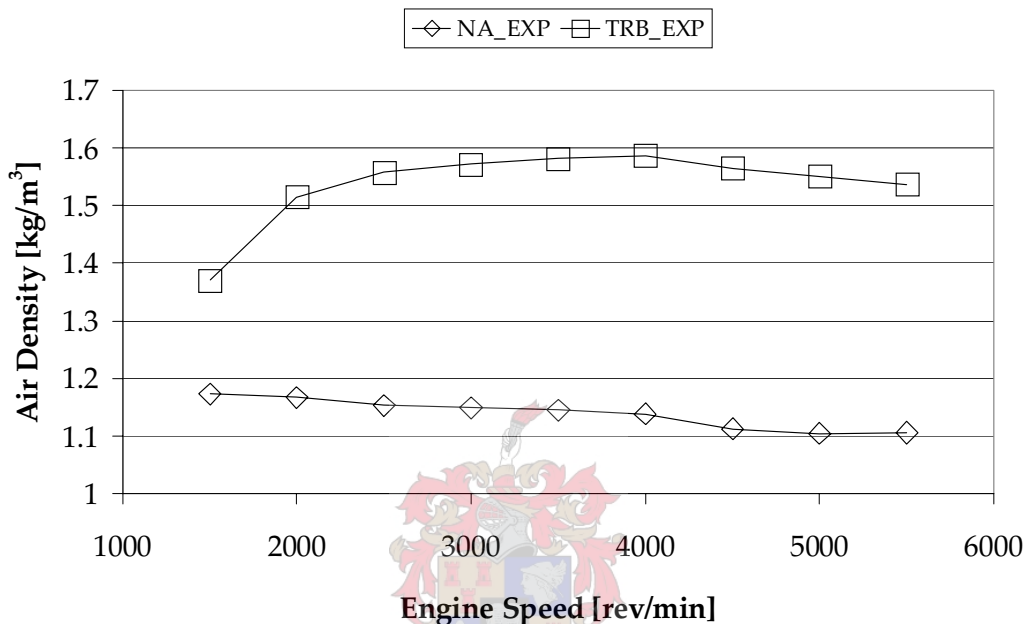


Figure 6-47 NA versus Turbocharged Results: Intake Manifold Air Density

The increase in TMAP for the NA engine is due to the ambient air temperature, as shown in Figure 6-48, which increased during the duration of the test. The ambient temperature increased, since the test-cell did not have controlled air temperature.

The temperature increase from ambient to TMAP for the turbocharged engine is due to the compression of the air through the compressor. If an intercooler had been installed, the TMAP could have been reduced. This would have had a major effect on the density, since density is inversely proportional to temperature. Thus it would have been possible to develop the same amount of torque with a lower boost pressure. If a moderate temperature difference of 30°C could be achieved across the intercooler, it would be possible to obtain the same density with a decrease of 9% on boost pressure, thus the boost pressure could be lowered to about 0.43 bar instead of 0.58 bar (gauge).

Therefore if this engine would be developed for production, it should not be considered without an added intercooler. The main reason why an intercooler was not included on the experimental engine is that the target power output could be achieved without an intercooler.

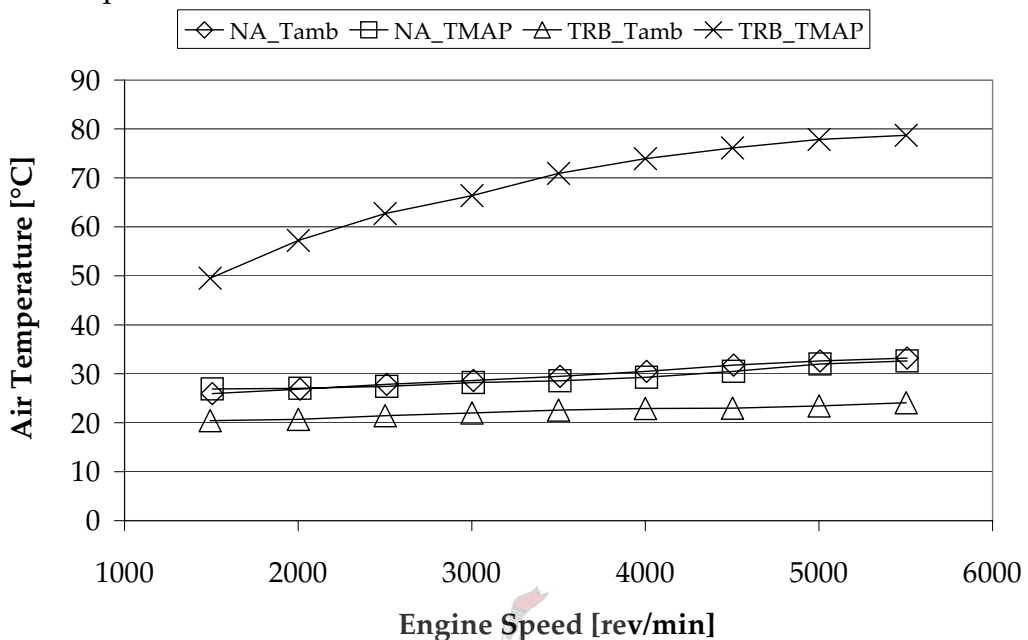


Figure 6-48 NA versus Turbocharged Results: Ambient and Intake Manifold Air Temperature

The airflow is compared in Figure 6-49. The maximum airflow at 5500 rev/min was increased by 37% to 400 kg/h.

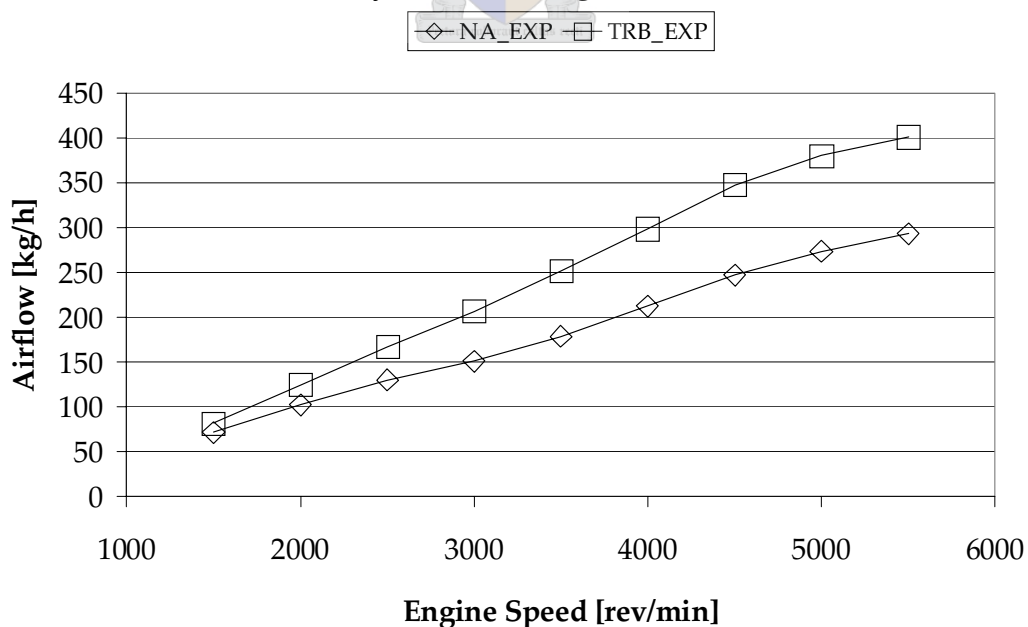


Figure 6-49 NA versus Turbocharged Results: Airflow

When considering the volumetric efficiency, which is based on the manifold conditions, as shown in Figure 6-50, the NA engine has a higher volumetric efficiency below 2500 rev/min than the turbocharged engine. Above 2500 rev/min the higher air density increases the volumetric efficiency of the turbocharged engine above that of the NA engine.

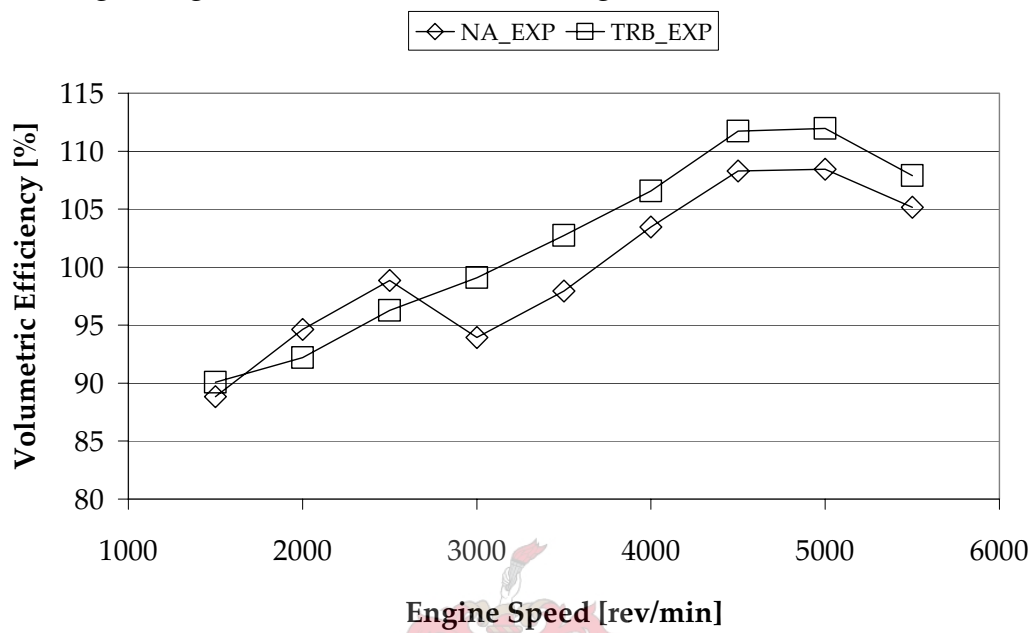


Figure 6-50 NA versus Turbocharged Results: Volumetric Efficiency

When considering the exhaust manifold pressure as shown in Figure 6-51, it can be seen that the turbine causes a very large backpressure.

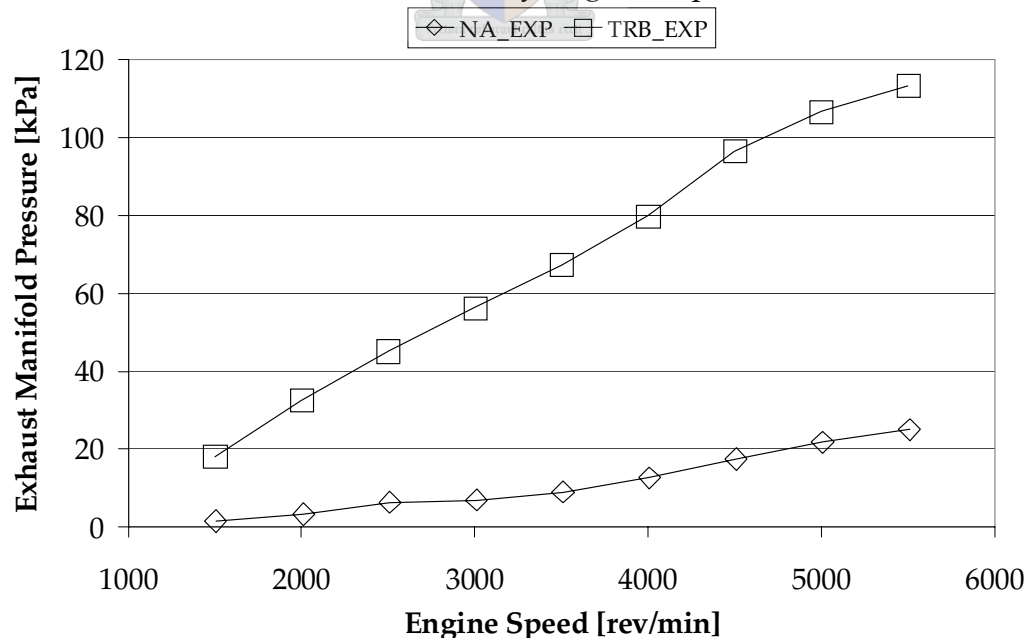


Figure 6-51 NA versus Turbocharged Results: Exhaust Manifold Pressure

To put the exhaust manifold pressure into perspective, let us consider the pressure difference between the intake and exhaust manifold. This pressure difference is shown in Figure 6-52. The turbocharged engine's pressure difference is positive at engine speeds below 2500 rev/min. This is also the range where a lower SFC was recorded for the turbocharged engine. Thus above 2500 rev/min the engine does pumping work, which might seem contradicting to the principle of turbocharging. Due to the boost limitation on spark ignition engines this will always be witnessed for especially engines fitted with a small turbocharger to improve the engines response. On large compression ignition engines, it would be expected that there is always a positive pressure difference across the engine if it is a well designed system (Watson & Janota, 1984).

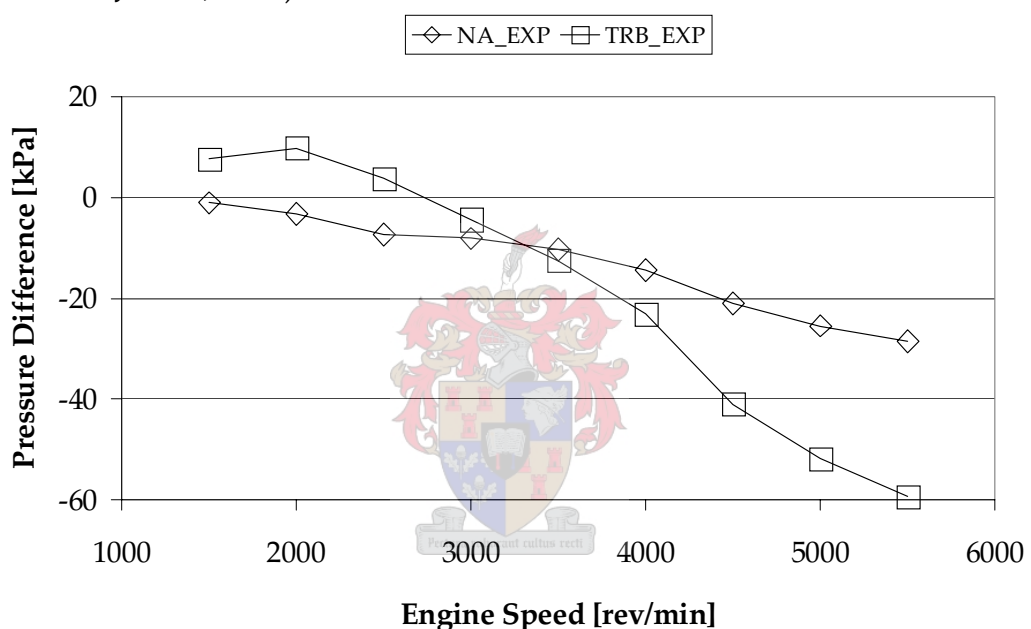


Figure 6-52 NA versus Turbocharged Results: Pressure Difference (Intake Manifold - Exhaust Manifold)

The exhaust backpressure (post turbine) is plotted as a function of mass flow, the sum of fuel flow and airflow, in Figure 6-53. This is where the advantage of the free flow exhaust is evident. The measured exhaust backpressures are about the same, but they occur at very different mass flow rates. Therefore the free flow exhaust system can handle more mass flow while producing the same backpressure as the standard exhaust system.

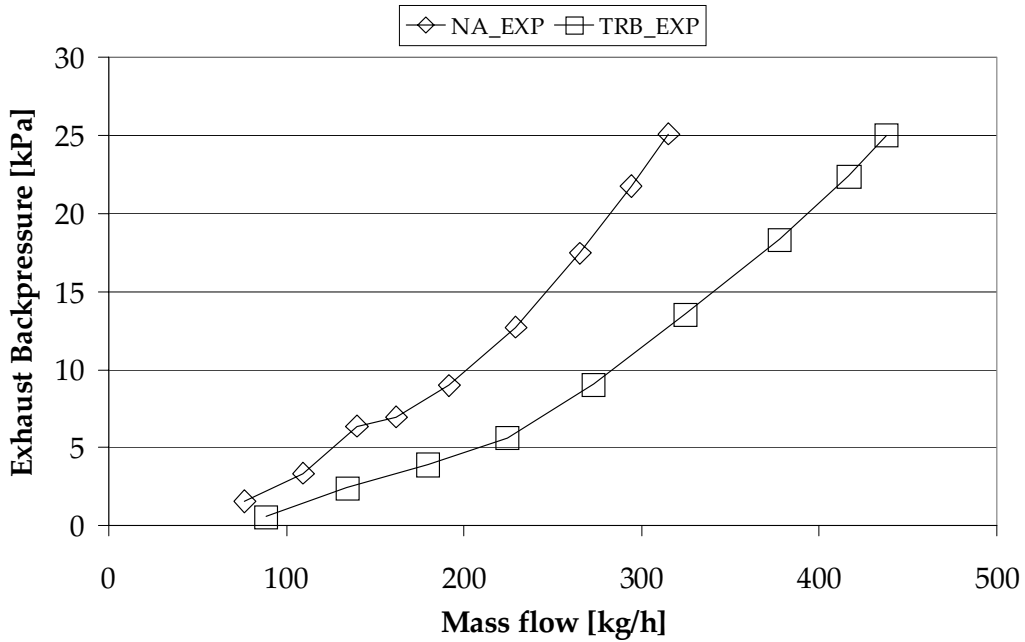


Figure 6-53 NA versus Turbocharged Results: Exhaust Backpressure

In general it can be assumed that the bigger the pressure difference across the turbine the more energy can be extracted. Whereas the difference in temperature across the turbine gives an indication of the amount of energy extracted. Thus it is important to reduce the exhaust backpressure to make more energy available to the turbine. A too low backpressure and a too small wastegate could result in the turbine extracting too much energy and exceeding its speed limit. This could result in rotor failure and serious damage to the engine and turbocharger.

When comparing the exhaust manifold temperatures as shown in Figure 6-54, the trends for both engines are similar. The difference in exhaust manifold temperature varies from 50°C up to 100°C for the two versions of the engine. This offset can be attributed to a variety of factors such as the retarded ignition timing, higher initial charge temperature, higher residual mass in the cylinders due to the high exhaust manifold pressure and the higher exhaust manifold pressure. The higher exhaust manifold pressure limits the amount of expansion and thus causes an increase in the exhaust temperature.

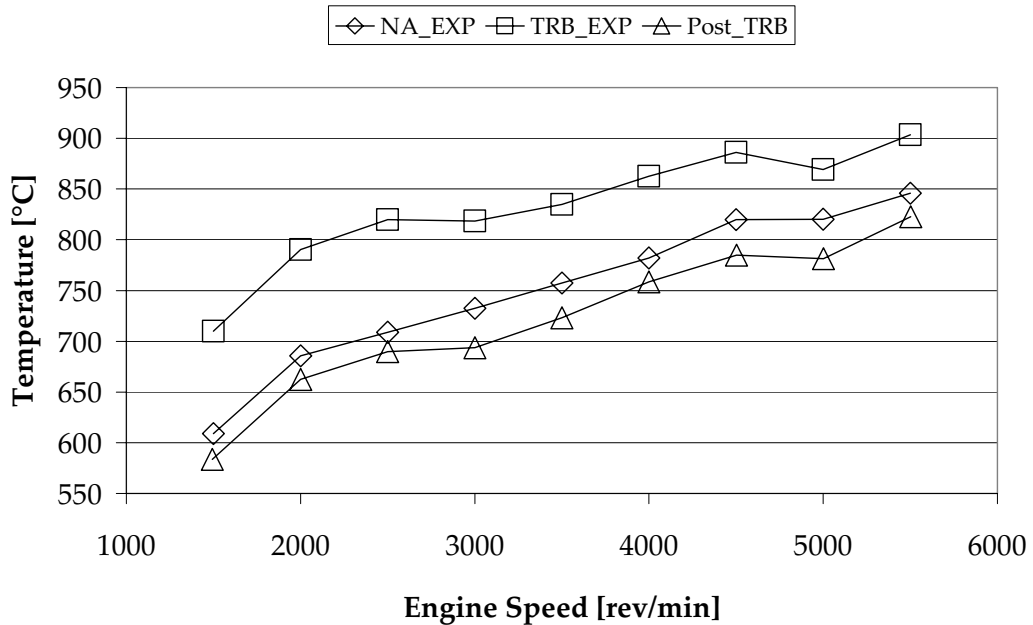


Figure 6-54 NA versus Turbocharged Results: Exhaust Manifold Temperature

Post turbine temperatures are on average 30°C lower than the NA exhaust manifold temperatures. The difference between pre and port turbine temperatures decreases with increasing engine speed. This is due to the increasing amount of exhaust gas flowing through the wastegate and not passing through the turbine. The energy of the gas passing through the wastegate can not be recovered by the turbine.

When considering the fuel consumption as a function of the power developed, as shown in Figure 6-55, it is clear to see the non-linearity when developing more than 93 kW at 5000 rev/min and 5500 rev/min. This is a result of the very rich mixtures that had to be used in order to cool the exhaust temperatures. But when considering the fuel consumption at lower engine speeds, both engines have similar fuel conversion efficiencies, thus the same amount of fuel is used to develop the same amount of power. This relation would not hold if the CR of the turbocharged engine were lowered. If the CR were lowered, the engine would be less likely to knock, but a lower CR is less efficient (Ferguson, 1986). Using a lower CR could enable the use of more advanced ignition timing and leaner mixtures, thus improving the combustion and recovering part of the inefficiency associated with a low CR, especially at WOT. However at part load where knock is not a limitation and lean mixtures are used to improve fuel consumption, it would thus not be possible to recover the inefficiency of a lower CR at part load.

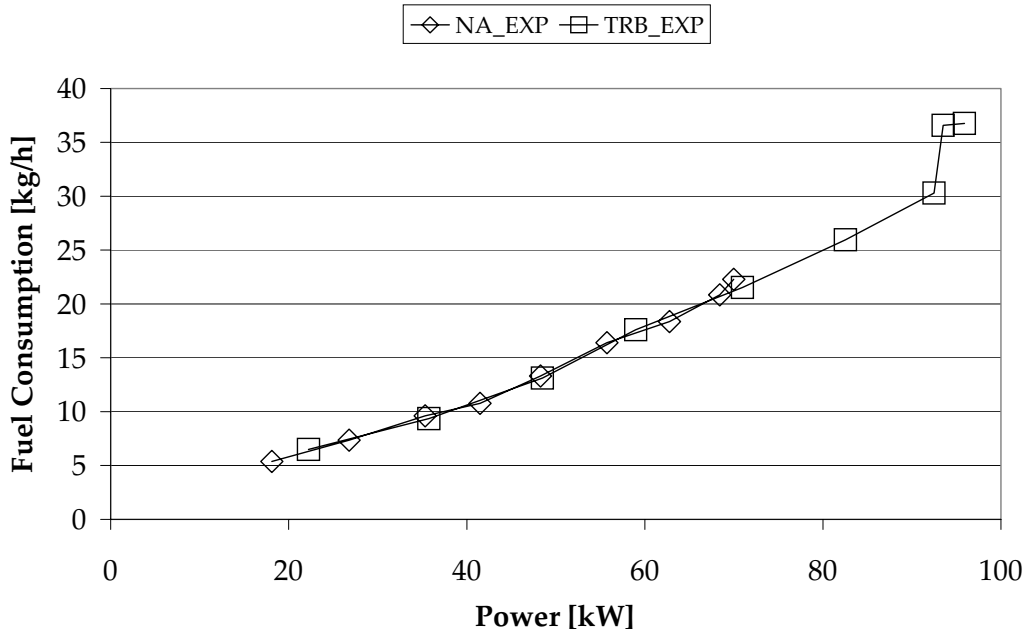


Figure 6-55 NA versus Turbocharged Results: Fuel consumption vs Power Output

When comparing the burn duration from the 10% to 90% burn point as shown in Figure 6-57, it can be seen that the turbocharged engine's burn duration is relatively constant up to 3500 rev/min. Above this speed, the burn duration continually increases. This can be explained by the fact that the ignition timing remains rather constant, but the mixture is enriched for engine speeds above 3500 rev/min as shown in Figure 6-56. At 5000 rev/min and 5500 rev/min, where the lambda is below 0.75, the burn duration is considerably longer.

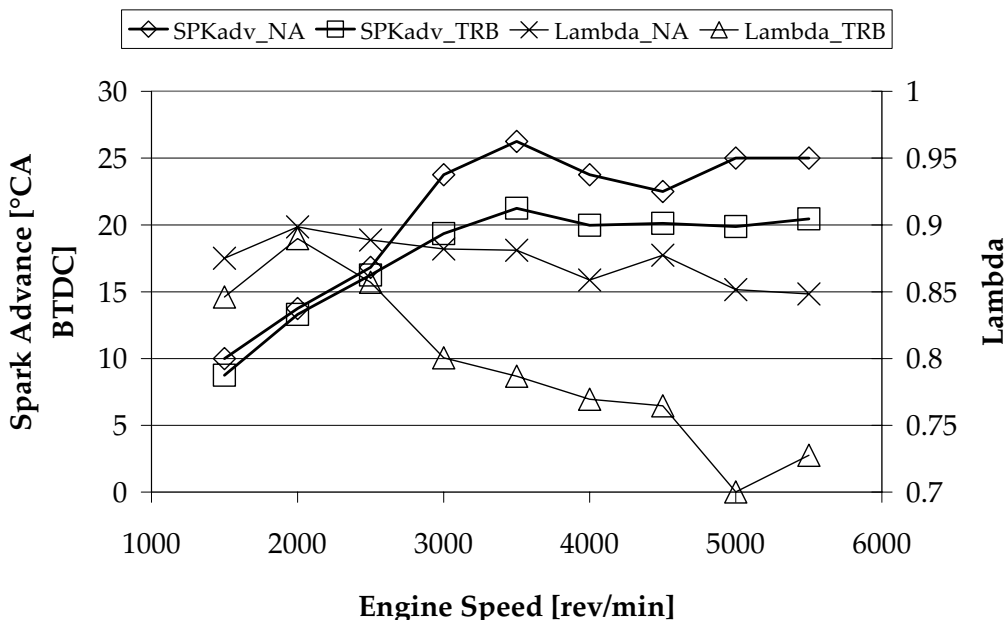


Figure 6-56 NA versus Turbocharged Results: Spark Advance and Lambda

The reason why the burn duration at 4500 rev/min of the NA engine is longer than that at 5000 rev/min is due to the timing that was retarded at 4500 rev/min. Thus the burn duration is not only dependent on the air/fuel ratio, but also on the ignition timing.

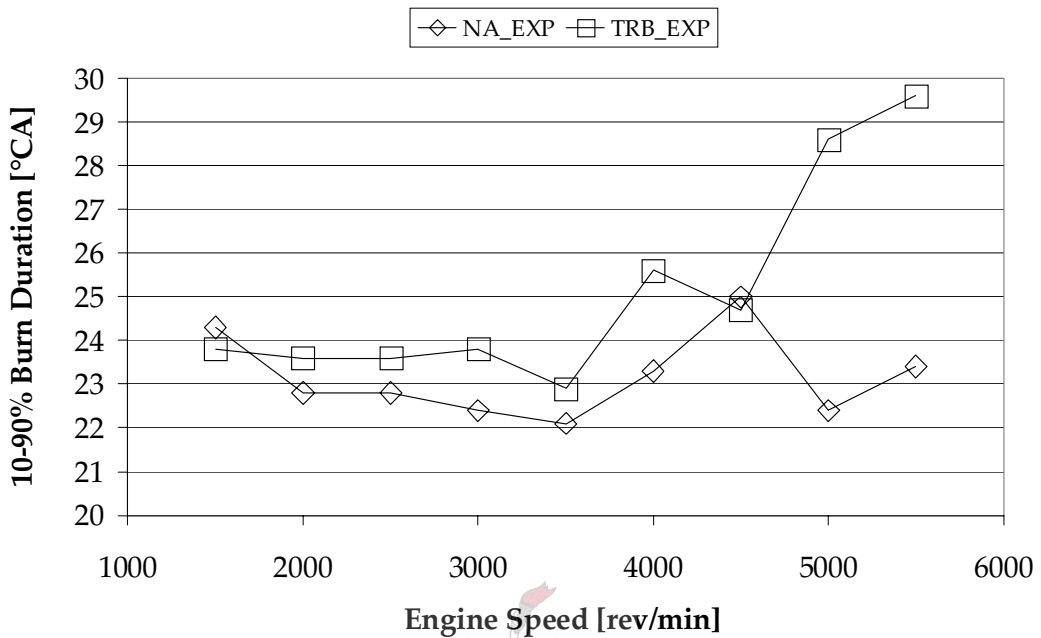


Figure 6-57 NA versus Turbocharged Results: Burn Duration

Figure 6-58 compares the 50% burn point. This is the crank angle at which 50% of the mass of fuel was burned. It is an indication of ignition timing and burn duration, however where ignition occurs before TDC, the 50% burn point usually only occurs after TDC.

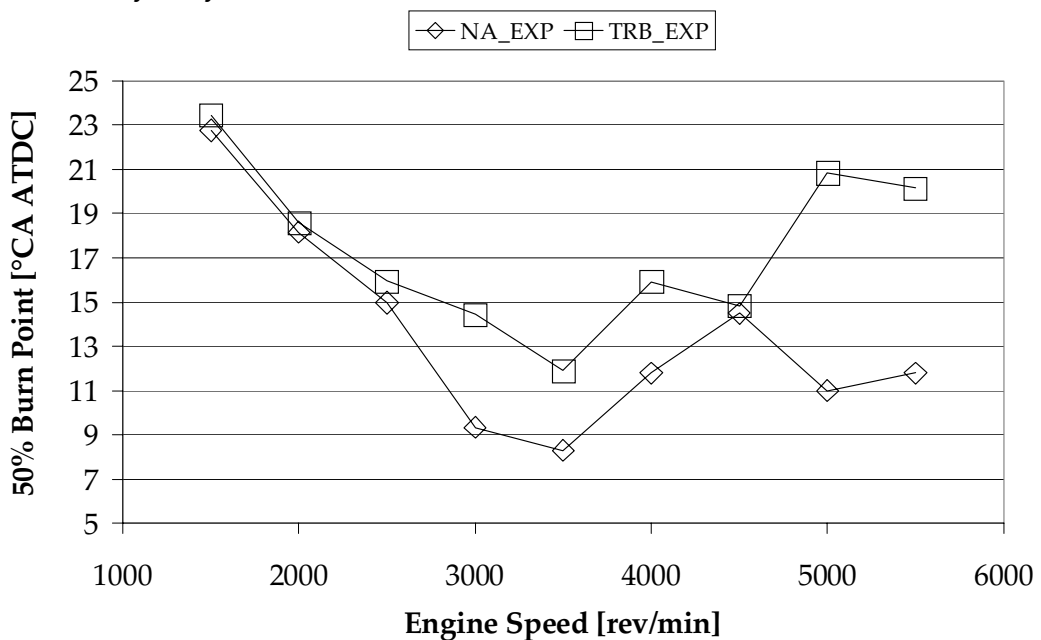


Figure 6-58 NA versus Turbocharged Results: 50% Burn Point

The maximum combustion pressure is shown in Figure 6-59. The maximum pressure for the turbocharged engine was more than that of the NA engine, as could be expected due to the higher charge and heat release in the combustion chamber. This is true except at 5000 rev/min, where the maximum combustion pressures of both engines were nearly the same. This is due to the long burn duration and the retarded ignition timing.

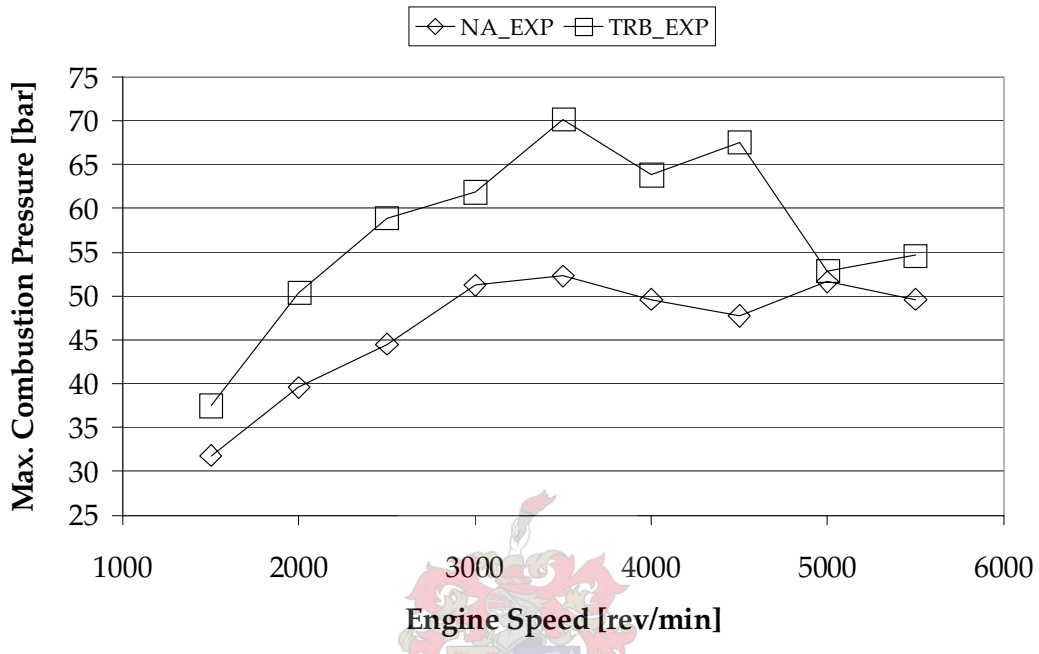


Figure 6-59 NA versus Turbocharged Results: Maximum Combustion Pressure

When further considering the maximum combustion pressure of the turbocharged engine, it can be seen that it nearly represents the shape of the torque curve. The maximum combustion pressure of 70 bar was measured at 3500 rev/min, but the maximum percentage increase of 41% in combustion pressure was witnessed at 4500 rev/min.

6.3.5. Part-load Comparison

During part load calibration, the same lambda values as the NA engine were used, as long as the exhaust port temperatures remained below 815°C. The ignition timing was optimised and thus it was set at MBT or KLSA, whichever occurred first. The calibration for the NA engine was not altered, since it is a standard factory calibration and should already have been optimised.

Testing was done only at two speeds, 2500 rev/min and 4000 rev/min, which are the engine speeds where maximum torque was developed for the NA engine and turbocharged engine, respectively. The maximum torque of the NA engine at both speeds was used as the baseline, and assigned a value of 100%. All the comparisons are made in terms of percentage load, thus percentage load of the NA engine at that speed.

Considering the part load SFC as presented in Figure 6-60, it is very interesting to note that the SFC values for both engines at the different speeds are fairly similar up to 60% load. At 80% load and 4000 rev/min, the turbocharged engine's exhaust temperature was very high and lambda was reduced from 1.05 to 0.95 to keep the exhaust temperature within the limits, thus the higher SFC for the turbocharged engine at 4000 rev/min can be explained.

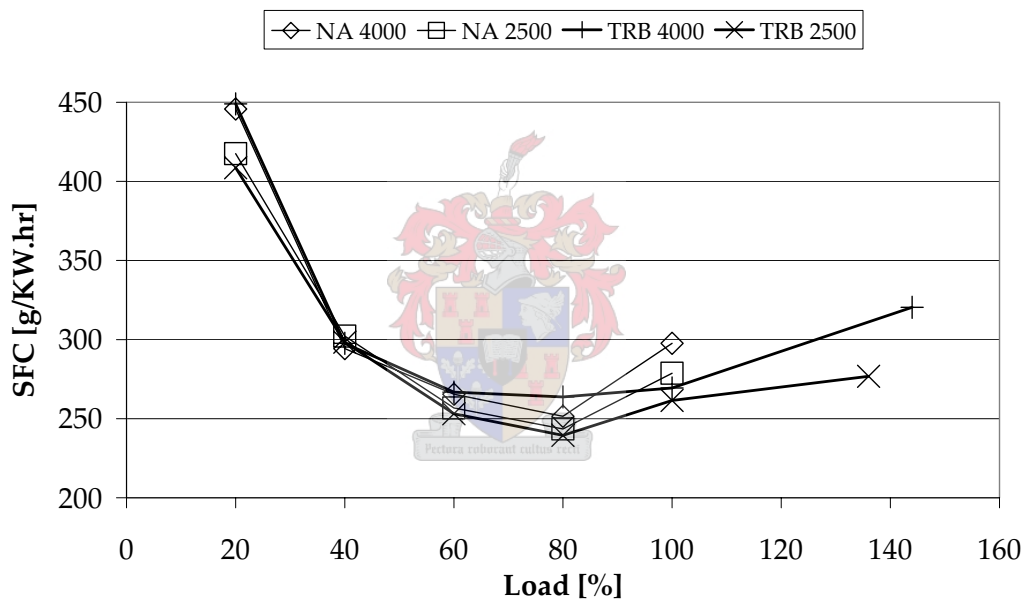


Figure 6-60 NA versus Turbocharged Results: Part load SFC

The main reason why the SFC at 100% load for the turbocharged engine is better than the NA engine is due to the fact that the same lambda values could not be reached due to the full load mixture enrichment necessary on the NA engine. The turbocharged engine did not require a rich mixture to cool the exhaust temperatures when operating at 100% of the NA engine's torque. Thus a lambda was adjusted for best fuel consumption while maintaining the exhaust temperature below the upper limit. The spark advance and lambda used during part load testing are presented in Figure 6-61 and Figure 6-62 respectively.

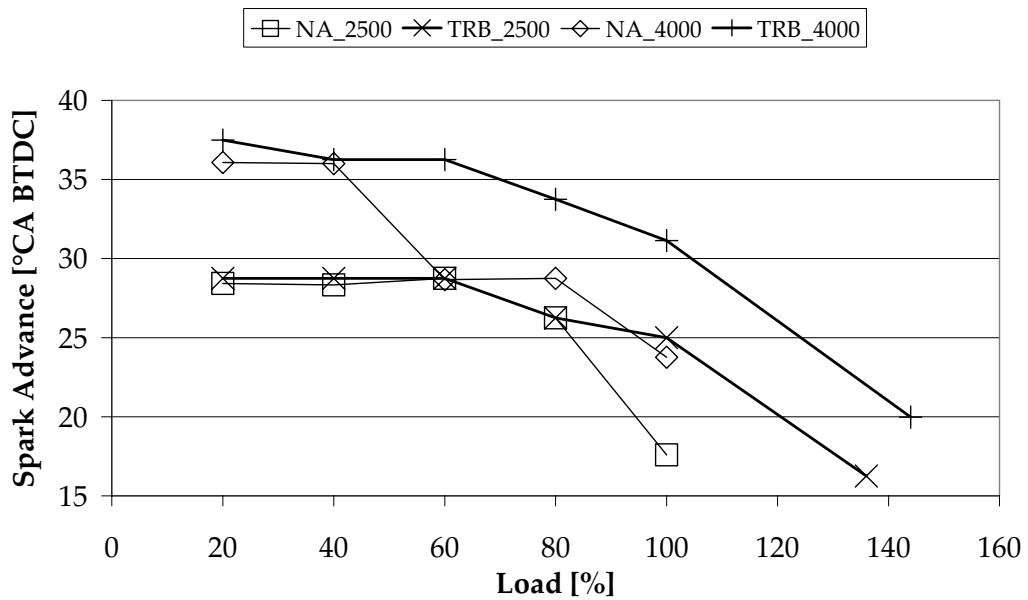


Figure 6-61 NA versus Turbocharged Results: Part load Spark Advance

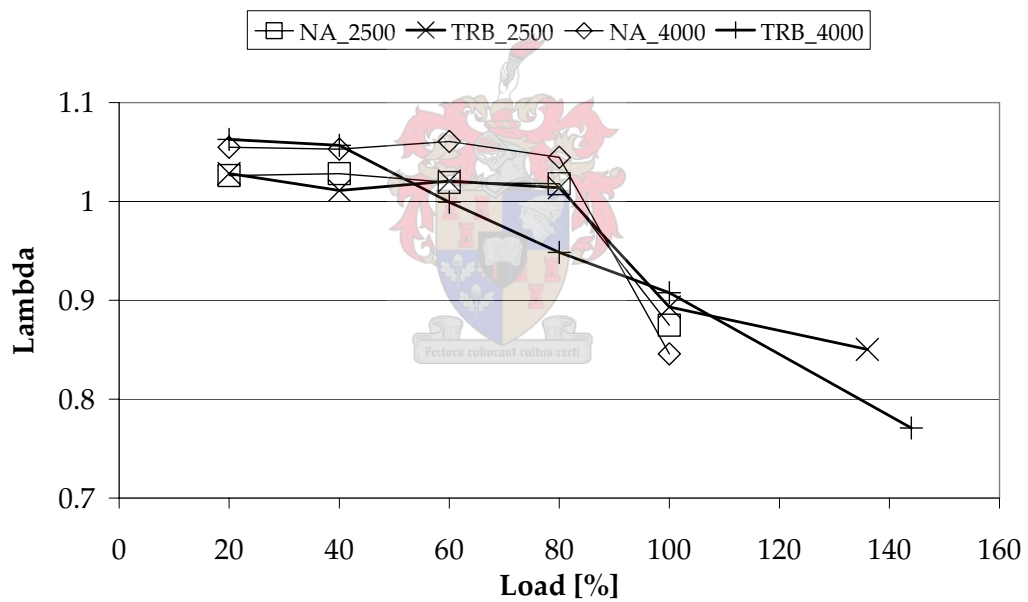


Figure 6-62 NA versus Turbocharged Results: Part load Lambda

At 4000 rev/min the turbocharged engine was severely limited by the high exhaust temperatures and thus the lambda was reduced to keep the exhaust temperature within the limits.

When operating the turbocharged engine at 2500 rev/min and lambda close to 1, about 92% of the fuel energy, as shown in Figure 6-63, can be accounted for by the sum of shaft, cooling and exhaust energy, which is referred to as Energy [%]. The exhaust energy is the potential thermal energy. The chemical energy in the carbon monoxide (CO) and unburned fuel that exist in the exhaust gas are not accounted for. For the NA engine about 88% of the fuel energy can be accounted for when operating at lambda close to 1. However, when lambda was decreased below 0.9, the percentage of accounted energy decreased to 80% and decreased even further if lambda was decreased more. This indicates that there is a lot of partially burned (carbon monoxide) and unburned fuel leaving the engine through the exhaust. This is verification of the fact that a large percentage of unaccounted, or "other", energy as shown in Figure 6-38 and Figure 6-39 is partially burned and unburned fuel at WOT.

The reason why the NA engine can only account for about 88% of the fuel energy when operating close to lambda 1, while the turbocharged engine can account for about 92% of the fuel energy, is because the turbocharged engine uses less fuel to develop the same amount of power. The actual amounts of shaft, exhaust and cooling energy are very much similar for both engines, but because the turbocharged engine uses less fuel it can account for a high percentage of the fuel energy. The radiation losses for both engines should be nearly the same because the operating temperatures of both engines were the same. The unaccounted for energy can thus be attributed to unburned and partially burned fuel in the exhaust as well as a percentage measurement error.

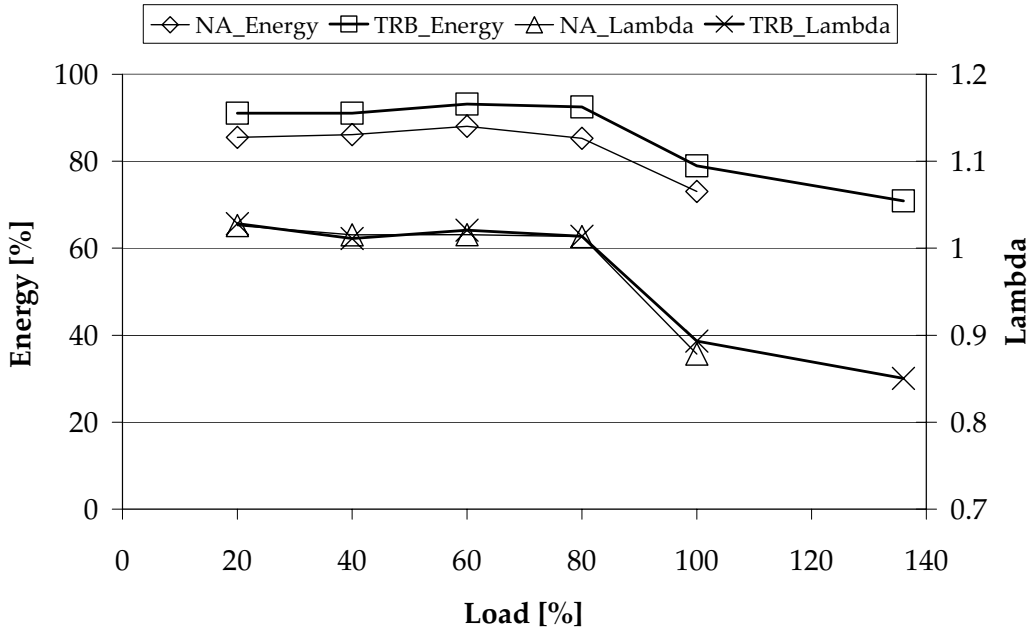


Figure 6-63 NA versus Turbocharged Results: Part load Energy Balance at 2500 rev/min

Probably the most significant results are represented by fuel flow and can be seen in Figure 6-64. It can be seen that fuel flow at part load is nearly the same for both engines. It is only at WOT that the turbocharged engine uses more fuel than the NA engine. This extra fuel is not only used to cool the exhaust temperature, but also to produce more power. This indicates that the turbocharged engine not only develops more power, but could also match the fuel economy at part load of its NA engine counterpart.

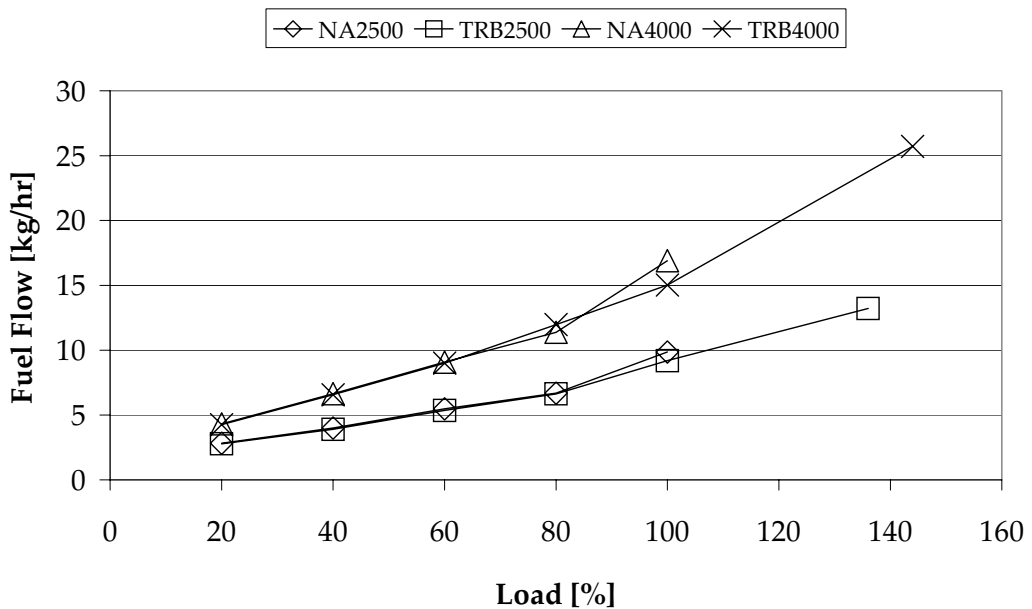


Figure 6-64 NA versus Turbocharged Results: Part load Fuel Flow

At a load equal to 100% of the NA WOT load the turbocharged engine is 7% and 11% more fuel efficient at 2500 rev/min and 4000 rev/min respectively and only 5% less fuel efficient at 80% and 4000 rev/min. It can thus be concluded that a vehicle would be equally or more fuel efficient given the same loading conditions.

When comparing part load fuel consumption, the turbocharged engine's consumption should be compared to a NA engine with the similar power rating. Only then could the real advantage of having a small-displacement, high-power output engine be put into perspective.

When comparing the rated power output of NA engines that are available on the market at the time of writing this report, it was found that the 2-litre class develops around 95 to 100 kW. Thus this turbocharged engine is 25% smaller than similar rated NA engines. When comparing the peak torque the turbocharged engine develops about 14% more torque than the average 2-liter NA engine

Typical engine power requirements to maintain a constant speed on a level road with a medium size passenger vehicle such as a mid '90s Toyota Corolla was determined by Bell, A J (2005) and shown in Figure 6-65.

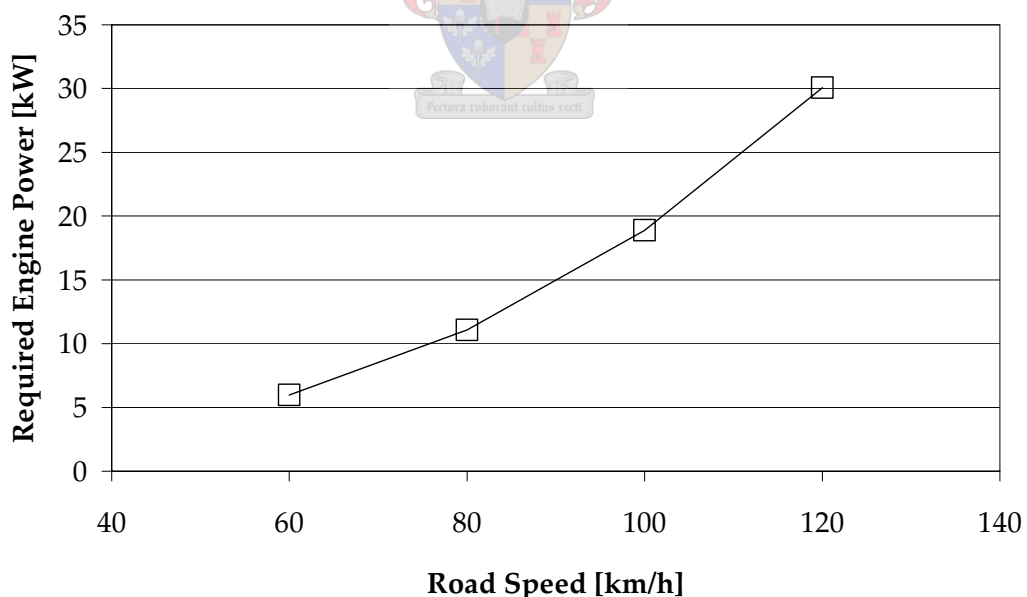


Figure 6-65 Required Engine Power

To illustrate the advantage of a small turbocharged engine to a similar rated bigger NA in this case a 1.6-liter turbocharged versus a 2.0-litre NA engine, the torque of the 1.6-litre NA engine was scaled up by 25% which would be the increase in displacement. It was assumed that the SFC of both NA engines would be similar at a specific percentage load. These scaled torque values were used as reference and maximum torque at a specific engine speed was assigned a value of 100%. The torque developed by the turbocharged engine was calculated as a percentage of the 2.0-liter NA engine's torque. The SFC was plotted against the turbocharged engine's SFC as measured. This was done for both 4000 rev/min and 2500 rev/min and is shown in Figure 6-66 and Figure 6-67 respectively. Superimposed on these graphs are the percentage load required to maintain constant speeds of 80, 100 and 120 km/h and corresponding SFC indicated by the shaded markers.

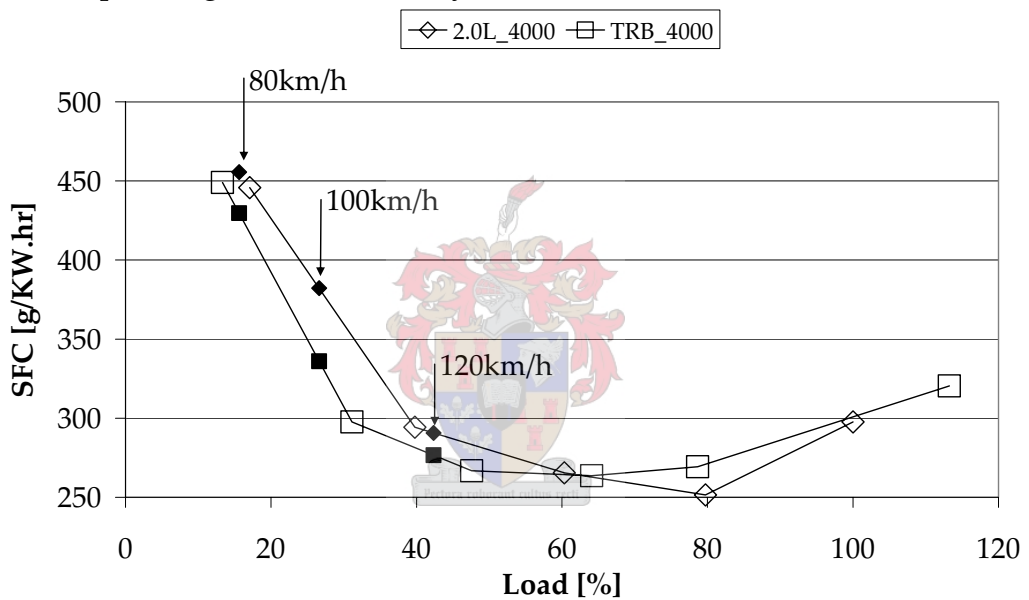


Figure 6-66 2.0L NA versus Turbocharged SFC at 4000 rev/min

The markers for 60km/h could not be included in either graph, since the required power was outside the tested range.

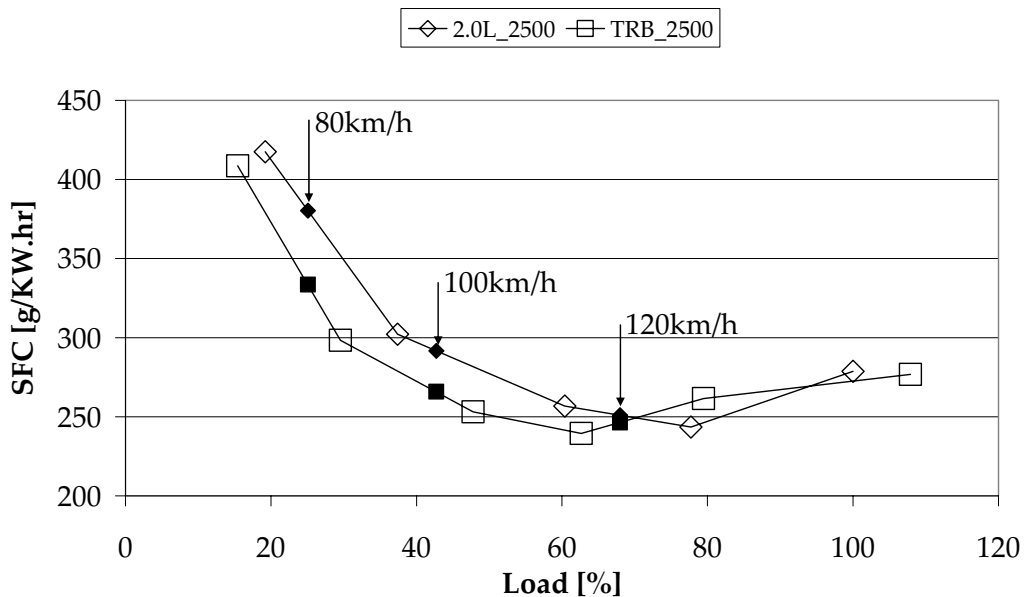


Figure 6-67 2.0L NA versus Turbocharged SFC at 2500 rev/min

Table 6-1 illustrates the percentage fuel saved by using the turbocharged engine instead of the big NA engine.

Table 6-1 Estimated Fuel Saving

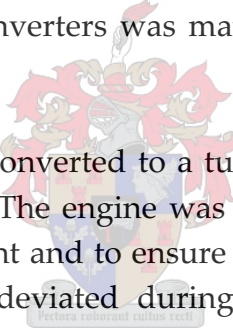
Load [%]	Engine Speed	Road Speed [km/h]	Fuel saving [%]
42	4000	120	5.3%
27	4000	100	9.6%
16	4000	80	12.8%
68	2500	120	1.0%
43	2500	100	8.8%
25	2500	80	11.6%

It can thus be concluded that the turbocharged engine is 12.8% and 11.6% more fuel efficient than the bigger NA engine at 80km/h with engine speeds of 4000 rev/min or 2500 rev/min respectively. The turbocharged engine is more fuel efficient while having the capability to produce 14% and 8% more torque than the bigger NA engine at 4000 rev/min and 2500 rev/min respectively.

7. CONCLUSION

The development of a turbocharged spark ignition engine from a naturally aspirated engine and the simulation and prediction of its performance were the objectives and scope for this research project. These objectives were successfully accomplished enabling the comparison of NA and turbocharged engines.

Relevant literature was reviewed and was presented to the reader to familiarise them with the theory behind turbocharging. The functionality of the simulation package was briefly discussed. Simulation was used to optimise valve timing and to illustrate the advantage that optimised valve timing would have over the standard valve timing. Simulation was also used to evaluate two exhaust manifold concepts. The exhaust manifold concept evaluation showed that the concept using simple pulse converters was the better of the two concepts. However, differences in overall performance were very small and due to the advantage of simplicity and ease of manufacture the concept without pulse converters was manufactured and used in actual testing.



The engine was successfully converted to a turbocharged engine and testing was completed successfully. The engine was then converted back to NA in order to bracket the experiment and to ensure that neither the engine nor the experimental apparatus has deviated during the evaluation. The engine performed equally well before and after the converted period, thus the engine's condition remained consistent throughout the process while also illustrating that the test facility produced reproducible results. This also indicates the high degree of repeatability of the testing process.

The correlation between the measured and predicted torque for the NA engine was within 6%. This error in predicting the NA engine torque can mainly be attributed to the valve flow coefficients. The flow coefficients used in the simulation were known to have not been accurately determined for this specific engine. This inconsistency in the valve flow coefficients also caused a shift in the predicted volumetric efficiency as a function of engine speed.

If the wastegate was controlled during simulation to match the boost pressure that was measured on the actual engine, the predicted torque was within 9% of the actual measured torque. It was found that the simulation predicted more torque than was actually developed with the same boost pressure. The trends of the predicted versus the measured engine parameters are the same, as with the NA engine; therefore the simulation could be used to investigate the sensitivity or influence of different design parameters on a desired output such as torque.

The actual wastegate area and that predicted by the simulation did not correlate well. The problem is believed to be due to inaccuracies both in the simulated amount of air flowing through the wastegate and the calculation of the wastegate area from the actual measured rack travel. The simulation predicts very small opening areas when compared to what was calculated by measuring the rack travel.

The turbocharged engine developed 96 kW at 5500 rev/min. At 2000 rev/min 84% of the maximum torque was produced, a maximum of 197 N·m was developed at 4000 rev/min and at 5500 rev/min 82% of the maximum torque was still available. Thus the torque curve was not perfectly flat, but it was the best that could be achieved without electronic boost control using the standard cam shaft and valve timing. The turbocharged conversion increased the maximum power by 37% and maximum torque by 48%.

When comparing this turbocharged engine with the NA engine, it has been shown that this turbocharged engine could match the full load fuel economy of the given NA engine up to the rated power of the NA engine, after which the fuel consumption increased significantly as more power was developed. This increase in fuel consumption was due to the rich mixture used to keep the exhaust temperature below the limit.

The most significant fact was that at part load conditions this turbocharged engine could match the SFC of the NA engine. Thus not only was more power developed at WOT, but the fuel efficiency can be matched even at part load. It is known that a big engine is less fuel efficient than a small engine when both are developing the same torque at part load. Thus when comparing the turbocharged engine to a average 2.0-litre NA engine of similar rated maximum power output, the fuel savings of the turbocharged engine at part load was estimated between 1% and 11.6% at 2500 rev/min and between 5.3% and 12.8% at 4000 rev/min.

Developing a turbocharged engine from a NA engine is an attractive option for motor companies that want to offer a higher-performance engine in their premium model, but do not have the resources to develop an all-new engine. It could also be used as a downsizing option and could be used to lower the fleet average fuel consumption.

The first research question asked in the beginning was: what are the implications of adding a turbocharger to a NA engine? The implications can be summarised as:

- It is possible to increase the maximum power output by 37% without reducing the CR or increasing the engine speed at which it is developed;
- Using mechanical boost control and the NA engine's camshaft and valve timing, 82% of maximum torque was available from 2000 rev/min up to 5000 rev/min;
- The loading on the components such as bearing forces would be increased by the same percentage that the maximum torque is increased provided the same speed range is considered;
- The percentage increased loading on the cooling system is similar to the percentage increase in maximum power output;
- Part load efficiency could be matched if the turbocharged engine is compared to a similar sized NA engine or the turbocharged engine could be superior under certain conditions compared to an equally powerful NA engine.

The second part of the research question: to determine whether the performance of a turbocharged engine can be predicted accurately by using 1-D flow simulation? The simulation results can be summarised as:

- The predicted torque was higher than the measured torque, but within 6% of the actual measured torque on the NA engine;
- The predicted torque was higher than the measured torque, but within 9% of the actual measured torque on the turbocharged engine when developing the same boost pressure;
- The trends for both cases were very similar than that measured.

It can be concluded that if 6% and 9% accuracy on NA and turbocharged engines respectively are within the acceptable limits of the purpose of the simulations, then 1-D simulations would be accurate enough to be used.

8. RECOMMENDATIONS

When considering upgrading the performance of an engine by adding a turbocharger, there are certain aspects that must be taken into consideration. The strength of the crankshaft, connecting rods and pistons should be investigated, since this will not only transfer more torque but also have higher bearing loadings. The quality of the exhaust valve and seat are important due to the higher exhaust temperatures typically experienced by a turbocharged engine.

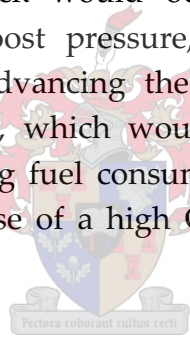
If a turbocharger with a water-cooled bearing housing is used, the degradation of the oil due to high temperatures in the turbocharger is not a concern. The cooling system should, however, be upgraded depending on the reserve capacity of the standard engine's cooling system. As a general guideline the cooling system should be able to cope with the same percentage increase in loading as the percentage increase in power output.

It may be necessary to upgrade the fuel injectors to supply the extra fuel needed to develop the higher power. If the fuel pressure is raised, the fuel rail must be certified to be able to operate at this higher pressure. The fuel pump must be able to deliver the desired flow rate at the designed operating pressure and thus the fuel filter should also satisfy these requirements.

The exhaust system should be upgraded in order to keep the exhaust backpressure (post turbine pressure) within reasonable limits due to the higher airflow caused by the turbocharger. Since the turbine damps most of the blow-down noise that is carried by the exhaust gas, a free flow exhaust system might be considered without increasing exhaust noise above the legal limit. The amount of energy that the turbine can extract is proportional to the pressure difference across the turbine, thus the lower the exhaust backpressure the better. Care must be taken that, if the backpressure is too low, it does not result in a situation where the wastegate is fully open, but the boost pressure developed is too high. This could cause the turbine speed to exceed its maximum and the results could be disastrous.

The variable wastegate actuator that was designed and manufactured proved to be a useful and valuable tool. Although only one spring was used during testing, different boost pressures could be achieved by only adjusting the preload on the spring. If this variable wastegate actuator could be modified such that it does not rely on the diaphragm to deform, its opening characteristics would only be dependent on the spring and therefore it would be a linear function of pressure and its operation would be consistent, independent of the operating temperature.

Whilst not investigated specifically in this research, the importance of an intercooler on a turbocharged engine cannot be over-emphasised. The main advantage of an intercooler is lower intake air temperatures. The lower air temperatures will result in lower initial charge temperatures and would thus reduce the chances that knock will occur. The lower air temperatures would also make it possible to reduce the boost pressure, but still maintain the same density of the air in the intake manifold. Lower boost pressure would further reduce the chances that knock would occur. Thus, with reduced air temperatures and reduced boost pressure, the ignition timing could be advanced closer to MBT. Advancing the ignition timing may result in reduced exhaust temperatures, which would enable leaner AFR mixtures being used and thus improving fuel consumption. The use of lower boost pressure might facilitate the use of a high CR which would greatly benefit engine efficiency.



In this research project a turbocharged engine was developed, thus a test engine is available in either NA or turbocharged format. This project sets the pathway for further research and development in turbocharging. Possible research could include valve optimisation coupled with boost pressure optimisation, development of control strategies for electronic boost control and electronic throttle control to minimise turbo lag.

Adding a turbocharger to a NA engine is not a simple or trivial task, but a properly designed system will yield fruits in proportion with the engineering excellence that was invested.

9. REFERENCES

- Audi AG, 1998, *Audi TT self study programme 207*, Ingolstadt.
- Azzoni, P, Moro, D, Ponti, F & Rizzoni, G, 1998, *Engine and load torque estimation with application to electronic throttle control*, SAE paper, No. 980795, Society of Automotive Engineers.
- Bell, AJ, 2005, *The effect of fuel formulation on the exhaust emissions of spark ignition engines*, Ph.D. thesis, University of Stellenbosch.
- Birmann, R, 1946, *Exhaust energy converting means for internal combustion engines*, US Patent, No. 2406656.
- British Iron and Steel Research Association Metallurgy, 1953, *Physical constants of some commercial steels at elevated temperatures*, London Butterworth Scientific Publications, London.
- Ferguson, CR, 1986, *Internal-combustion engines – applied thermodynamics*, John Wiley, New York.
- Gatowski, JA, Balles, EN, Chun, KM, Nelson, FE, Ekchian, JA, & Heywood, JB, 1984, *Heat release analysis of engine pressure data*, SAE paper, No. 841359, Society of Automotive Engineers.
- Gerhardt, J, Honninger, H & Bischof, H, 1998, *A new approach to functional and software structure for engine management systems – BOSCH ME7*, SAE paper, No 980801, Society of Automotive Engineers.
- Heywood, JB, 1988, *Internal-combustion engine fundamentals*, McGraw-Hill, United States of America.
- Kingwill, AC, 2000, *The calculation of the factors for power correction in IC engines*, Internal report, Stellenbosch Automotive Engineering, October.
- Kühnle, Kopp & Kausch, 1994, *Öldurchsatz K0 mittlere Ölzufluss*, (datasheet).
- Krabbendam, P, 2004, Telephonic interview, February, Stellenbosch.

Kröger, DG, 1998, *Air-cooled heat exchangers and cooling towers thermal-flow performance evaluation and design*, Mechanical Engineering Department, University of Stellenbosch.

Mabie, HH & Reinholtz, CF, 1987, *Mechanisms and dynamics of machinery*, 4th edition, John Wiley, New York.

Mills, AF, 1995, *Heat and mass transfer*, Richard D. Irwin, United States of America.

Moran, DP, Bell, AJ & Williams, PNT, 1997, *RACER – Engine combustion data acquisition and burn-rate analysis system*, Unpublished in-house system operations manual, Centre for Automotive Engineering, University of Stellenbosch, September.

Nelder, JA & Mead, R, 1965, A simplex method for function minimization, *The Computer Journal* Vol. 7, p. 308-313.

Press, WH, Teukolsky, SA, Vetterling, WT & Flannery, BP, 2001, *Numerical recipes in Fortran 77: The art of scientific computing*, 2nd edition, Volume 1, The Press Syndicate of the University of Cambridge, New York.

Ricardo, 2002, WAVE v5 Engine reference manual.

Sayers, AT, 1990, *Hydraulic and compressible flow turbomachines*, AT Sayers, Cape Town.

Streib, H & Bischof, H, 1978, *Electronic Throttle Control (ETC): A cost-effective system for improved emissions, fuel economy and driveability*, SAE paper, No. 960338, Society of Automotive Engineers.

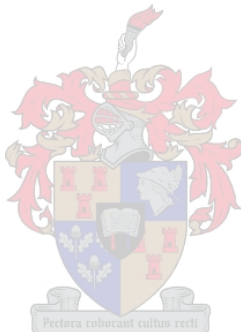
Van der Spuy, J, 2003, Personal interview, 2 October, Stellenbosch.

Van der Weshuizen, HJ, 2003, *Computational and experimental investigation of chamber design and combustion process interaction in a spark ignition engine*, MSc. thesis, University of Stellenbosch.

Venter, J, 1999, Automotive turbocharging, *Car*, December, p. 78.

Watson, N & Janota, M, 1971, *Non-steady flow in an exhaust system with a pulse converter junction*, Paper 27, Conference on Unsteady Flow, University of Salford.

Watson, N & Janota, M, 1984, *Turbocharging the internal-combustion engine*, MacMillan, Great Britain.



APPENDIX A OPTIMISATION ALGORITHMS

A.1. Nelder-Mead Algorithm

The Nelder-Mead algorithm (Nelder & Mead, 1965) was proposed as a method for minimizing a real-valued function $F(\mathbf{x})$ for $\mathbf{x} \in \mathbb{R}^n$. Four scalar parameters must be specified to define a complete Nelder-Mead method: coefficients of reflection (ρ), expansion (χ), contraction (γ), and shrinkage (σ). According to the original Nelder-Mead paper, these parameters should satisfy:

$$\rho > 0; \chi > 1; \chi > \rho; 0 < \gamma < 1; \text{ and } 0 < \sigma < 1.$$

(The relation $\chi > \rho$, while not stated explicitly in the original paper, is implicit in the algorithm description and terminology.) The nearly universal choices used in the standard Nelder-Mead algorithm are:

$$\rho = 1; \chi = 2; \gamma = \frac{1}{2}; \text{ and } \sigma = \frac{1}{2}$$

One iteration of the Nelder-Mead algorithm for n variables:

1. **Order:** Order $n+1$ vertices to satisfy $f(x_1) \leq f(x_2) \leq \dots \leq f(x_n) \leq f(x_{n+1})$
2. **Reflect:** Calculate the reflection point x_r

$$x_r = (1 + \rho)\bar{x} - \rho x_{n+1} \quad (\text{A-1})$$

$$\text{where } \bar{x} = \sum_{i=1}^n \frac{x_i}{n}, \text{ Evaluate } f_r = f(x_r)$$

if $f_l \leq f_r \leq f_n$, accept the reflected point x_r and terminate iteration.

3. **Expand:** If $f_r < f_l$, calculate the expansion point x_e ,

$$x_e = (1 + \rho\chi)\bar{x} - \rho\chi x_{n+1} \quad (\text{A-2})$$

Evaluate $f_e = f(x_e)$. If $f_e < f_0$, accept x_e and terminate iteration; otherwise (if $f_e \geq f_r$), accept x_r and terminate the iteration.

4. **Contract:** If $f_r \geq f_n$, perform a contraction between x and the better of x_{n+1} and x_n .

- a. **Outside:** If $f_n \leq f_r \leq f_{n+1}$, perform a outside contraction

$$x_c = (1 + \rho\gamma)\bar{x} - \rho\gamma x_{n+1} \quad (\text{A-3})$$

Evaluate $f_c = f(x_c)$. If $f_c \leq f_r$, accept x_c and terminate the iteration; otherwise go to step 5 (perform a shrink step).

- b. **Inside:** If $f_r \geq f_{n+1}$, perform a inside contraction

$$x_{cc} = (1 - \gamma)\bar{x} + \gamma x_{n+1} \quad (\text{A-4})$$

Evaluate $f_{cc} = f(x_{cc})$. If $f_{cc} < f_{n+1}$, accept x_{cc} and terminate the iteration; otherwise go to step 5 (perform a shrink step).

5. **Perform a shrink step:** Evaluate f at the n points $v_i = x_1 + \sigma(x_i - x_1)$,

$i = 2, \dots, n+1$. The unordered vertices of the simplex at the next iteration consist of x_1, v_2, \dots, v_{n+1} .

A.2. Initial Value Scaling for Optimisation

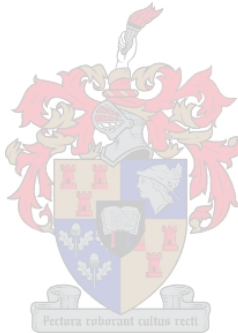
Consider an optimisation problem with n variables and x_1, x_2, \dots, x_n the initial values. Calculate a scaling factor S_i by:

$$S_i = \frac{\sum_{i=1}^n |x_i|}{n \cdot x_i} \quad (\text{A-5})$$

The scaled input is then calculated by:

$$y_i = \frac{x_i}{S_i} \quad (\text{A-6})$$

Then y_1, y_2, \dots, y_n is used as the initial values. The boundary conditions must also be scaled accordingly. Thus when the optimisation has been completed, the end-values must be multiplied by the scaling factor to get the real value.



APPENDIX B TURBOCHARGER OIL FLOW

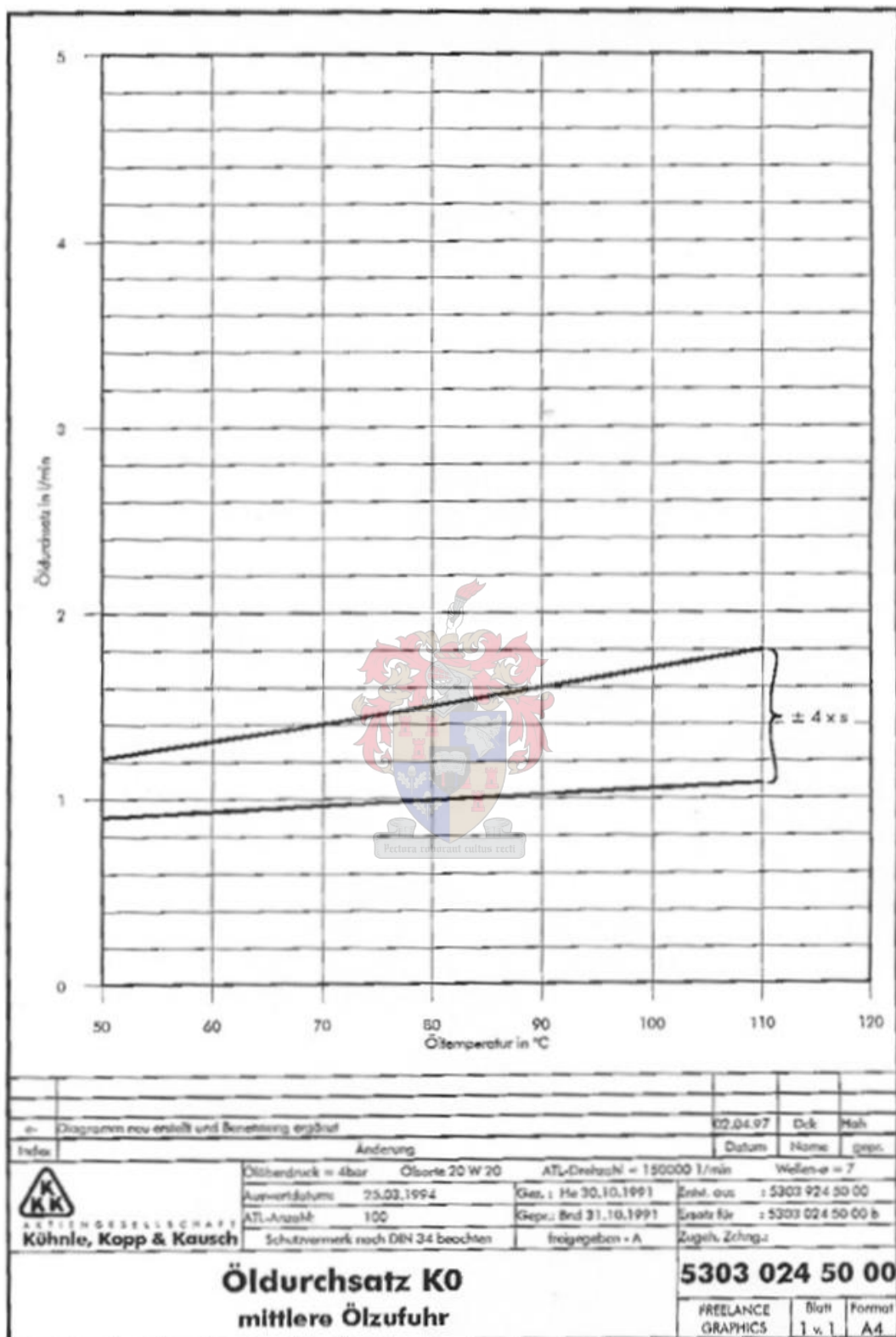


Figure B-1 K03 Oil Flow Specification (Kühnle, Kopp, Kausch, 1994)

APPENDIX C POWER CORRECTION FACTORS

For the purpose of determining the corrected power of internal-combustion engines, the following standard reference conditions are defined and tabulated in Table C-1:

Table C-1 ECE-Standard Reference Conditions

Quantity:	Symbol:	Reference Value:	Unit:
Total barometric pressure	P_r	100	kPa
Air temperature	T_r	298	Kelvin [K]
Relative humidity	ϕ_r	30	%

The ECE-correction factor can be calculated as follows:

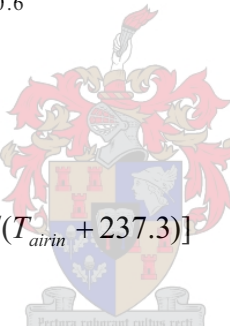
$$CF = \left(\frac{99}{P_a}\right)^{1.2} \times \left(\frac{T_{airin} + 273}{298}\right)^{0.6}$$

Where:

$$P_a = P_{baro} - (\phi \times P_{vsat})$$

$$P_{vsat} = \text{Exp}[(16.78 \times T_{airin} - 116.9) / (T_{airin} + 237.3)]$$

Note: P_a in kPa and T_{airin} in °C:



It must be stressed that the correction factor is only valid within a range of ±2% adjustment and must therefore be applied carefully.

APPENDIX D FORCE ANALYSIS

Derived equations of motion for the piston:

$$x = \sqrt{l^2 - \left(\frac{r}{2} \sin(\omega t) - h\right)^2} \quad (\text{D-1})$$

$$\dot{x} = \frac{-1}{2\sqrt{l^2 - \left(\frac{r}{2} \sin(\omega t) - h\right)^2}} \cdot \left(\frac{r}{2} \sin(\omega t) - h \right) r \omega \cos(\omega t) - \frac{r \omega}{2} \sin(\omega t) \quad (\text{D-2})$$

$$\ddot{x} = \frac{-\left(\left(\frac{r^2 \cdot \sin(\omega t)}{2} - h \right)^2 \cdot r^2 \cdot \omega^2 \cdot \cos(\omega t)^2 \right)}{4 \left(l^2 - \left(\frac{r}{2} \sin(\omega t) - h \right)^2 \right)^{3/2}} - \frac{r^2 \cdot \omega^2 \cdot \cos(\omega t)^2}{4 \left(l^2 - \left(\frac{r}{2} \sin(\omega t) - h \right)^2 \right)^{1/2}} \quad (\text{D-3})$$

$$+ \frac{\left(\frac{r \cdot \sin(\omega t)}{2} - h \right) r \omega^2 \cdot \sin(\omega t)}{2 \left(l^2 - \left(\frac{r}{2} \sin(\omega t) - h \right)^2 \right)^{1/2}} - \frac{r \omega^2 \cdot \cos(\omega t)}{2}$$

Where: x : is the distance from the centre of the crankshaft (O) to the Centre of Gravity (COG) of the piston (B) [m]

l : length of the connecting rod [m]

r : stroke [m]

h : wrist pin offset [m]

ω : angular velocity of the crankshaft [rad/s]

t : time [s]

With equations (D-1), (D-2) and (D-3) the position, velocity and acceleration of the piston can be calculated for any instance in time. It is assumed that at $t=0$ the piston is at TDC and at the beginning of the intake stroke.

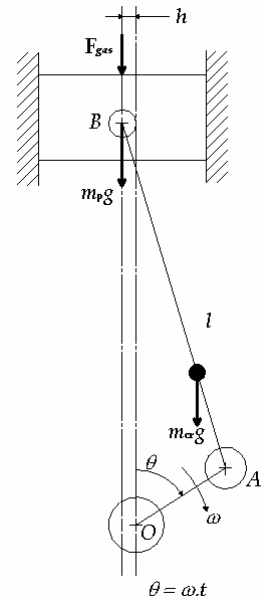


Figure D-1 Piston-Crank: Free Body Diagram